Global Modeling of Persistent Organic Pollutants in an Era of Changing Emissions and Climate

HARVARD UNIVERSITY

Graduate School of Arts and Sciences

DISSERTATION ACCEPTANCE CERTIFICATE

The undersigned, appointed by the

Harvard John A. Paulson School of Engineering and Applied Sciences
have examined a dissertation entitled:

"Global Modeling of Persistent Pollutants in an Era of Changing Emissions and Climate"

presented by: Charlotte Christine Wagner

Signature _____
Typed name: Professor E. Sunderland

Signature _____
Typed name: Professor S. Wofsy

Signature _____
Typed name: Professor A. Pearson

March 26, 2021

Global Modeling of Persistent Organic Pollutants in an Era of Changing Emissions and Climate

A DISSERTATION PRESENTED
BY
CHARLOTTE CHRISTINE WAGNER
TO
THE DEPARTMENT OF HARVARD JOHN A. PAULSON SCHOOL OF ENGINEERING AND APPLIED SCIENCES

IN PARTIAL FULFILLMENT OF THE REQUIREMENTS
FOR THE DEGREE OF
DOCTOR OF PHILOSOPHY
IN THE SUBJECT OF
ENGINEERING SCIENCES: ENVIRONMENTAL SCIENCE AND ENGINEERING

HARVARD UNIVERSITY
CAMBRIDGE, MASSACHUSETTS
MARCH 2021

Dissertation advisor: Professor Dr. Elsie M. Sunderland Charlotte Christine Wagner

Global Modeling of Persistent Organic Pollutants in an Era of Changing Emissions and Climate

Abstract

Certain anthropogenic organic pollutants persist in the environment, bioaccumulate and are toxic to humans and wildlife. They accumulate in the global oceans where marine biogeochemical cycles drive their fate and distribution. An increasing number of compounds has been included in the Stockholm Convention on Persistent Organic Pollutants (POPs) and some have been banned for several decades. Yet, they continue to be ubiquitous in the environment.

Most POPs are neutral and display strong particle affinity. Particle scavenging removes POPs like polychlorinated biphenyls (PCBs) from biologically relevant zones of the ocean to marine sediments or the deep ocean, which can become a source of legacy POPs when emissions decline. In the past two decades poly- and perfluorinated alkyl substances (PFAS) with low particle affinity and no known degradation mechanisms have emerged as global pollutants of concern. The presence of PFAS like perfluorooctane sulfonate (PFOS) in the environment has been attributed to direct releases from rivers, but recently, atmospheric transport of precursors and transport with sea spray aerosol (SSA) were suggested to be important drivers of elevated concentrations in polar regions.

This work presents 3-D simulations for four PCBs and PFOS embedded in the MIT general circulation model and applies them to explore the timescales of removal from the global ocean and the effectiveness of regulation for human exposure. I develop a novel inventory of riverine and atmospheric PFOS inputs to the ocean constrained by seawater observations in a Bayesian framework. I

model global transport of PCBs and PFOS with ocean circulation, diffusion, particle settling, air-sea exchange and transport with SSA for PFOS. By propagating PFOS and precursor concentrations through the food web of the North Atlantic pilot whale, I determine the the contribution of changing seawater concentrations to human exposure in the Faroe Islands.

I estimate that 75% of historic PCB inputs to the ocean have been buried in the marine sediments and evasion from the ocean's surface is an important contributor to releases in remote regions. Preferential burial of heavier molecular weight PCBs has resulted in an enrichment in lighter congeners. Climate-driven changes have increased evasion of low molecular weight PCBs but increased deposition of higher molecular weight PCBs in the Arctic Ocean. I find that atmospheric deposition of PFOS contributes up to 98% of seawater concentrations in the mixed layer of remote ocean basins, but the contribution of riverine discharges from China and Brazil to cumulative ocean inputs is small. Transport with SSA is important for the Southern Ocean, doubling mixed layer concentrations in certain regions. Marginal burial in marine sediments since 1958 indicates that the half-life of PFOS in the ocean likely exceeds 300,000 years. I estimate that PFOS exposure from whale meat consumption in Faroese children would have been four-fold higher without regulation, emphasizing the effectiveness of international regulation of global pollutants. The PFOS precursor FOSA continues to contribute 60% to the $\sum(PFOS, FOSA)$ concentrations in whale muscle in 2015.

My dissertation work provides new insights into the timescales of removal of POPs from the global ocean in response to declining emissions and changing climate and shows that the importance of atmosphere-ocean interactions will likely increase in the future for neutral POPs as well as PFAS. Identifying how biogeochemical processes and changes in primary releases impact the longevity and hazard potential of POPs in the ocean is key to estimating the effectiveness of regulation.

Contents

List of Figures

List of Tables

To Alex and my family without whom this dissertation may been never been completed.

Acknowledgments

First and foremost, I want express my gratitude to my advisor Prof. Elsie Sunderland, who was an enormous source of encouragement and mentorship. She gave me the freedom to explore my scientifc interests, and ensured I had the support I needed along the way. I also want to thank my co-authors who kindly shared their knowledge and scientific passion with me: Carey Friedman, Clifton Dassuncao, Colin Thackray, Elizabeth Lundgren, Gael Forget, Heidi Pickard, Helen Amos, Jennifer Sun, Noelle Selin and Rainer Lohmann. Without being able to build my research on their knowledge and prior work my dissertation would have been a lesser contribution. Finally, I want to thank the entire Sunderland Group, past and present members, who have been the social and intellectual fabric of my graduate experience.

0

Introduction

Since the 1940s, there has been an unprecedented increase in the manufacturing of synthetic chemicals ranging from pest and disease control, crop production, industrial use and consumer products, many of which have subsequently entered the environment. Today, more than 350,000 chemicals are commercially registered and for many little or no data on environmental behavior and human health effects exists.[203] Persistent organic pollutants (POPs) receive particular attention due to their persistence in the environment, ability to bioaccumulate and potential to cause a variety of reproductive, endocrine and developmental disorders in humans and wildlife.[196] Since 2001, the Stockholm Convention on POPs has added an increasing number of compounds to its list of banned contaminants. These chemicals are targeted for elimination, or in cases of a competing health benefits, have their production and application restricted to a maximum extent feasible.[196] POPs known to be harmful to human and ecological health continue to be pervasive in the global environment.

The resistance to degradation and volatility of many POPs means they are subject to long range transport from source regions to remote locations.[55,134] Many POPs accumulate in the oceans due to inputs from rivers and the atmosphere.[134] In the ocean, their fate is driven by biogeochemical processes. Their removal from different regions of the ocean depends on circulation, particle scavenging, and exchange across the ocean-atmosphere boundary.[134,69,123] Previous efforts to characterize biologically relevant global reservoirs of these pollutants have not accounted for heterogeneity in spatial inputs from the atmosphere and rivers, circulation patterns, and ocean biogeochemistry. Past research has hypothesized that air-sea exchange of POPs and emissions with sea spray aerosol (SSA) may be a particularly important source of emissions on a global scale,[148,125,182,103] but these fluxes are poorly characterized. As such, declining atmospheric and surface ocean concentrations may remobilize contaminant reservoirs in the deep ocean and contribute to a prolonged residence time of POPs in the biologically relevant ocean layers and the marine food web.

In addition, ongoing changes in ocean biogeochemistry will alter the fate and transport of POPs in the oceans. For example, warming in the Arctic is accelerating and is much larger than in mid-latitude ecosystems.[159] Weakened meridional overturning is expected to result in greater inputs from the North Atlantic to the high Arctic.[223] Rising air temperatures and large resulting decreases in ice cover are expected to dramatically shift air-sea exchange of many POPs.[158,110] Climate-driven shifts in wind, precipitation and are expected to trigger complex feedback mechanisms impacting nutrient discharge, stratification, biological productivity, ocean oscillation and salinity,[131] which have implications for bioavailability and magnification of POPs in marine ecosystems. Already today, we observe some of the highest concentrations of POPs in the Arctic Ocean and climatic shifts will likely have a significant impact oncontaminant cycling and residence times.

Polychlorinated biphenyls (PCBs) are a class of 209 persistent organic compounds that were widely used in electronic applications and transistors due to their high dielectric constant and low flammability. They bioaccumulate in food webs and some have been associated with cancer, neuro-

toxicity, endocrine and thyroid disorders.[23,24,155] PCBs were banned from production in the US in 1979 and were included among the original 12 chemicals listed by the Stockholm Convention. As neutral POPs with strong particle affinity they represent ideal benchmarking compounds to better understand how the distribution of neutral hydrophobic POPs in seawater is affected by variability in ocean biogeochemistry. The variable physical-chemical properties across PCB congeners enables exploring the impact of climate-driven changes in surface temperatures, sea ice cover, and ocean circulation across a range of molecular weights and volatilities.

The past two decades have seen the emergence of poly- and perfluorinated alkyl substances (PFAS), which are potent immune suppressants detectable in virtually all human populations and wildlife in remote regions such as the Arctic.[108,17,160,189] PFAS have contrasting physical-chemical properties to neutral POPs. They are both hydrophobic and oleophobic, and some, such as perfluorooctane sulfonate (PFOS), are present as stable anions in solution and are not known to degrade in the environment. Marine seafood is an important exposure source of PFAS for coastal communities,[56] driving research efforts to quantify PFAS bioaccumulation in marine organism.[160] PFOS is of particular concern due to its long elimination time in organisms.[149] Production of the PFOS parent compound POSF (perfluorooctanesulfonyl fluoride) and its precursors was phased out between 2000-2002, leading to large reductions in releases in Europe and North America.[139,150] By contrast, environmental concentrations have not declined simultaneously, especially in remote regions where increasing trends have been observed in some media and organisms.[114,212] Some studies have suggested a potential increase in releases from Asia and South America[156,79] and atmospheric transport of precursor substances may explain continued elevated concentrations observed in polar and other remote regions.[14,73] More recently, sea spray aerosols (SSA) have been shown to be many thousandfold enriched in PFOS and transport mediated by SSA has been suggested an important transport vector to remote regions.[103,32]

The non-linear propagation of environmental releases across environmental media, ecosystems

and human exposure poses a challenge to international conventions aiming to control pollutant releases. Impact evaluations of such regulations rely on the assumption of causal, and often linear, links between declining pollutant releases in response to regulation and human and environmental monitoring data. Establishing such links is especially difficult when moving from the global (i.e. releases, environmental transport processes) to the local scale (i.e. bioaccumulation in local ecosystems, human exposure). As such, the complexity of the human-environmental system has limited our ability to attribute observed patterns in human exposure data to changes in environmental releases and assess whether existing regulations are effective at protecting public health.

In this work, I present global 3-D simulations for four neutral PCBs and PFOS embedded in the MIT general circulation model. In Chapter 1, I investigate how ocean circulation, biological productivity and particle export fluxes affect residence times of PCBs in biologically relevant regions and the potential of marine reservoirs to function as secondary environmental sources in an era of declining primary emissions. In Chapter 2, I develop an inventory for PFOS inputs to global oceans from riverine and atmospheric sources constrained by global ocean observations. I add transport with SSA to the ocean simulation and investigate the importance of deposition of PFOS oxidized from precursor substances and transport with SSA for observed ocean seawater concentrations. Finally, in Chapter 3, I apply the PFOS simulation to explore the impact of regulation on PFOS exposure in a subsistence fishing community in the North Atlantic. I propagate environmental concentrations through the food web of the North Atlantic pilot whale and deconstruct the contribution of changing seawater concentration trends and dietary changes on exposure patterns observed in human biomonitoring data collected in three children cohorts on the Faroe Islands. With this case study, I demonstrate how global biogeochemical modeling can be integrated with local ecosystem models and human biomonitoring data to close important gaps in environmental monitoring and quantify avoided exposures to POPs. Finally, I identify key sources of uncertainty that need to be considered when employing monitoring data for regulatory impact evaluations.

1

A global 3-D ocean model for polychlorinated biphenyls (PCBs): Benchmark compounds for understanding the impacts of global change on neutral persistent organic pollutants

1.1 Introduction

Human activities release large numbers of persistent organic pollutants (POPs) to the environment, hundreds of which are known to be persistent, bioaccumulate in food webs, and may pose health risks to exposed wildlife and humans. [168] The ocean is a terminal sink for many of these chemicals, some of which are regulated internationally under the Stockholm Convention. [123,196] Multimedia box models have been applied to better understand the global environmental fate of compounds with different molecular weights and volatilities. [13,133,169,204] However, effects of climate-driven variability in ocean biogeochemistry on POPs are poorly characterized. [10] Such an analysis is enabled by satellite observations and ocean state estimates incorporated into Earth systems models. Here we develop a 3-D ocean simulation for polychlorinated biphenyls (PCBs) within such a model (the MITgcm) to better understand how variability in ocean biogeochemistry affects the transport, accumulation and removal of hydrophobic neutral POPs. PCBs are a class of 209 chlorinated aromatic compounds that were used extensively in industrial equipment and consumer products prior to a global phase out in the 1970s. [21,22] PCB emissions peaked (ca. 1970) at approximately 3000 Mg a^{-1} before they were phased out in most regions globally and they have subsequently declined to several hundred Mg a^{-1} (ca. 2010). [21,22] Atmospheric deposition is the main source of PCBs to the global oceans, and rivers are a minor contributor. [106,113,204] High PCB concentrations in crustaceans from the deep Pacific Ocean illustrate their penetration to even the most remote regions of the ocean. [101] Prior work has characterized PCB behavior in the environment, quantified their physical-chemical properties, and developed global release inventories. [22,37,78,137,170] This makes PCBs ideal as benchmark compounds for better understanding the behavior of persistent, bioaccumulative and toxic POPs in the ocean and interactions with different biogeochemical processes. The global residence time and distribution of many organic contaminants is affected by biogeochemical characteristics of the ocean such as productivity, photochemistry, circulation, suspended particle dynamics, and

sea-ice cover.[122,170,179] Both evasion and particle scavenging can remove organic chemicals from the surface ocean.[69] Chemicals evaded from the ocean to the atmosphere will be redeposited elsewhere and thus have an extended lifetime in the biosphere. Chemicals with a stronger propensity to sorb to particles will have a shorter lifetime in biologically relevant components of the environment due to faster burial and sequestration. Thus, the relative importance of evasion and sorption to particles is essential for understanding chemical fate and lifetime in the ocean. The balance between these processes depends on both the physical-chemical properties of pollutants as well as ecosystem conditions such as productivity, temperature, wind-speed and turbulence .[220] The main objective of this study is to better understand how the distribution of neutral hydrophobic POPs in seawater is affected by variability in ocean biogeochemistry. We develop a 3-D global simulation for PCBs within an ocean general circulation model (MITgcm) forced by atmospheric inputs from the GEOS-Chem Chemical Transport Model (CTM).[62,65] We evaluate the model against observations and apply it to better understand the relative importance of different input and removal processes. We explore variability across PCB congeners spanning a range of molecular weights and volatilities and use our simulation to estimate impacts of climate-driven changes in surface temperatures, sea ice cover and ocean circulation in the Arctic, where the largest changes are occurring.

1.2 Model Description

1.2.1 General Model Description

We added four PCBs (chlorinated biphenyl (CB)-28, CB-101, CB-153, CB-180) as tracers to the Massachusetts Institute of Technology general circulation model (MITgcm). Tracers were selected from the seven congeners frequently measured by the International Council for the Exploration of the Sea (ICES-7) and represent a range of physicochemical properties.[51] The MITgcm has a horizontal resolution of 1°×1° globally, with higher resolution in the Arctic (40 km×40 km) and near

the equator (0.5°×1°). It has 50 vertical layers spanning 5 m intervals at the surface and 500 m near the ocean floor.[62] Advection and diffusion of PCBs is based on ocean state estimates from the Estimating the Circulation & Climate of the Ocean (ECCO-v4) climatology. Surface boundary conditions (e.g., wind stress, seawater temperatures, and sea-ice cover) from the ERA-Interim re-analysis fields spanning 1992-2015 and ocean transport parameters are optimized in ECCO-v4 to produce a best fit to *in situ* and satellite observations of the physical ocean state and sea ice cover.[64,62,63] We forced the ocean model with monthly atmospheric concentrations and deposition of PCBs between 1930-2015 from the GEOS-Chem global atmospheric model.[65] We assumed negligible concentrations of PCBs in the ocean prior to the onset of global production in 1930. The GEOS-Chem simulation estimates primary releases based on the high anthropogenic emissions scenario recommended in prior work and surface temperature.[22,65] Projected emissions to 2015 were based on continued product use trends suggested by the same authors.[22] We neglected inputs to the ocean other than atmospheric deposition because other work suggests they are small.[106,113]

1.2.2 Model parameterization and sensitivity analysis

Air-sea exchange of PCBs was modeled using a standard two-layer thin film transfer model.[104] Chemical evasion in the polar oceans is thought to be enhanced by turbulence from sea ice-rafting.[127] We thus doubled the piston velocity over regions partially covered with sea-ice, following previous work.[224] Model parameters for air-sea exchange of PCBs are provided in the supporting information (Table A.1).[50,65,67,99,104,111,121,147,166,177,194,195,211] PCBs rapidly reach equilibrium between the dissolved and solid phases in seawater.[180] Partitioning to suspended particles was therefore represented as a reversible equilibrium based on an empirically measured organic carbon partition coefficient (K_{OC}) adjusted for temperature and salinity.[180] The physicochemical properties of the four congeners are detailed in the supporting information (Table A.3).[119,167,170,204] Particle concentrations and vertical transport of PCBs associated with export fluxes were simulated using the ecolog-

ical simulation (DARWIN-ECCO v4) embedded within the MITgcm. The ecological simulation has been described and evaluated elsewhere.[53] Some sorption to dissolved organic carbon (DOC) is also known to occur and is particularly important in the coastal environment.[28] However, typical surface ocean DOC concentrations for pelagic marine regions (51-79μM) and the mean partition coefficient for dissolved organic carbon (log K_{DOC}=0.71 log K_{OW}-0.50) suggest less than 5% of PCBs will be bound in this phase.[28,53,89] Sorption coefficients for DOC may vary depending on organic carbon composition but such data are not available to parameterize our model simulations and we thus neglect sorption to DOC in our ocean simulation. We conducted sensitivity simulations to explore the impacts of uncertainties in K_{OC} values, particle concentrations, carbon export fluxes and degradation rates. Prior work has hypothesized that stronger relative sorption to organic carbon occurs in low productivity ecosystems such as the open ocean.[180]Marine primary productivity predicted by satellite measurements ranges from 44 - 57 Pg C a^{-1}.[31] Estimates of annual export of carbon from the euphotic zone vary widely (5 to >12 Pg C a^{-1}) and the simulation used here is on the lower end of this range (6 Pg C a^{-1}).[19,94] This results in a low bias in particle concentrations in the subsurface ocean.

We ran the 1930-2015 simulation using the range of log K_{OC} values reported in prior work (5.82 to 8.31) for CB-153, which is the most prevalent congener in many regions of the ocean.[92,119,167,179,180] The upper bound of K_{OC} values reported by Sobek et al.[180] is higher than supported by recent data.[152,183] It can be used to explore model sensitivity to a potential underestimate in carbon export since both higher K_{OC} values and higher particle concentrations will result in greater PCB partitioning to the solid phase. We found the low and mid-range values of K_{OC} for CB-153 resulted in modeled dissolved concentration peaks (9-16 pg L^{-1}) at three tropical Atlantic Ocean stations that exceeded the ranges of measurements (0.06 to 3.5 pg L^{-1}) (Figure A.1). The best model performance was obtained using the upper 95^{th} percentile confidence limit of the K_{OC}, reflecting combined influences of higher PCBs sorption to particles than predicted by the geometric mean K_{OC}

and likely higher carbon export fluxes from the surface ocean. Gustafsson et al. (1997) reported PCB settling fluxes from the surface ocean mixed layer of the North Atlantic for CB-52, CB-128, and CB-194 that ranged from 0.02-12 pmol m^{-2} d^{-1} based on ^{234}Th and PCB concentrations in suspended particles. This compares well to our modeled results for different congeners (CB-28, CB-101, CB-153, and CB-180) of 0.0002-7 pmol m^{-2} d^{-1}. Annually averaged settling fluxes in this study are lower than those reported by Galbán-Malagón et al. (2012) for the polar North Atlantic during peak biomass production. At this time, particle concentrations are approximately one order of magnitude higher than outside the spring-summer season.[185] Polychlorinated POPs degrade through both photolytic and biological processes but rate data are not specifically available for PCBs.[1,66,175] Assuming uniform degradation with depth, which has been used in other models,[204] results in decreasing PCB concentrations with depth. Measured PCB concentrations increase with depth in the water column and peak between 400 m and 3000 m (Figure A.2).[18,86,187] Prior research suggests microbial degradation of PCBs is approximately one order of magnitude lower than photolytic degradation.[175,224] We thus used the following expression to represent degradation of PCBs in the water column:

$$k_{deg} = (0.9\frac{k_{(base,T)}}{RAD_{surf}} \times RAD_z + 0.1k_{(base,T)} \times f_{(remin,z)}) \times 100$$

where $k_{base,T}$ is the temperature adjusted degradation base rate, RAD_{surf} and RAD_z are the shortwave radiation intensity at the surface and at depth z, and $f_{remin,z}$ is the remineralized fraction of organic carbon at depth z. Organic carbon remineralization rates are used as a proxy for bacterial activity in the water column.[52,224] Resulting modeled degradation half-lives in the upper ocean (top 1000 m) for CB-28 (3.8 years), CB-101 (10.4 years), CB-153 (20.9 years), and CB-180 (27.2 years) agree well with those reported elsewhere.[70,175,204]

Figure 1.1 ***(following page)*****:** Modeled dissolved seawater concentrations of chlorinated biphenyl (CB)-28, CB-101, CB-153 and CB-180 at 5 m depth in 2008. Observations collected between 2000 and 2015 are shown as circles and the modeled year represents the mid-point of measurements. Data sources are as follows: **Arctic Ocean**: Booij et al. 2014; Galbán-Malagón et al. 2012; Gioia et al. 2008a; Gustafsson et al. 2005; Sobek & Gustafsson2014; Sobek et al.2004, **North Atlantic Ocean**: Galbán-Malagón et al. 2012; Gioia et al. 2008b; Gioia et al. 2008b; Lohmann et al.; 2012; Sun et al. 2016, **South Atlantic Ocean**: Sun et al. 2016; Booij et al. 2014; Gioia et al. 2008b; Lohmann et al. 2012; Sun et al. 2016, **Mediterranean Sea**: Berrojalbiz et al. 2011; Lammel et al. 2016, **Pacific Ocean**: Zhang & Lohmann 2010a, **Indian Ocean**: Booij et al. 2014, **Southern Ocean**: Galbán-Malagón et al. 2013.

Figure 1.1: (continued)

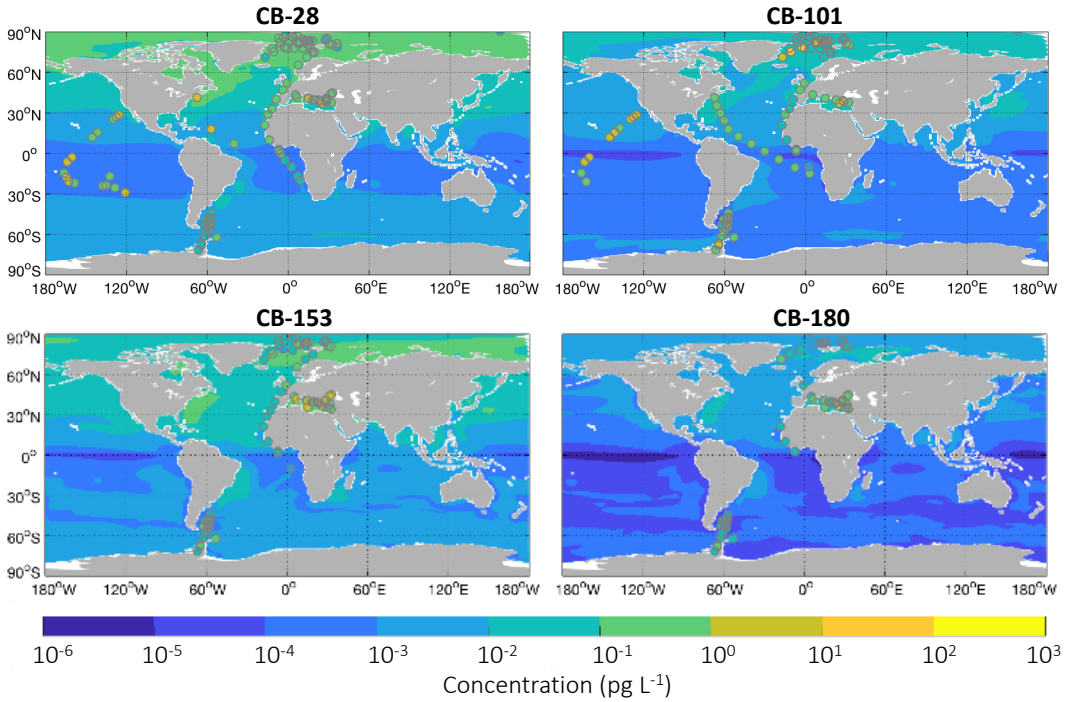

1.3 Results and Discussion

1.3.1 Modeled global distribution of PCBs in seawater

Figure 1.1 shows the modeled global distribution of PCBs in the surface ocean (5 m depth, ca. 2008) compared to measurements collected between 2000-2015. Modeled seawater PCB concentrations were highest in the Northern Hemisphere for all four congeners due to proximity to historic sources. Seawater measurements between 2000-2015 were clustered in the Mediterranean Sea and Arctic Ocean, and sparse data have been collected from other ocean regions (Figure 1.1, Table A.4). The atmospheric model used to force our ocean simulation has a relatively coarse resolution (4°×5°) and when combined with the narrow shape of the Mediterranean Sea produces anomalous deposition patterns due to multiple atmospheric grid cells that contain only a small fraction of water. We thus focus model evaluation on the Arctic Ocean. Median modeled concentrations overlap with the measured ranges in surface seawater for all four PCB congeners and capture important spatial patterns (Figure 1.1 and 1.2). Both modeled and measured concentrations peak in the Norwegian and Greenland Seas and are lowest in the high Arctic. Variability in observations is greater than for modeled concentrations, which reflects the coarser spatial resolution and associated spatial averaging that occurs in the model. Both the model and measurements indicate the most volatile congener (CB-28) is most abundant in the Arctic, and the highest molecular weight congener (CB-180) is approximately two orders of

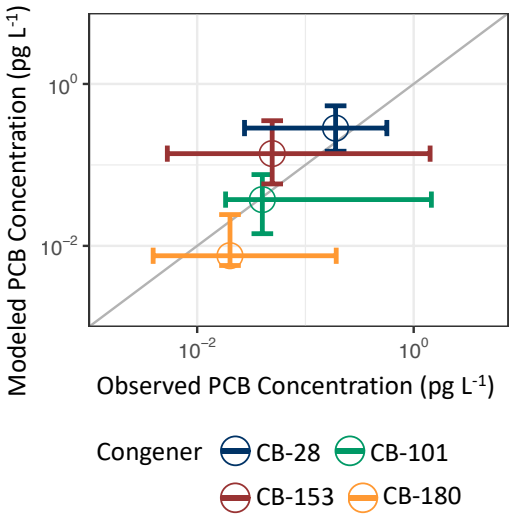

Figure 1.2: Comparison of modeled (2008) and observed (2000-2015) dissolved concentrations of chlorinated biphenyl (CB)-28, CB-101, CB-153 and CB-180 in the upper 1000 m of the Arctic Ocean.[18,69,77,86,179,180]

magnitude lower in concentration (Figures 1.1 and 1.2).

This contrasts the modeled distribution at mid-latitudes and in the tropics (Figure 1.1, Table A.4) where the higher molecular weight congener, CB-153, is most abundant due to higher deposition. Fractionation of more volatile congeners with increasing latitude is consistent with measurements in ocean water and sediment cores.[87,178] For other ocean regions, insufficient data are available to perform a quantitative model evaluation. In addition, ship-based sampling always faces the issue of shipboard contamination due to the potential presence of trace-level contaminants on the ship itself.[124] During active sampling, incomplete separation of the dissolved and solid phases in reported PCB measurements is known to occur.[2] Such issues may explain the lack

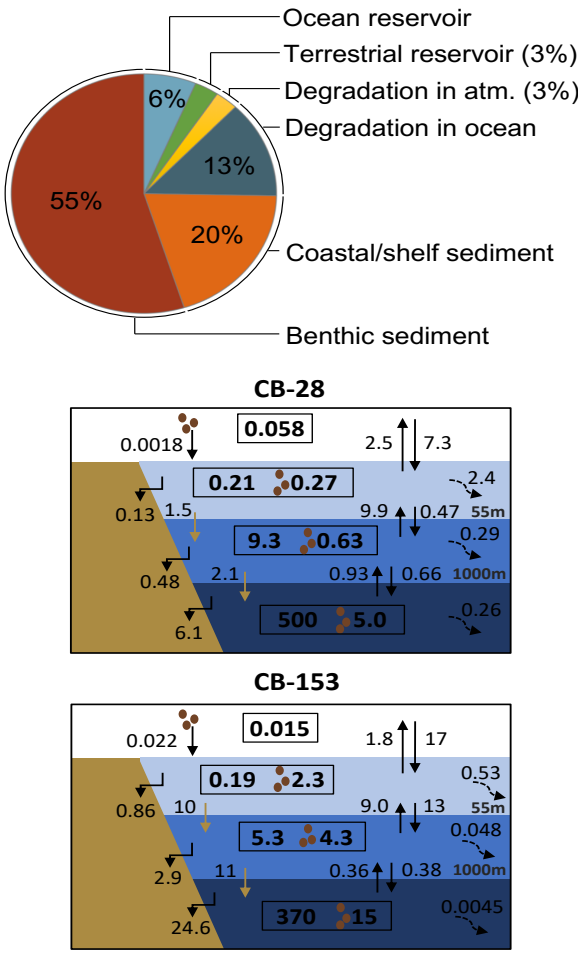

Figure 1.3: Modeled fate of polychlorinated biphenyls released to the global environment between 1930 and 2015 (sum of historical CB-28, CB-101, CB-153, and CB-180 releases) and major removal processes through degradation in the atmosphere and ocean. The 2015 atmospheric reservoir is estimated to be <0.01% of the cumulative releases since 1930.[65,204] Bottom panels show 2015 global ocean budget of CB-28 and CB-153. Atmospheric deposition includes wet and dry particulate, and wet gaseous deposition; vertical transport includes advective and diffusive transport. Upward diffusive transport at the air-sea boundary denotes gross evasion and downward diffusive transport denotes gross gaseous deposition. Superscripted asterisk (*) indicates that the terrestrial reservoir is based on the difference between environmental releases and cycling/loss pathways included in our analysis and does not account for localized point sources not included in Breivik et al. (2007). CB = chlorinated biphenyl.

of clear latitudinal variability in ocean measurements compared to the distinct enrichment in the Northern Hemisphere in the model.

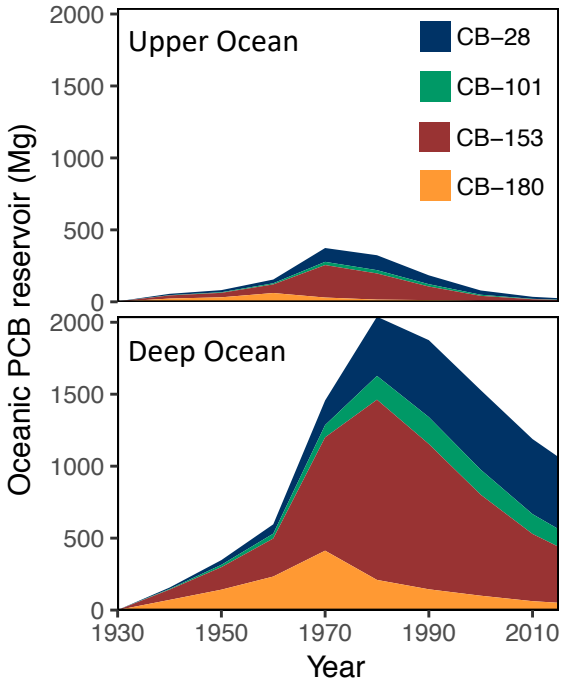

Figure 1.4: Modeled changes between 1930 and 2015 in the reservoir of PCBs in the upper ocean (top 1000 m) and deep ocean (below 1000 m to the seafloor).

Model results indicate the global oceans contain approximately 6% of the $\sum$ 4PCBs (sum of CB-28, CB-101, CB-153 and CB-180) released to the environment between 1930 and 2015. In 2015, only 2% of the $\sum$ 4PCBs (approximately 22 Mg) was present in the ocean above 1000 m depth (Figures 1.3 and 1.4). Burial of PCBs in benthic sediment in the deep ocean (9400 Mg) and in coastal/shelf regions (3400 Mg) has sequestered 75% of cumulative releases between 1930 and 2015 (Figure 1.3), emphasizing the importance of this pathway as a removal process.[107] Our parameterization for PCB degradation in seawater suggests it has removed an additional 13% from environmental reservoirs (2200 Mg). This is substantially higher than in previous modeling studies and more than the present ocean reservoir.[204] Thus, better observational constraints on PCB degradation rates in seawater have global significance for understanding their ultimate fate in the environment. As noted elsewhere, atmospheric oxidation is a less important loss pathway (3%).[13,65] The terrestrial environment contains the remainder of environmental releases included in our analysis since 1930. These results emphasize the effectiveness of natural sequestration mechanisms at reducing concentrations in the biosphere following a global phase out in chemical production.

1.3.2 Temporal shifts in the global ocean reservoir

The modeled global upper ocean reservoir (top 1000 m) of PCBs peaked during the highest atmospheric releases in the 1970s and 1980s and has declined by more than 90% since this time (Figure 1.4). In the deep ocean, the reservoir of CB-180 peaked in 1968, followed by CB-153 in 1979, CB-101 in 1990 and CB-28 in 1997 (Figure 1.4). This timing follows their molecular weight and associated volatilities, particle affinities and hydrophobicities.[170] More rapid scavenging of high molecular weight PCBs increased the proportion of lighter congeners (CB-28 and CB-101) in the ocean from 20% of the $\sum$ 4PCBs in 1970 to 58% in 2015 and is consistent with enrichment of moderately chlorinated congeners in modern sediments.[87] Shifts in congener composition led to a 37% increase in modeled global residence time of the sum of four PCBs in the upper ocean between 1970 and 2015 (Figure A.3). The spatial distribution of PCBs in the ocean has shifted over time toward the Southern Hemisphere (Figure

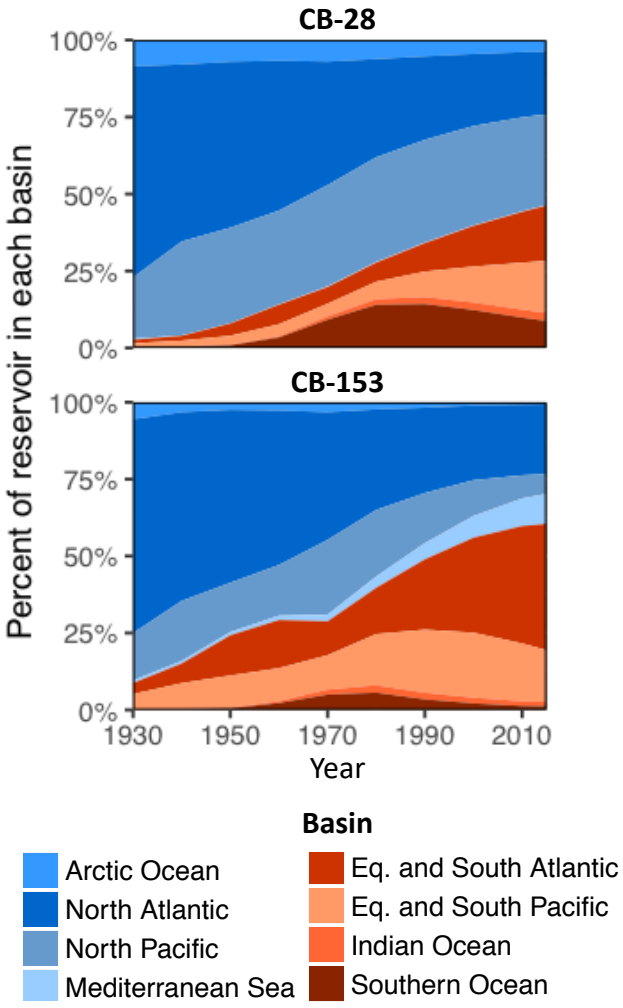

Figure 1.5: Changes in the mass distribution of chlorinated biphenyl (CB)-28, and CB-153 between ocean basins between 1930 and 2015. Northern hemisphere basins are shades of blue and southern hemisphere basins are shades of red/orange.

1.5, Figure A.4). In 1970, when primary emissions of PCBs were very high, 64% of the global ocean reservoir in the ocean was contained in the North Atlantic and North Pacific Oceans. By 2015, this declined to 39%. Over the same time period, the Southern Hemisphere ocean reservoirs increased from 30% to 54% of the global total. These results illustrate the role of the Northern Hemisphere oceans as an ongoing exporter of historic pollution to the equatorial and southern ocean basins over multi-decadal timescales.

1.3.3 Major biogeochemical processes driving global distribution

Figure 1.6 shows the relative importance of different biogeochemical processes for PCB inputs and losses across the upper ocean (top 1000 m). Despite declines in PCB releases, atmospheric deposition to the surface ocean is still the most important input source to all ocean regions and accounted for 49-99% of total inputs across basins and congeners in 2015 (Figure 1.6a, Table A.5). Almost 60% of modeled total deposition occurred in the North Pacific and North Atlantic basins even though they make up only 33% of surface area of the ocean.[54] This reflects their continued proximity to emissions sources from PCBs used in historic manufacturing in the global PCB inventory.[22] More recent studies have suggested that global inventories of PCB releases should be updated to account for missing recent sources in the Southern Hemisphere.[78,125,220]

As discussed above, advection of PCBs from the Northern Hemisphere to the Southern Hemisphere ($\sum$ 4PCBs = 2.5 Mg in 2015) though lateral ocean circulation has become substantial in recent years for some basins. Modeled fluxes of PCBs with lateral ocean circulation accounted for 48% of total inputs to the upper Equatorial and South Atlantic Ocean and 20% of inputs to the Indian Ocean in 2015. Other sources to the upper ocean such as upwelling from the deep ocean accounted for less than 10% of the modeled total inputs across basins. Globally, we find modeled particle-associated scavenging of PCBs from the upper ocean accounted for 69% of total losses in 2015 (Figure 1.6b, Table A.5). This is consistent with observational studies that have suggested the marine

biological pump is a globally significant removal mechanism for PCBs from the upper ocean.[41,69] Across basins, particle-associated export of PCBs from the top 1000 m of the water column accounted for between 25% and 75% of losses in 2015 (Figure 1.6b, Table A.5). The Arctic Ocean has a water column depth of less than 1000 m in many regions due to an expansive continental shelf. Thus, particle-associated removal is reflected by burial in benthic sediment in the Arctic basin (42% of the $\sum$ 4PCBs losses), as has been noted elsewhere.[179]

The importance of other PCB removal processes from the upper ocean varies spatially and by congener. Globally, evasion accounts for 16% of total losses from the upper ocean, degradation for 11%, and deep water formation for 4% (Figure 1.6b, Table A.5). For the higher molecular weight congeners (CB-153 and CB-180), scavenging by particles is the dominant removal process across all basins (59-97%, Figure 1.7b, Table A.5). These two compounds have log octanol water partition coefficients (K_{OW}) of greater than 7.31, which is linearly related to their K_{OC} (upper bound greater than 8.31) and a good proxy for partitioning to lipids.[35,180]

A single dominant removal process for PCBs from the upper ocean is less identifiable for the lower molecular weight congeners CB-28 and CB-101 with lower log K_{OW} values. For CB-28, modeled degradation is the dominant removal process in the Equatorial and South Atlantic (57%), Equatorial and South Pacific (54%), Indian Ocean (62%) and Mediterranean Sea (70%) but evasion is more important in the Arctic, North Pacific and Atlantic Ocean basins (21-41%) (Figure 1.6b, Table A.5). This reflects higher winter wind speeds in Northern Hemisphere oceans that enhance PCB losses through evasion and greater shortwave radiation intensity near the tropics that enhance water column degradation. Removal processes for CB-101 in the upper ocean are diverse and depend on basin specific characteristics. The lack of a single dominant removal process for lower molecular weight PCB congeners demonstrates that the removal of some POPs can only be determined after characterizing basin-specific differences in biogeochemical properties. Prior work suggests that accumulation of persistent organic contaminants in the subsurface ocean

may provide an ongoing source to the surface ocean and atmosphere after elimination of primary emissions sources.[96,182] These studies have proposed that the ocean could act as source rather than sink for some legacy POPs due to mixing, seasonal entrainment of the mixed layer, and diffusion of volatile chemicals back to the surface ocean, followed by evasion to the atmosphere.[125,148,182] Such processes have been proposed as one explanation for slowing declines in atmospheric concentrations of PCBs and even increases at some Arctic monitoring stations.[78,96] The simultaneous peak in environmental releases and the upper ocean reservoir of CB-153 and CB-180 suggest seasonal entrainment does not exert a major influence on surface and atmospheric concentrations of these congeners (Figure 1.4).

For CB-28, we find an upper ocean response lag of ten years and a short half-life against evasion (2 months) in ocean surface mixed layer (Figure 1.3, 1.4 and 1.6). Vertical transport contributes similar amounts of CB-28 (9 Mg) and CB-153 (10 Mg) to the mixed layer (upper 55m). However, the ratio of inputs to losses of CB-153 (1.0) in the mixed layer is less than half that of CB-28 (2.5), mainly due to rapid particle-associated removal and downward vertical transport (Figure 1.3). Thus, model results suggest in ocean basins with significant evasion, such as the Arctic, North Pacific and Atlantic Oceans, the subsurface PCB reservoir is a potential source of more volatile congeners to the atmosphere. Our findings show that differing meteorological conditions between basins drive removal of lighter molecular weight congeners indicating they will be affected more strongly by climate-driven changes to ocean biogeochemistry.

Figure 1.6 ***(following page)*****:** Relative importance of different input (panel a) and loss (panel b) processes for PCBs across ocean basins and congeners. Modeled mass flows of PCBs for 2015 are normalized to the magnitude of the dominant process to illustrate their relative importance for each congener. Polygons with small, pointed areas indicate a single dominant removal process. Part. sinking denotes sinking sorbed to particles at 1000 m. Hor. transport denotes net horizontal advective and diffusive transport. Vert. transport denotes gross vertical advective and diffusive transport at 1000 m.

Figure 1.6: (continued)

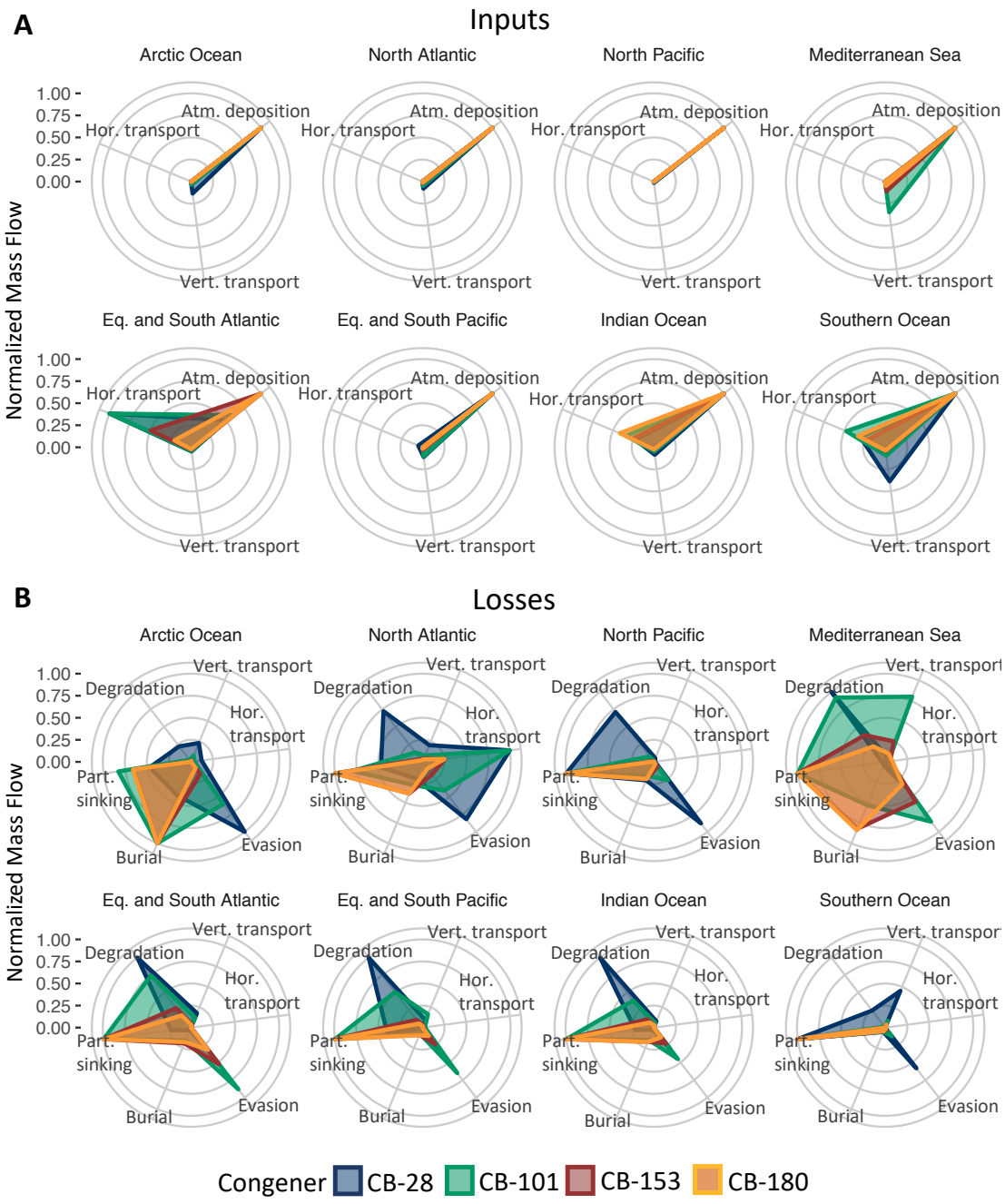

1.3.4 Climate-driven changes in the Arctic Ocean

In the Arctic, global temperature anomalies are two times higher than the global average.[97] In 2017, September sea ice extent was 25% lower than the 1981-2010 average, reflecting changes in atmospheric circulation, weakened Atlantic Meridional Overturning Circulation and increased poleward heat transport.[47,48,97,162,163,186] We examined the impacts of such rapid changes on PCB cycling in the Arctic Ocean by forcing the model with the ERA-Interim re-analysis fields that capture changes in temperature, sea-ice cover, and ocean circulation observed in the Arctic Ocean between 1992-2015.[62]

Figure 1.7 shows modeled differences in 2015 seawater PCB concentrations due to variability in ocean circulation and sea-ice cover between 1992-2015 compared to a baseline simulation with constant ocean state conditions (1992-1996). Results show changes in ocean conditions resulted in a decline in CB-28 seawater concentrations by an additional 54% compared to the constant meteorology scenario. In contrast, model results show an increase in concentrations of CB-153 in Arctic

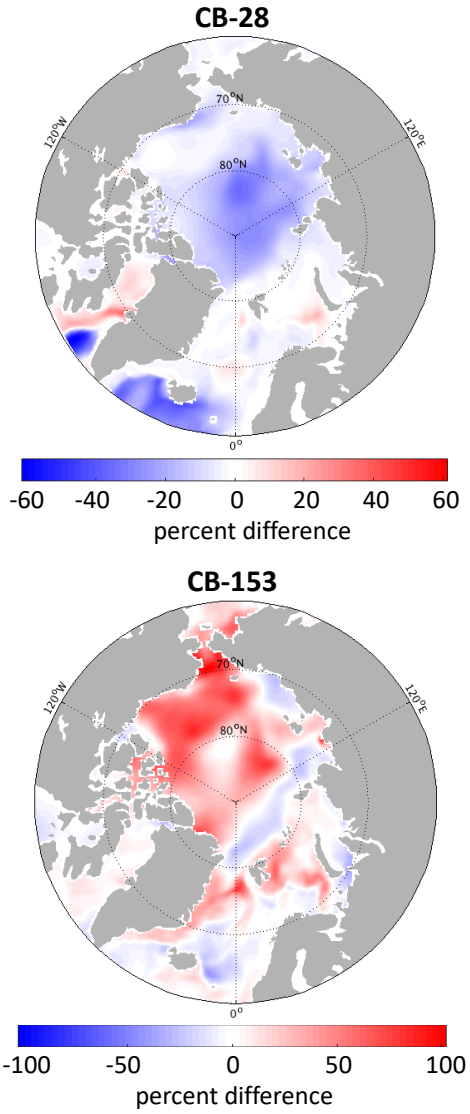

Figure 1.7: Modeled differences in PCB concentrations in the Arctic Ocean simulated using 1992-2015 meteorology, ice cover, and ocean circulation relative to base results using constant 1992-1996 conditions. Upper panel shows results for CB-28 and lower panel shows CB-153.

surface seawater relative to the constant climate scenario. Differences in the directionality of changes in PCB concentrations between congeners reflect their contrasting sensitivity to physical/chemical processes. CB-28 is much more volatile and thus ice-free waters and longer seasonal ice-free periods resulted in greater losses through increased evasion (41% change) and degradation (28% change) using the 1992-2015 climatology. The net increase in mean 2015 CB-153 concentrations with varying meteorological conditions relative to the constant climate scenario was small in our simulation (0.0004 pg L^{-1} or 1%). Larger increases of up to 100%, or 0.06 pg L^{-1} were apparent in the areas with greatest sea-ice cover retreat such as the Canadian Basin, the East Greenland Rift Basin and on the Barents shelf (Figure 1.7).

CB-153 has a greater propensity for binding to particles leading to greater stability and retention in the surface ocean. Thus, declining sea-ice cover in the Arctic Ocean resulted in a net increase in atmospheric deposition and overall increase in seawater concentrations in some regions. Such patterns are consistent with observed increases and stabilization in biotic concentrations in the Arctic. For example, data from 358 time-series covering Arctic mussels, marine fish, seals and polar bears suggest that the annual rate of decline in CB-153 concentrations in biota was reduced from 3.7% in the 1980s and 1990s to 2.5% after 2000.[8] Arctic sea-ice cover is projected to retreat 60% in the coming decades and mean fall temperatures may increase by as much as 13°C by the end of the 21st century.[97] This is likely to further increase evasion of more volatile congeners. Extended seasonally ice-free waters and associated increases in light availability increased ocean productivity in the Barents Sea and the Eurasian Arctic between 2003-2017.[163] Melting of permafrost is expected to increase riverine inputs of labile DOC to the Arctic Ocean.[153] Satellite data suggest that net primary productivity increased by 20% between 1998-2009 and may reach 730 Tg C yr^{-1} in an ice-free Arctic.[12] Increases in particle-associated removal in a more productive ocean may attenuate any increases in atmospheric deposition of higher molecular weight congeners and ultimately reduce the residence times in the ocean of high molecular weight compounds. Our findings suggest that

changes in ocean biogeochemistry resulting from projected sea ice retreat, increasing surface temperatures, and changing ocean circulation will decrease concentrations of lighter molecular weight POPs and slow concentration declines of POPs with higher molecular weights. For PCBs, the large decline in emissions exerts the dominant influence on concentration trends. However, for neutral hydrophobic POPs with increasing production trends, such as organophosphate esters, changes in Arctic ecosystem properties may exert a much more pronounced pattern and result in differing trends among low and high molecular weight compounds. [118,190]

1.4 Summary and Conclusions

We developed a global ocean simulation for four PCB congeners between 1930 and 2015. PCB concentrations in the upper ocean have declined by over 90% since 1970, mainly due to declines in primary emissions and particle-associated removal from the water column. We estimate that burial in coastal and marine sediment accounts for cumulative removal of approximately 75% of the PCBs released to the atmosphere since 1930. In 2015, the global ocean reservoir of the four PCBs modeled in this study was equivalent to 6% of releases since 1930, with only 2% in the upper ocean above 1000 m. The slowest decline in seawater PCB concentrations has occurred among the lightest molecular weight congeners, resulting in an increase in their proportion in the upper ocean reservoir in recent years. The enormous lack of data in the Southern, South Pacific, Indian, and South Atlantic Oceans highlights critical research needs for the future. Biogeochemical processes driving PCB inputs and losses vary among basins and by congener. Atmospheric deposition is the most important input source for the surface ocean. Model results suggest 56% of global deposition was located in the North Atlantic and North Pacific basins in 2015. Lateral transport of legacy PCB pollution from the Northern Hemisphere to the Southern Hemisphere oceans through thermohaline circulation has become increasingly important in recent years, particularly for the Equatorial and

South Atlantic Ocean. For the higher molecular weight PCB congeners, particle-associated removal dominates losses across all basins but a combination of evasion, degradation, particle settling and lateral transport is important for the lighter molecular weight congener removal. For the lighter molecular weight congeners, basin-specific biogeochemical conditions such as high winds in the North Atlantic determine the major loss processes, suggesting the importance of future climate-driven changes in the global oceans for the fate of many anthropogenic pollutants. Differences among high and low molecular weight PCB congeners observed in this study may be more pronounced for neutral hydrophobic POPs with stable or increasing emissions. Increases in seawater temperature, changes in circulation and reductions in sea-ice cover between 1992 and 2015 in the Arctic Ocean increased evasion of the lowest molecular weight PCB (CB-28). A small increase in net deposition to the surface ocean occurred for CB-153 due to sorption to particles and thus greater stability in seawater. Continued declines in sea-ice cover and increases in seawater temperature are projected for the next several decades.[97] Thus, increases in Arctic seawater concentrations of some persistent pollutants (e.g. CB-153) and neutral POPs with high Kow (>7.3 in this study), but decreases for more volatile compounds (e.g. CB-28), may be expected. Potential climate-driven mobilization of legacy POP reservoirs in permafrost, glaciers and sea-ice should also be considered.[7]

Further publication of this work

Ma, Y., Adelman, D. A., Bauerfeind, E., Cabrerizo, A., McDonough, C.A., Muir, D., Soltwedel, T., Sun, C. Sunderland, E. M., **Wagner, C. C.**, and Lohmann, R. (2018). Concentrations and water mass transport of legacy POPs in the Arctic Ocean. *Geophysical Research Letters*, 45, 23, 12,972-12,981.

Lohmann, R., Markham, E., Klanova, J., Kukucka, P., Přibylová, P., Gong, X., Pockalny, R., Yanisheswki, T., **Wagner, C. C.**, & Sunderland, E. (2021). Trends of diverse POPs in air and water across the Western Atlantic Ocean: Strong gradients in the ocean, but not in the air. *Environmental Science & Technology (in press)*.

2

The fate of a forever chemical: A global 3-D model of the removal timescales for continental and atmospheric PFOS inputs in the ocean and transport by sea spray aerosol

2.1 Introduction

Per- and polyfluoroalkyl substances (PFAS) are aliphatic, highly fluorinated compounds that have been widely used in commerce and by industry since 1958.[27] PFAS exposures are associated with

immune suppression, metabolic disruption and certain cancers.[189] The extreme stability of the fluorine-carbon bond[176] in PFAS like perfluorooctane sulfonate (PFOS) has resulted in lay references to "forever chemicals." In reality, environmental PFAS releases contain abundant polyfluoroalkyl precursors that degrade into terminal compounds like PFOS.[201,202,200]The magnitude of precursors released to the environment, their relative importance compared to direct releases, and the overall timescales for PFAS cycling in the environment are highly uncertain. The ocean is thought to be the main terminal sink for PFAS.[215,216] Thus, understanding the timescales for PFAS contamination due to human activities relies on estimating the removal times from the ocean. Few environmental and biological measurements are available for most PFAS.[114,141] It is therefore essential to glean lessons from relatively well-studied PFAS like PFOS. Production of the parent chemical to PFOS (perfluorooctane sulfonyl fluoride: POSF) and POSF-based precursors (*x*FOSA/Es) that degrade into PFOS was voluntarily phased out by the main global manufacturer in North America between 2000-2002.[27] PFOS was added to the Stockholm Convention on Persistent Organic Pollutants (POPs) in 2009.[197] This decision stemmed in part from concern about high levels of PFOS in wildlife such as polar bears and marine mammals in remote environments, reflecting the propensity of PFOS to accumulate in food webs.[76] Biological PFOS concentrations are still increasing in some regions[114] and elevated PFOS concentrations in seawater and biota from coastal waters of China, Brazil and Australia suggest releases from these regions may be substantial.[130,144,193,225] Global production is thought to be much lower than peak values in the early 2000s,[200] but all prior studies have noted large uncertainty in emissions estimates for PFOS and POSF-based precursors.[9,154,200,223] Seawater PFAS measurements are too sparse for robust temporal trend analysis, even on a regional basis.[223] Most measurements are in coastal waters and lack of systematic sampling at fixed sites and interannual variability in concentrations means temporal trends summarized in past work are qualitative in nature.[141] Thus, prior studies have relied on modeling analyses forced by reconstructed time-resolved environmental releases.[9,200]

Early box modeling efforts forced by ground-up inventories for PFOS and POSF-based precursors suggested PFOS concentrations would decline slowly following the phase out of POSF production and PFOS precursor concentrations would decline rapidly.[9] Past modeling studies have suggested atmospheric inputs of POSF-based precursors to the ocean are a small fraction of direct continental releases but simulated concentrations in seawater were underpredicted relative to observations.[9,200] Recent work has shown that sea spray aerosol (SSA) transport at the ocean surface may be an important atmospheric transport mechanism that was previously overlooked.[103]

The main objective of this work is to better understand the timescales of PFOS removal from the ocean as the terminal sink for anthropogenic contamination. As part of this analysis, we examine the cumulative importance of different continental PFOS source regions to the ocean compared to atmospheric deposition using a global modeling analysis. We present new data on PFOS seawater concentrations in undersampled regions of North Pacific and Atlantic Oceans between 2017-2018 and use a synthesis of all available seawater PFOS measurements to provide a statistically optimized estimate of total ocean inputs using Bayesian inference. We use the model to examine the contemporary (ca. 2015) reservoir of PFOS in the ocean and the magnitudes of various removal pathways, including SSA transport. Our findings provide novel insights into the expected timescales of legacy PFAS contamination in the global environment.

2.2 Methods

2.2.1 Continental PFOS releases to the ocean.

Uncertainty in emissions estimates for PFOS and POSF-based precursors has hampered previous attempts to model global accumulation and cycling in the oceans. For example, bottom-up global release estimates between 1958-2015 constructed by Wang et al. (2017) were 1228-4930 tonnes for PFOS and 12230-8738 tonnes for *x*FOSA/Es. No global inventory for inputs to marine ecosystems

is available. To address this gap, we extended the approach for estimating continental PFOS releases from North America and Europe from Zhang et al. (2017) to Japan, Australia, China, and Brazil. We follow the same general approach for estimating releases as described in earlier inventories. Measured PFOS discharge rates (concentration × volumetric water discharge) in rivers or wastewater treatment plants (WWTPs) were compiled for a baseline year with the most abundant observational record.[223,71,143] We used population within a river watershed or population served by WWTPs to derive power regression relationships with PFOS discharge.[157,223] Power regression relationships for each region (Figure B.1) were used to estimate discharges from regional WWTP and river catchments databases. Catchment boundaries from the HydroBASINS database were used to spatially allocate estimated PFOS discharges to corresponding rivers discharging into the ocean.[116] Releases for the baseline year were scaled by relative changes in regionally resolved releases to water from Wang et al. (2017) to create a spatially resolved historical release inventory from 1958-2015. For each region, uncertainty bounds for releases were estimated from 95% confidence intervals around the mean of coefficients in the power regression relationships. In Brazil, most PFOS releases originate from agricultural run-off from direct application to soil of ant baits containing EtFOSA rather than wastewater treatment plants.[130,129,157,223] Therefore, we calculated spatially resolved EtFOSA application rates to agricultural land based on 2014 sales data by province and GlobCover land use data.[58,130,129,138] We assumed a mean conversion rate of EtFOSA to PFOS of 4% and 30% conversion representing one $\log_{10}$-standard deviation around the mean.[130,129,138]

2.2.2 Atmospheric inputs of POSF-based precursors to the ocean

The GEOS-Chem atmospheric chemistry transport model was used to simulate atmospheric PFOS deposition to the ocean from oxidation of POSF-based precursors (*x*FOSA/Es) initiated by hydroxyl radicals,[136,9] building on the atmospheric PFAS simulation that is described in detail in Thackray et al. (2020). We estimated annual releases of *x*FOSE precursors to the atmosphere from

POSF-based products and *x*FOSA releases to air from the application of sulfuramide in Brazil based on estimates provided in Wang et al. (2017) and Löfstedt Gilljam et al. (2016b). Following previous work, we estimated *x*FOSE releases of 2% of global PFOS production in North America, Europe and Japan with an uncertainty bound of 0.3-11%, following procedures outlined in Wang et al. (2017). We assumed 10% emissions to air following the application of EtFOSA and log-normally distributed uncertainty bounds of 0-100% as up to 80% of EtFOSA applied to soil may ultimately volatize to air.[200] Emissions were uniformly distributed across populated areas. We neglected xFOSA emissions from POSF production and use because they accounted for less than 2 percent of *x*FOSE/As used in products.[200]

2.2.3 New seawater PFAS concentration data

We collected seawater samples from the North Atlantic Ocean between March 31 and April 4, 2017 on board the R/V Endeavor, and in the North Pacific Ocean on board the R/V Exxpedition between June 30 and July 10, 2018. In the North Atlantic, we collected vertical profiles from the surface up to 4151 m depth from seven stations using a CTD-Niskin bottles rosette array (n=36). Sites occupied were located between the Eastern Shore of North Carolina and Fort Lauderdale, Florida (34 11.82°N, 76 24.67°W -27 32.93°N, 79 52.12°W; Figure 2.1 and Table B.3). In the North Pacific, we collected surface samples (depth = 8 m) at 10 stations using HDPE bottles between North America (Washington State, USA) and the Central North Pacific (45 37.31°N, 133 04.74°W –32 01.12°N, 152 32.12°W). Samples were analyzed for suite of 25 PFAS at Harvard University following previously published extraction procedures and analytical methods that are summarized in the SI Section B.0.1.[223] Details of the cruises, including sampling locations and depths, measured PFAS concentrations, detection limits and recoveries are provided in the SI (Table B.3 and Section B.0.1).

2.2.4 Synthesis of existing PFOS seawater observations

We compiled global seawater measurements collected in the open ocean between 2002-2015. Data from locations with water depths <200 m were not included in model evaluation because local sources and fine scale circulation patterns make global model simulations unreliable in these regions. We imputed values for non-detects using robust regression on order statistics (ROS).[93] We excluded data from one sampling campaign identified to have anomalous variance (paired t-test, p-value<0.05). The final dataset contains 540 measurements from eight ocean basins.[3,4,15,25,29,30,192,207,214,215,216,217,218,222,226] Most (76%) were from the surface ocean (above 55 m, n=403) and less than 10% of measurements were from below 1000 m (n=44).

2.2.5 Model description and updates

We extended the PFOS simulation embedded in a 3-D ocean circulation model (the MITgcm)[223] to the global domain as part of this study. The model simulates transport of ionic, neutral and particle bound PFOS with ocean circulation, mixing, diffusion and particle settling. Recent work has shown that SSA transport at the ocean surface may be an important transport mechanism that was previously overlooked.[103] Production of SSA results from wind-driven entrainment of air into the ocean's surface creating air bubbles that burst at the sea surface. SSA are abundant in the marine boundary layer and the surfactant properties of PFAS lead to large enrichment in the aerosol relative to the aqueous phase. For example, one study in the Southern Ocean observed PFAS 522-4690-fold enrichment compared to seawater concentrations.[32] These data are consistent with laboratory experiments showing a several thousand-fold PFAS enrichment in SSA relative to seawater[103] emphasizing the need to incorporate SSA transport into modeling of oceanic PFAS cycling. We implemented a new source function for SSA for three modal diameters of aerosols based on Salter et al. (2015, Table B.1). The SSA flux follows a cubic function of wind and sea surface temperature.

We apply SSA enrichment factors for PFOS relative to Na observed experimentally to calculate the PFOS flux (Table B.2).[103] Wind driven aerosol transport is simulated using a pseudo-first order advective transport scheme, followed by deposition after an average residence time of the three aerosol modes based on prior work.[165]

2.2.6 Bayesian inference for optimizing inputs to the ocean

The PFOS simulation is initialized by assuming negligible concentrations in seawater prior to human releases beginning in 1958. It is forced with time dependent riverine discharges and atmospheric deposition of PFOS between 1958-2015. We used uncertainty in continental discharge and atmospheric deposition estimates and the synthesis of observed seawater concentrations, described above, to develop a statistical best estimate of ocean inputs. Specifically, we developed a statistical prior by using distributions for PFOS ocean inputs from rivers and atmospheric deposition and the range of possible global releases reported in Wang et al. (2017, 1228-4930 Mg). We applied Bayesian inference to solve for the release rate within this uncertainty range that best explained seawater observations (minimized the least-squares of the log difference between measured and modeled ocean concentrations) given the transport and mixing simulated using the MITgcm. We used an iterative sequence of proposed scaling factors for each input region using Metropolis Hastings Markov Chain Monte Carlo (MCMC) simulations. We implemented the MCMC model using the mcmc package in *R*. A complete description of the modeling is provided in the SI (Section B.0.2).

2.3 Results and Discussion

2.3.1 PFOS most detected PFAS in new seawater measurements

Of the 25 targeted analytes, PFOS was most detected PFAS in the seawater samples collected in the North Atlantic and Pacific Oceans in 2017 and 2018 (98 % detection frequency, Figure 2.1). PFOA

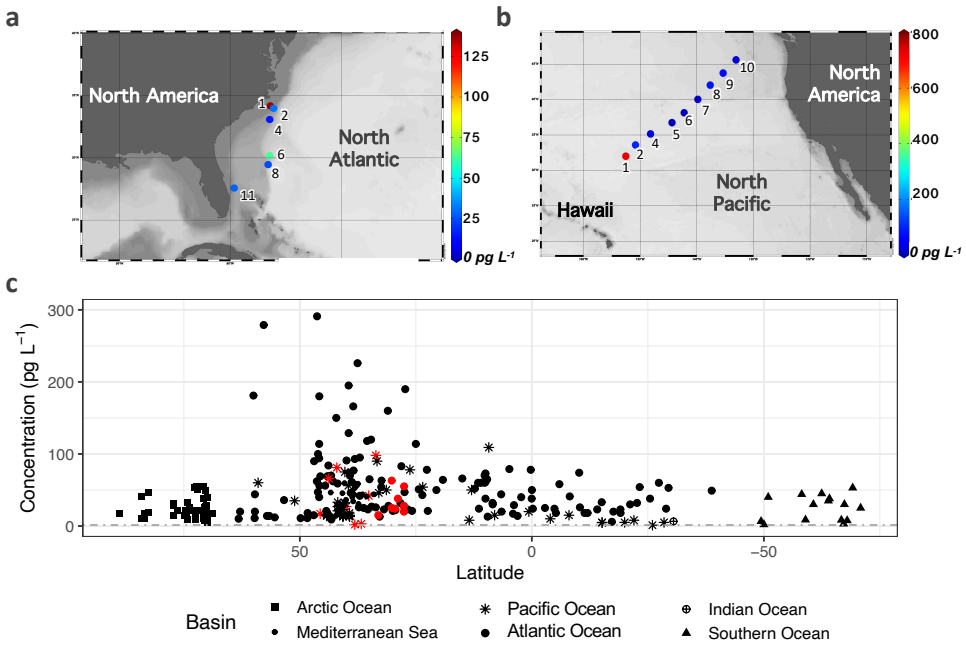

Figure 2.1: Measured PFOS concentrations in seawater collected: a) for this study on the R/V Endeavor in the North Atlantic in 2017, b) for this study on the R/V Exxpedition in the North Pacific in 2018, and c) compiled from the literature for all open ocean measurements collected between 2002-2015. Red marks denote samples collected in this study. The horizonal line on panel (c) indicates the Method Detection Limit (MDL) of 1.4 pg L^{-1} for the sum of linear and branched PFOS from this study. One high value of 732 pg L^{-1} was omitted for clarity in panel (c).

was detectable in 68% of the samples, followed by PFNA (60% detection), PFHpA (47% detection) and 6:2 FTS (43% detection) Figure 2.1, Table B.3). All other PFAS were detected in <20% of the samples.

In the North Atlantic, PFOS concentrations ranged between 9-137 pg L^{-1} with geometric mean of 24 pg L^{-1} (Figure 2.1). This is comparable to previous sampling campaigns in the North Atlantic (22 pg L^{-1}, <MDL-514 pg L^{-1}, Figure 2.2, Mann-Whitney U test; p-value=0.9) and suggests that concentrations outside major source areas in the North Atlantic are declining slowly.[114,142,141] Vertical profiles showed higher PFOS concentrations at the surface compared to subsurface waters (Figure B.2). By contrast, vertical profiles for PFOA mainly showed enrichment near the fluorescence maximum used as a proxy for productivity (Figure B.2). Compared to PFOA, PFOS has a higher

observed enrichment in experimentally generated SSA.[103] Enrichment in the ocean microlayer and SSA has been previously observed.[32,105] PFOS enrichment at the air-water interface may therefore reflect upward transport of dissolved PFOS by entrained air bubbles, and greater PFOS enrichment in SSA and associated retention in near surface waters compared to PFOA.

In the North Pacific Ocean, PFOS concentrations were in the same range as those observed in the North Atlantic (2-98 pg L^{-1}) in 9 of the 10 surface water sampling locations, and were comparable (geometric mean: 33 pg L^{-1}) to previous North Pacific sampling campaigns (11 pg L^{-1}, <MDL-90 pg L^{-1}, Mann-Whitney U test; *p*-value=0.1, Figure 2.2). One offshore sample approaching Hawaii was an outlier for both PFOS (732 pg L^{-1}, inter-quartile range criterion (IQR)) and PFOA (785 pg L^{-1}, IQR). PFOA-to-PFOS ratios are sometimes used to indicate the approximate magnitude of atmospheric deposition because a greater number of volatile precursors degrade into PFOA as the terminal PFAS compared to PFOS.[38,172,219] In the North Pacific, PFOA concentrations were consistently greater than PFOS, except at one station (Station 2, Figure 2.1). PFOA and PFOS concentrations were similar at the anomalously high station, but PFOA-to-PFOS ratios were greater in most of the remaining samples (2.9, 0.4-5.4). This is suggestive of atmospheric inputs as a contributing source to background levels in the open ocean.

2.3.2 Global distribution of PFOS in the surface mixed layer of the ocean.

Our synthesis of global open ocean seawater measurements in the surface mixed layer (Figure 2.1C) shows a pronounced enrichment in PFOS concentrations between 20°N-60°N. Sampling stations with a bathymetry of less than 200 m were excluded to ensure concentrations reflected those in the offshore ocean. Between 20°N-60°N in the Atlantic Ocean, the geometric mean concentration (22 pg L^{-1}, range <MDL-291 pg L^{-1}) is significantly higher than concentrations North of 60°N (7 pg L^{-1}, range:<MDL-39 pg L^{-1}, Arctic and North Atlantic Oceans, Mann-Whitney U test; *p*-value«0.01) and south of 20°N (16 pg L^{-1}; South Atlantic and Southern Ocean, Mann-

Whitney U test; p-value <0.05, Figure B.2A). Similarly, concentrations are elevated in the mid-latitude North Pacific Ocean (26 pg L^{-1}, range:<MDL-765 pg L^{-1}) compared to below 20°N (7 pg L^{-1}, range:<MDL- pg L^{-1}, Mann-Whitney U test; p-value<0.01) and above 60°N (14 pg L^{-1}, range:<MDL-109 pg L^{-1}, Mann-Whitney U test; p-value<0.01). This pattern is consistent with large riverine discharges of PFOS in North America and Asia that occur next to mid-latitudes source regions and offshore currents such as the Gulf Stream in the North Atlantic and the Oyashio and Kuroshio currents in the North Pacific.

In the polar oceans, PFOS concentrations are more uniform (Figure 2.2c). For example, the geometric mean concentration in the Southern Ocean (6 pg L^{-1}, range:<MDL-53 pg L^{-1}) is comparable to the Arctic Ocean (9 pg L^{-1}, range:<MDL-55 pg L^{-1}) even though water from the North Atlantic requires 50-700 years to reach the Antarctic shore. PFOS precursors (xFOSE/As) have been detected in air above the Southern Ocean and the Arctic Ocean.[5,49,184,199,213] providing evidence for atmospheric transport of precursor substances as a source of PFOS to remote environments.

Figure 2.2 ***(following page)*****:** Optimized cumulative PFOS inputs to the global ocean (1958-2015) and simulated seawater concentrations based on inputs from rivers only (panels a and c), and combined inputs from rivers and atmospheric deposition (panels b and d). In panels (c) and (d), measurements between 2002 and 2015 are shown as circles. Background color shows modeled 5-year average seawater concentrations around the median year of observations (2008). Errorbars in panels (a) and (d) show 90^{th} percentiles around the median based on Markov Chain Monte Carlo (MCMC) Bayesian inference.

Figure 2.2: (continued)

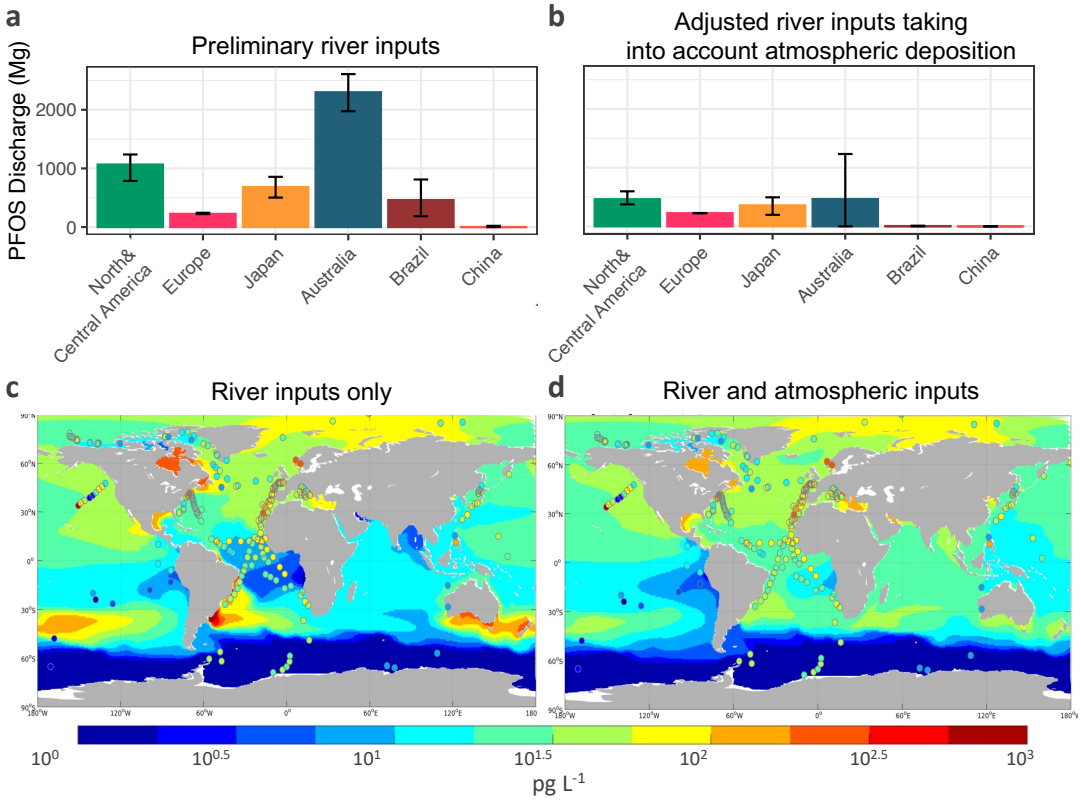

2.3.3 Cumulative PFOS inputs to the ocean (1958-2015)

Modeled open ocean seawater PFOS concentrations based on both rivers and atmospheric deposition (Figure 2.2b, d) better reproduce the magnitude and spatial patterns of open ocean observations (Figure 2.2c, d) than river discharges only. For example, modeled median concentrations in the Equatorial and South Atlantic with both riverine and atmospheric inputs (23 pg L^{-1}, 90^{th} percentile confidence intervals (CIs): 0-41 pg L^{-1}) fall within the range of observations (18 pg L^{-1}, 90^{th} percentile CIs: 2-73 pg L^{-1}) but are biased low (7 pg L^{-1}, 90^{th} percentile CIs: 0-48 pg L^{-1}) when only riverine inputs are considered. Modeled median concentrations for the North Atlantic (38 pg L^{-1}, 90^{th} percentile CIs: 1-50 pg L^{-1}) agree well with our measurements from 2017 (25 pg L^{-1}, range 11-139 pg L^{-1} and the synthesis of precious observations (22 pg L^{-1}, 90^{th} percentile CIs: <MDL-514 pg L^{-1}). Cumulative PFOS discharges from Australia proposed in the optimization that only considers riverine discharges are implausibly high (2000-2600 Mg) because the majority (80%) of POSF production occurred in the United States and other known manufacturing sites are located in Italy, Japan and China.[200] We therefore focus our analysis on the simulation that includes inputs from both atmospheric and riverine sources.

Cumulative riverine discharges from Australia in the optimization that includes atmospheric deposition are smaller but still uncertain (90^{th} percent CIs: 1-1200 Mg; Figure 2.2b). Measured PFOS concentrations in Australian WWTP effluents (130 ng L^{-1}) are an order of magnitude higher than those measured in the late 2000s in North America and higher than those measured in wastewater treatment plants in China.[36,223] The lower 90^{th} percentile confidence interval (1 Mg) may be a more realistic estimate of discharges from Australia based on historical production estimates[200] but additional riverine and seawater measurements are needed to constrain the optimization for PFOS inputs performed in this study.

For other regions, the optimization that includes atmospheric inputs reduces uncertainty in the

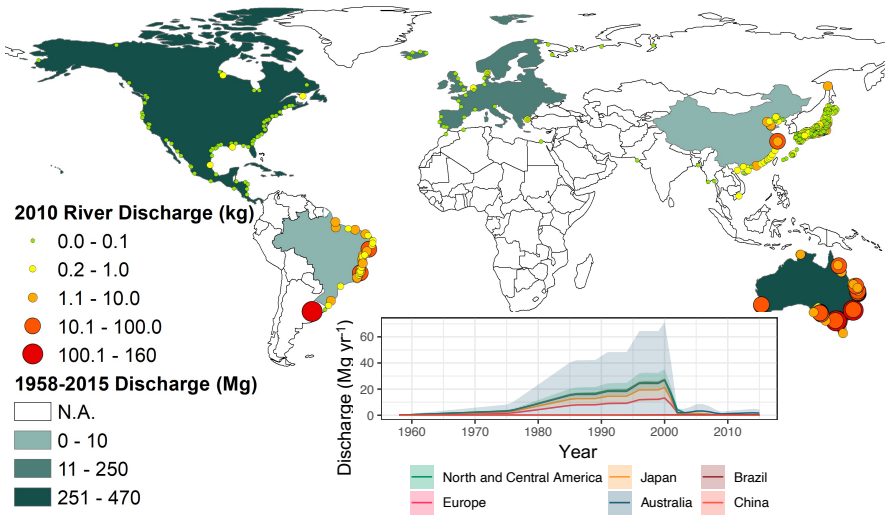

Figure 2.3: Historical and annual river discharges to the ocean. Results of optimized PFOS discharges from rivers based on Bayesian Inference that includes atmospheric deposition (Figure 2.2b). Contemporary (ca. 2010) discharges are shown as filled circles. Colors of source regions indicate the relative magnitudes of cumulative historical discharges (1958-2015). The inserted panel shows the temporal trajectory of riverine releases and shaded areas indicate 90^{th} percentile confidence interval around the median estimate.

riverine discharges to the ocean. The 90^{th} percentile confidence interval for cumulative riverine discharges between 1958-2015 is 370-600 Mg for North and Central America and 220-230 Mg for Europe but uncertainty is higher for Japan (200-500 Mg). The 90^{th} percentile confidence intervals indicate cumulative releases from Brazil (2-11 Mg) and China (0-3 Mg) are relatively small compared to North America and Europe (Figure 2.2). This is not surprising because Brazil and China only began producing PFOS in the late 1980s, compared to the 1950s in North America. [120,130]

2.3.4 Contemporary riverine PFOS discharges

Contemporary (ca. 2010) PFOS discharges from rivers in Brazil (300 kg), China (36 kg) and Australia (1300 kg) represent the major ongoing global source regions to the ocean (97%, Figure 2.3). Australian inputs are highly uncertain due to lack of monitoring data for rivers and adjacent marine regions, as discussed above. The Korean Peninsula and Japanese archipelago provide physi-

cal barriers that prevent much of the pollution from large Asian rivers from reaching the offshore North Pacific, which is instead retained in coastal and shelf regions.[224] This land barrier for offshore transport helps to explain the relatively low PFOS concentrations in the offshore western North Pacific Ocean offshore compared to highly contaminated coastal regions (Figure 2.2d).[142] High PFOS concentrations (ng L^{-1} range) have been reported in the rivers and coastal regions of both China[151,225,227] and Brazil[130,144]. Offshore of Brazil, riverine discharges result in elevated PFOS concentrations along the coast and south of 20°S that are transported with the South Brazil current that turns east at the Rio de la Plata. This circulation pattern is inconsistent with the full extent of elevated seawater concentrations in the South Atlantic.[15,79,6] PFOS precursors have been measured in air and water across the South Atlantic,[3,15,49] suggesting atmospheric inputs from degradation of EtFOSA are another important source.

2.3.5 Atmospheric inputs to the ocean

Results of our simulation suggest large atmospheric PFOS inputs to the open ocean, especially in the Southern Hemisphere (Figure 2.4a). For example, preliminary modeling suggests atmospheric inputs account for more than 90% of the PFOS in the contemporary surface mixed layer of the Indian and Southern Ocean (ca. 2015). Large historical river inputs and a comparatively small surface area of the North Atlantic Ocean mean atmospheric sources account for a smaller fraction in this basin. In the South Atlantic, modeled inputs from the degradation of *x*FOSE/As contribute 77% of the surface mixed layer PFOS reservoir. Degradation of EtFOSA released from sulfuramide application is estimated to contribute 17% of the PFOS deposited to the South Atlantic (80 Mg, 1958-2015).

The dominant role of atmospheric inputs for surface concentrations in remote ocean basins is supported by past observations. For example, detectable levels of PFOS that have been reported in the Southern Ocean before 2007.[207] However, the Antarctic Circumpolar Current (ACC) acts as a

barrier for surface transport from northern latitudes. PFOS discharges to the North Atlantic could not have reached the Southern Ocean over the time scales relevant to PFAS production because deep water from the North Atlantic takes at least 50 years to upwell in the Antarctic Polar Front Zone.[100,181] This is supported by the observation of detectable levels of PFAS in marine species foraging in the ACC but not in those foraging in upwelling zones of North Atlantic Deep Water south of the ACC.[14] A constant diffusive atmospheric source from populated areas in South America and Southern Africa has been suggested as the source of elevated atmospheric (*x*)FOSA/Es in the polar cell.[49,199] The reaction of sulfonamidoethanols with OH is approximately 5-fold faster than for fluorotelomer alcohols suggesting it may yield PFOS more efficiently,[57,136] and underscores the overlooked role of atmospheric PFOS sources.

2.3.6 Atmospheric transport with sea spray aerosols (SSA).

Model results suggest global PFOS transport with SSA leads to lower seawater concentrations in the surface mixed layer of the ocean due to transport and deposition in coastal land areas (Figure 2.4b). SSA enrichment is linearly related to surface water concentrations.[103,171] Thus, the highest SSA emissions occur in the mid-latitude regions of the North Atlantic and the North Pacific Oceans where seawater concentrations are enriched (Figure B.3a; Figure 2.1d). Greater land mass in the Northern Hemisphere compared to the Southern Hemisphere leads to higher terrestrial PFOS deposition. Only 59% of SSA emissions in the Northern Hemisphere are redeposited on to the ocean (net loss of 5 Mg, ca. 2015), whereas 90% of emissions with SSA resettle on the ocean in the Southern Hemisphere (net loss of 2 Mg). SSA increases mixed layer PFOS concentrations in the Southern Ocean and other ocean convergence zones like the Equatorial Pacific. Simulated transport with SSA aerosol doubles surface water PFOS concentrations in some regions of the Southern Ocean (Figure 2.4b), reinforcing the importance of SSA for observed PFAS distributions in seawater.

Figure 2.4 *(following page)*: Panel (a) shows the modeled contribution of atmospheric deposition as a fraction of total inputs to the surface mixed layer of the ocean (ca. 2015). Panel (b) shows contributions to concentrations in the surface mixed layer of the ocean (ca. 2015, above 55 m) from sea spray aerosol (SSA) inputs. In panel (b), red indicates an increase and blue indicates a relative decrease in seawater concentrations due to transport with SSA.

Figure 2.4: (continued)

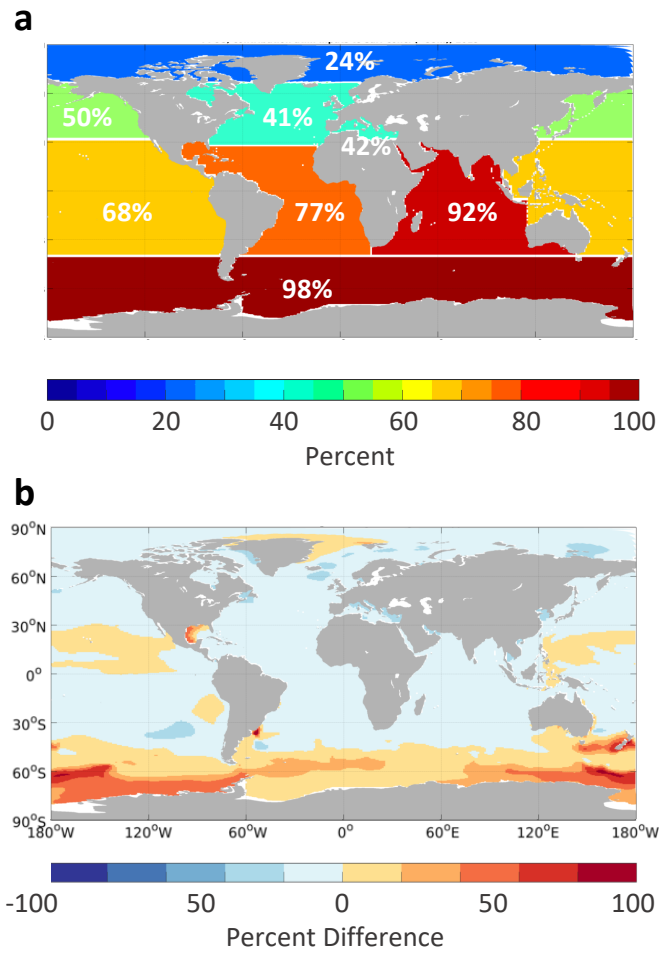

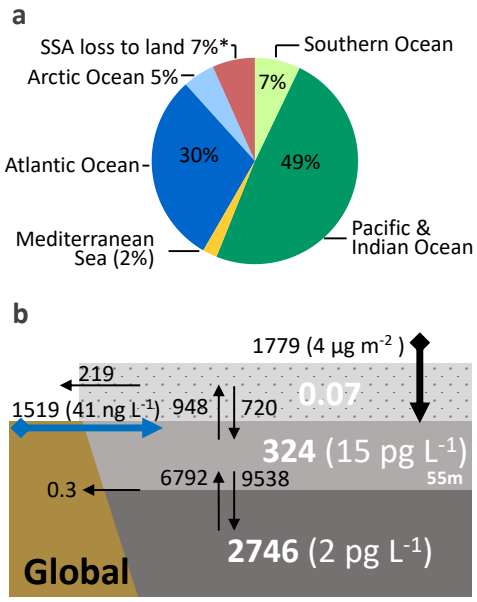

Figure 2.5: Modeled fate of PFOS released to the ocean between 1958 and 2015. Model estimated cumulative burial in ocean sediment is 0.3 Mg. Panel (b) shows the cumulative global ocean budget for 1958-2015, with reservoirs for 2015 and average concentrations indicated in brackets. Total deposition fluxes are based on the total surface area of the ocean in the MITgcm. Total riverine fluxes are cumulative (1958-2015) and based on global freshwater discharge. Superscripted asterisk (*) indicates that loss with sea spray aerosol to land is based on the difference between sea spray aerosol emission and deposition fluxes.

2.3.7 Global PFOS budget.

The global budget for PFOS in the ocean (Figure 2.5, ca. 2015) suggests less than 0.01% of the cumulative global PFOS releases have been buried in marine sediment (0.3 Mg). Sediment burial represents the major terminal sink for anthropogenic PFOS releases to the global environment. This corresponds to a half-life of PFOS against burial in the ocean since the onset of production of more than 300,000 years. Atmospheric modeling and our inventory of PFOS discharges from rivers to the ocean suggest 3300 Mg (2600-4100 Mg) of PFOS has entered the global oceans since 1958. The majority is still present in the ocean (93%, Figure 2.5), with 12% in the surface mixed layer that is most relevant to biological exposures. The Pacific and Indian Oceans contain half of the cumulative

ocean inputs (1600 Mg). The Atlantic Ocean contains 30% of cumulative ocean inputs (990 Mg) but has relatively higher concentrations in the surface mixed layer due to its much smaller volume compared to the Indian and Pacific Oceans. The remaining 10% of discharges have been distributed between the Southern Ocean (230 Mg), the Arctic (160 Mg) and the Mediterranean Sea (75 Mg). We find that 7% of PFOS that has entered the oceans has been deposited over land with SSA (230 Mg). While transport back to the ocean may be slow,[26] this PFOS will eventually reenter the ocean with run-off and has not been permanently sequestered.

Ocean modeling suggests that there has been substantial exchange between the surface mixed layer of the ocean and subsurface waters. Vertical advection and diffusion has cumulatively transported 2700 Mg PFOS to the subsurface ocean, but much of this removal is returned through upwelling waters and entrainment/detrainment of the mixed layer. Average apparent upwelling rates between 1958-2015 of 120 Mg yr^{-1} (or 4% of the subsurface ocean reservoir) imply that the subsurface ocean will replenish the surface ocean for decades after inputs cease. Emissions of PFOS with SSA represents another important removal mechanism for the surface ocean (950 Mg, 1958-2015). We estimate that 76% of PFOS in SSA are redeposited to the ocean surface, with the remaining 24% deposited to coastal terrestrial regions.

Previous work that has shown that ocean circulation is a major driver of declining surface seawater concentrations in the Atlantic Ocean.[223] We similarly find it is the dominant transport process globally. In addition, processes associated with SSA transport help retain PFOS in the surface ocean and provide an important source PFOS to coastal regions. The ocean has long been identified as a legacy source of semi-volatile pollutants, like polychlorinated biphenyls (PCBs), extending their lifetime in the global environment.[125,221] In the case of PFAS, SSA may play a similar role by extending their lifetime through greater retention in the surface ocean and transport to coastal environments.

2.4 Further publication of this work

Sunderland, E. M., Hu, X. D., Dassuncao, C., Tokranov, A.K., **Wagner, C. C.**, & G. Allen, J. G. (2018). A review of the pathways of human exposure to poly- and perfluoralkyl substances (PFASs) and present understanding of health effects. *Journal of Exposure Science & Environmental Epidemiology, 29, 131–147.*

Kwiatkowski, C. F., Andrews, D. Q., Birnbaum, L. S., Bruton, T. A., DeWitt, J. C., Knappe, D. R. U., Maffini, M. V., Miller, M. F., Pelch, K. E., Reade, A., Soehl, A., Trier, X., Venier, M., **Wagner, C. C.**, Wang, Z. & Blum, A. (2020). The Scientific Basis for Managing PFAS as a Chemical Class. *Environmental Science & Technology Global Perspectives, 7, 8, 532–543*

Joerss, H., Xie, Z., **Wagner, C. C.**, von Appen, W.-J., Sunderland, E. M. & Ebinghaus, R (2020). Transport of legacy perfluoroalkyl substances and the replacement compound HFPO-DA through the Atlantic Gateway to the Arctic Ocean – Is the Arctic a sink or a source? *Environmental Science & Technology, 54, 16, 9958–9967.*

Kwiatkowski, C. F., Andrews, D. Q., Birnbaum, L. S., Bruton, T. A., DeWitt, J. C., Knappe, D. R. U., Maffini, M. V., Miller, M. F., Pelch, K. E., Reade, A., Soehl, A., Trier, X., Venier, M., **Wagner, C. C.**, Wang, Z. & Blum, A. (2021). Response to "Comment on Scientific Basis for Managing PFAS as a Chemical Class". *Environmental Science & Technology Global Perspectives, 8, 2, 195-197.*

3

From global pollutants to community health: An integrated biogeochemical modeling and environmental monitoring framework to identify environmental drivers of PFOS exposure from whale consumption on the Faroe Islands

3.1 Introduction

Nine million premature deaths are attributed to pollution annually.[115] An important subset of pollutants that has been largely ignored in these calculations persist in the environment for decades and are potent neuro- or immune toxicants meaning that they cause chronic sub-clinical adverse health outcomes even at low level developmental exposure.[85] Already neurological disorders are the leading cause of disability worldwide.[59] International conventions on persistent pollutants aim to reduce the environmental burden of these pollutants, but the complexity of the human-environmental system have limited our ability to assess whether existing regulations are effective at protecting public

health.

The ocean is an important reservoir of persistent pollutants in that it not only accumulates these chemicals, but also performs an important role as solute for marine food webs. Fisheries are crucial for food security, nutrition and livelihoods. 3.2 billion people globally rely on fish for protein intake and 10% of the world's population depend on fisheries for income.[61]

Small-scale subsistence communities in the Arctic whose traditional diets include marine mammals are especially vulnerable to global pollutants. These communities are exposed to amplified environmental accumulation due to cold-trapping of pollutants released from North America and Europe in the Arctic.[173,205] Further, the consumption of high-trophic level wild foods is integral to their nutrition as well as their cultural identity.[33] This two-fold dependence aggravates the adverse impact of global pollutant releases when wild foods become too contaminated for consumption.[198]

On the Faroe Islands, the pilot whale hunt (Grindadràp) and subsistence consumption of whale meat and blubber has existed since the late 16^{th} century.[60] Discovery of elevated contamination of pilot whales with mercury and and associated health effects resulted in consumption advisories for pilot whale consumption. In 2012, Faroese health officials recommended to eliminate pilot whale consumption entirely.[210,208]

Poly- and perfluoroalkyl substances are present in every Faroese individual[210] and prospective cohort studies have associated elevated exposures to perfluorooctanoic sulfonate (PFOS) with suppressed antibody response to vaccinations.[80,83,84] At age 5, 44% of children had antibody levels below those clinically considered protective against diphtheria (0.1 IU mL^{-1}).[82] Consumption of pilot whale meat is an important exposure source of PFAS in the Faroese population and perfluorooctanoic sulfonate (PFOS) contributes more than 50% to PFAS concentrations in the marine food web of the Norwegian Sea.[91] One whale meal per 2 weeks increased PFOS concentrations by 25% in children.[210]

Biomonitoring of pilot whale in the Faroe Islands suggests both PFOS and its precursor perfluo-

rooctane sulfonamide (FOSA), which is enzymatically transformed to PFOS in humans contribute to observed PFAS levels in the marine food web.[45] Following the voluntary phase out of PFOS and its precursors by the main manufacturer, precursor concentration have decreased in polar regions while PFOS levels have remained elevated, and even increased in certain locations and marine organisms.[114,135,212] In marine food webs, biological concentrations reflect environmental exposures, food web structure and assimilation efficiency. For example, whales biotransform FOSA to PFOS only at low or negligible rates as a result of different toxicant metabolism mechanisms.[135,20,34,68,117] Further, water-breathing organisms, like squid, which are the primary diet of pilot whales[98], and their prey, eliminate PFAS more efficiently than air-breathing mammals like whales.[46,109] These species differences will likely modulate observed concentration trends in pilot whales and their prey.

Predicting the impact of regulating persistent pollutants on local contaminant exposures is complicated by the limited understanding of magnitude and spatial patterns of pollutant releases, nonlinearity of relevant biogeochemical transport processes, the variability in marine food webs and a need to account for local dietary preferences to predict human exposure. A particular problem arises when changing the scale of analysis from the global to the local scale. Sparse data in environmental media often preclude the detection of trends and models play an important role in closing data gaps based on mechanistic understanding of environmental-biological relationships. Here we present a case study that quantifies the impact of regulation on dietary PFOS exposure from whale meat in children in the Faroe Islands by linking global releases to local biomonitoring data and identifies key uncertainties. The present study demonstrates how global modeling can be leveraged to improve impact evaluations of regulations. This work builds on previous work presented in Dassuncao et al. (2017); Dassuncao et al. (2018) and Chapter 2.

3.2 Methods

3.2.1 Global releases and environmental concentrations

We reconstruct FOSA concentrations in seawater from cruise measurements and temporal deposition flux trends recorded in an ice-core from the Devon Ice Cap.[45,132] PFOS seawater concentrations in the North East Atlantic are from the PFOS simulation embedded in the MITgcm, which has been constrained using observed seawater concentrations collected between 2002-2015 using Bayesian inference (Chapter 2). We extended the food web model for the Faroe Islands presented in Dassuncao et al. (2017) to include phytoplankton, zooplankton, and fish consumed by squid. PFAS enrichment in phytoplankton was calculated based on particle-water partitioning.[11] PFAS concentrations in all other organisms were calculated using a revised version a bioaccumulation model adapted to describe the bioconcentration of ionic surfactants in fish,[10,11] which we extended to describe PFAS bioaccumulation in invertebrates and whales. We further update the model by including (2) empirically observed aqueous and dietary chemical transfer efficiencies from fish toxicokinetic studies, (3) blood proteins as an additional partitioning compartment, using partitioning coefficients from studies with bovine serum albumin, and (3) inhalation and exhalation pathways for whales. We model steady-state whole-body concentrations for all species except whales, for which we model time-dependent age cohorts following Dassuncao et al. (2017). Modeled whole body concentrations in whales are converted to muscle concentrations based on tissue-specific concentrations and muscle-to-whole body proportions.[40,42,45,44,140] Biotransformation from FOSA to PFOS does not appear to occur in whales, but has been observed in carp.[117,68,34] Biotransformation rates in squid (*Todarodes sagitatus*) or their prey (f.e. argentines or blue whiting) are unknown and may vary due to differing toxicant metabolisms involved in biotransformation.[128,164] We test the importance of FOSA biotransformation for observed PFOS concentrations in pilot whale by evaluating model performance with 0%, 5%, 20%, and 100% biotransformation of FOSA to PFOS in

fish.

3.2.2 Human exposure

We calculate the "avoided" exposure to PFOS from pilot whale consumption as a result of regulation using scenario analysis. The baseline scenario assumes continued pilot whale consumption at levels observed in whale consuming children in 1993 and increases in FOSA and PFOS concentrations extrapolated to 2015 based on observed increases between 1986-2002. Consumption rates are simulated from log-normally distributed consumption rates observed in Cohort 1 in 1993.[43] FOSA and PFOS concentrations between 2003-2015 are predicted based on linear regression analysis of whale concentrations between 1993-2003. Scenario 2 applies observed PFOS and FOSA concentrations in whale between 1976-2015 while holding pilot whale consumption fixed at 1993 levels. Finally, both variables are allowed to change following observed changes in PFOS and FOSA concentrations in pilot whale and consumption rates (scenario 3). The estimated avoided exposure is calculated as the difference in serum concentration between the scenarios. We compare serum concentration for the same age only as serum concentrations will be affected by maternal serum concentrations and growth and ingested contaminants accumulating over time. Human exposure to PFOS from whale meat is estimated using modeled ingestion rates of pilot whale based on Hg concentrations in hair among three Faroese birth cohorts and observed PFOS and FOSA concentrations in pilot whale between 1986-2015. Ingestion rates are calculated using the US Environmental Protection Agency's one-compartment toxicokinetic model for methylmercury follwoing preivously published work.[43] Methylmercury is a reliable proxy for fish consumption and repeated measurements of methylmercury concentrations in Faroese pilot whale showed no statistically significant changes over time.[146,188]

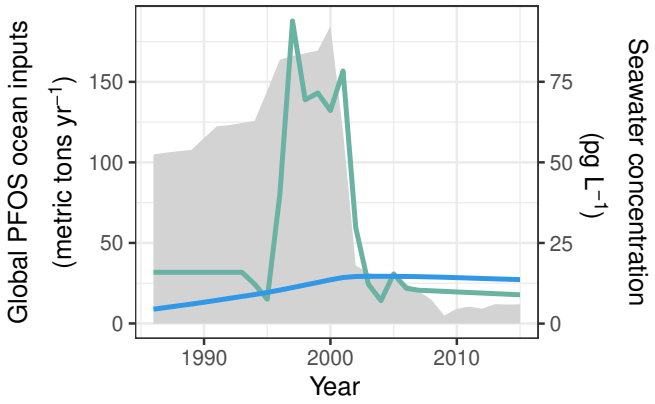

Figure 3.1: Global PFOS releases to the ocean and local modeled seawater concentrations of perfluorooctane sulfonamide (FOSA) and perfluorooctane sulfonate (PFOS) in the mixed layer of the North East Atlantic. FOSA concentrations are reconstructed from three cruise transects and deposition flux derived from the Devon ice cap, Nunavut, Canada. PFOS concentrations (above 100m) in the North East Atlantic are from the PFOS simulation embedded in the MITgcm that has been optimized using a global database of ocean observations.

PFOS serum concentrations attributable to pilot whale consumption are modeled based on the ingestion rates, temporal trends FOSA and PFOS concentrations in pilot whale, first-order elimination rates measured in retired fluorochemical factory workers (PFOS = 4.87 years) and 31% conversion of absorbed FOSA to PFOS, which has been established as a likely lower bound for humans in previous work.[135] PFOS and FOSA concentrations in pilot whale for each year from 1986-2015 were interpolated from observed concentrations using linear regression. A full model description is provided in Dassuncao et al. (2018).

3.3 Results

3.3.1 Source receptor relationship

We find distinct temporal patterns of PFOS and FOSA concentrations in seawater in the North East Atlantic after 2000. Reconstructed FOSA seawater concentrations decreased 8-fold between 2000 and 2015 (66 pg L^{-1} to 8 pg L^{-1}) closely following the decline of global inputs to the oceans during this time (190 Mg yr^{-1} to 15 Mg yr^{-1}) (Figure 3.1, and Chapter 2).[45] PFOS concentrations in the upper 500 m on the other hand remained unchanged (mean 23±5 pg L^{-1} (2000-2015). The distinct local seawater concentration patterns are a result of the turn-over times of the reservoirs that con-

stitute the main transport pathways of the two compounds to the Arctic. Atmospheric transporte is much more important for FOSA than for PFOS, which is primarily present in its ionic form in seawater. Accordingly, FOSA concentrations in the environment responded rapidly to decreasing emissions.[132] PFOS on the other hand is considered to be transported primarily with ocean circulation,[216] in locations hydrologically well connected to historical releases regions like the North Atlantic. In these regions, PFOS concentrations are thought to reflect releases magnitude at the time of their last contact with coastal source areas.[102] PFOS concentrations in Arctic water have been shown to contain elevated PFOS levels compared to Atlantic water.[102] Located half-way between Iceland and Norway, water masses surrounding the Faroe Islands are influenced by Arctic water masses to the north[90] and continued increases in PFOS concentrations may reflect past releases that have recirculated through the Arctic.

3.3.2 Bioaccumulation in the North Atlantic pilot whale food web

Concentration trends observed in seawater remain recognizable in pilot whales with decreasing concentrations of FOSA but not PFOS following the phase out in 2003. Observed FOSA concentrations in pilot whale muscle tissue peak at 25.2 ng g^{-1} in 1999, followed by a decline to 5.1 ng g^{-1} in 2015 (geometric mean), whereas PFOS levels increase by 2.54% yr_{-1} (p-value<0.01) from 1994 to 2015 (Figures 3.2c and 3.2d). Modeled concentrations reproduce key features of these observed trends in whales. After peaking at 29.5 ng g^{-1} (geometric mean, ca. 2001), modeled FOSA concentrations decline to 4.4 ng g^{-1} in 2015. During this time, modeled annual mean PFOS concentrations increase by 5% yr^{-1} (1994-2015, p-value <0.05). Overall, modeled annual mean concentrations agree with observed values within a factor of two (FOSA: 5.3-25.5 ng g^{-1} observed, 4.4-29.5 ng g^{-1} modeled; PFOS: 2.3-5.0 ng g^{-1} observed, 1.9-3.3 ng g^{-1} modeled, 1994-2015). The modeled trends in the piscivorous food web closely follow trends in aqueous concentrations, with an initial concentration peak occurring in 1997 (Figures 3.2a and 3.2b).

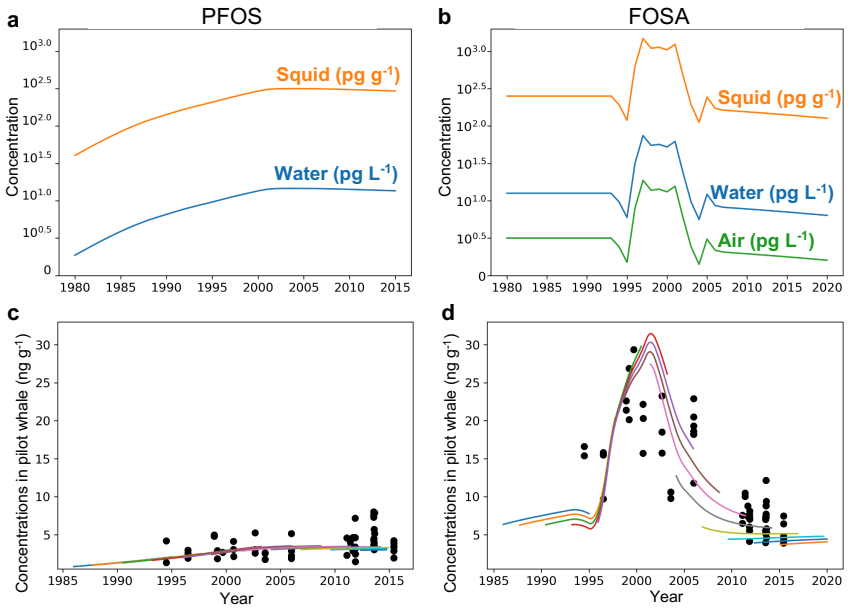

Figure 3.2: Modeled concentrations of perfluorooctane sulfonamide (FOSA) and perfluorooctane sulfonate (PFOS) in air, water, squid (*Todarodes sagitatus*), and pilot whales (*Globicephala melas*) compared to temporal measurements. Panel (a) shows reconstructed FOSA and PFOS concentrations in air (FOSA only), seawater and squid based on equilibrium partitioning. Panel (c) and (d) shows modeled concentrations of FOSA and PFOS in different pilot whale birth cohorts plotted against measured concentrations of FOSA and PFOS in juvenile male pilot whales shown as black circles.

We estimate that the half-life of FOSA (3.3-3.8 years) is twice as long as the half-life of PFOS (1.3-1.6 years) in pilot whale. As a result, the contribution of FOSA to the $\sum(PFOS, FOSA)$ burden in whales remains high post phase-out (61% in 2015), driven by the greater biomagnification of FOSA relative to PFOS in pilot whales. The greater biomagnification of FOSA compared to PFOS in pilot whales has also been observed in other ecosystems.[95] Modeled half-lives of both compounds in fish and squid (<2 weeks) are short compared to pilot whales.

Modeled dietary consumption contributed <85% of both FOSA and PFOS uptake in whales. Rapid concentration declines of FOSA but not PFOS after 2000 in both modeled seawater and observed whale concentrations suggest that biotransformation in the pilot whale food web is small. Modeled PFOS trends change substantially when including biotransformation, as the biotransformed PFOS is efficiently transferred along the food chain with dietary uptake. For example, FOSA biotransformation of 20% in fish would result in a peak in whale PFOS concentrations in the early 2000s that is not consistent with observed concentrations (Figure C.1). Model performance at a biotransformation rate of 5% in fish is comparable (mean absolute model bias = 1.25, range 1.10-1.43) to the model version previously discussed that does not include biotransformation (mean absolute model bias: 1.20, range 1.11-1.35). However, when including biotransformation modeled PFOS concentrations no longer reproduce increasing concentration trends observed in whale muscle (p-value=0.11). We therefore infer that the contribution of FOSA biotransformation to PFOS concentrations observed in pilot whale is negligible in this ecosystem.

3.3.3 Pilot whale consumption in the Faroese children

Between 1993 and 2014, the percentage of children consuming pilot whale declined from 90% to 33% (Figure 3.3a). Hair mercury levels indicate that the consumption of pilot whale among whale consuming children decreased from 0.34 g kg-bw^{-1} d^{-1} (1991, age 5) to 0.10 g kw-bw^{-1} d^{-1} (2012, age 5, Figure 3.3b). It is likely that these changes in consumption behavior occurred in response to

consumption advisories published in 1989, 1998 and 2010.[209]

Children who consume pilot whale meat continue to be exposed to substantial PFOS from whale meat consumption. Based on interpolated levels of PFOS and FOSA levels in pilot whales and estimated consumption rates, we calculate that whale eating children are exposed to 0.60 ng PFOS kw-bw^{-1} d^{-1} (range 0.35-0.91 ng kw-bw^{-1} d^{-1}) from pilot whale consumption alone (age 5, 2012), equivalent to the European Food and Safety Agency's (EFSA) proposed tolerable daily intake of 0.6 ng kg-bw^{-1} d^{-1} for the sum of PFOA, PFNA, PFHxS, and PFOS.[56]

Between 2000-2012, 80% of decreases in PFOS serum concentrations in whale eating children (37.5 ng mL^{-1} to 5.4 ng mL^{-1}, 2000-2012) can be attributed to declining exposure from sources other than whale meat (Figure 3.3c). Decreases in PFOS exposure attributable to whale meat consumption occurred between 2000 and 2005 following declining

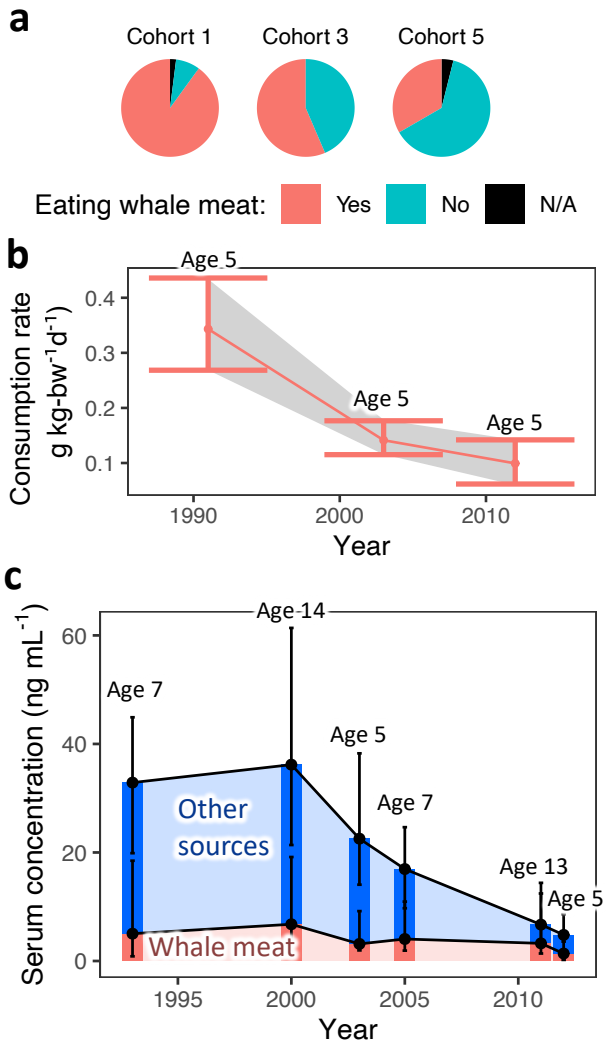

Figure 3.3: (a) Percent of whale consuming children in each cohort, (b) their modeled whale consumption rate at age 5, and (c) $\sum(PFOS, FOSA)$ serum concentration attributable to whale meat consumption and other sources. Modeled whale meat consumption is based on measured Hg concentrations in hair (adapted from Dassuncao et al. (2018). Error bars in Panel (b) indicate the bootstrapped 95 percent confidence interval around the mean. Error bars in Panel (c) indicate 95th percentiles around median PFOS exposure from whale meat and other sources.

FOSA concentration in pilot whale. The contribution of whale meat to the total PFOS burden in children increased from 17% (age 5, 2003) to 32% (age 5, 2012).

We find that avoided exposures are much greater than those indicated by temporal trends in whale and human biomonitoring data. Under scenario 1, we estimate PFOS serum concentrations attributable to whale consumption would have been 4-fold higher in children age 5 (geometric mean: 8 (5-12) ng mL^{-1}, ca. 2012) had FOSA and PFOS concentrations in pilot whale and whale meat consumption not decreased (Scenario 3, 2.2 (1.7-2.9) ng mL^{-1}, Figure 3.4a and 4b). 47% of the avoided exposure from pilot whale can be attributed to avoided increases in PFOS and FOSA concentrations in pilot whale (3 (2-5) ng mL^{-1}, Scenario1 - Scenario 2). Based on regression analysis of trends prior to 2002, we estimate PFOS and FOSA concentrations in pilot whale may have increased to 4 (2-7) ng g^{-1}, ca. 2012) and 52 (19-139) ng g^{-1}, ca. 2012) without regulation (Figure 3.4a).[45] The remainder of avoided exposure is due to reduced consumption of pilot whale of whale eating children since 1993 (3 (2-4) ng g^{-1}, Scenario 2- Scenario 3). EFSA has concluded that there is no adverse observed effect at serum concentrations below 17.5 ng mL^{-1}.[56] Another study considered based on serum concentrations measured at age 5 in 2003 on the Faroe Islands that serum concentrations of <2.6 ng mL^{-1} ensured antibody response to vaccinations against diphtheria was suppressed by less than 10%.[81] In 2012, none of the children at age 5 exceeded the EFSA Panel on Contaminants in the Food Chain (CONTAM Panel)'s No-Observed-Adverse-Effect-Concentration (NOAEC) of 17.5 ng mL^{-1}. Based on our scenario analysis, we estimate that without regulation and consumption changes in pilot whale consumption 42% of children age 5 would have exceeded serum concentrations considered safe by EFSA (median: 14 ng mL^{-1}, 90 percent confidence interval: 3-161 ng mL^{-1}, *Figure*3.4*b*).

Figure 3.4 ***(following page)*****:** Impact of regulation and consumption advisories on PFOS exposure in Faroese children between 1993 and 2012. Panel (a) shows modeled serum concentrations under a scenario of increasing concentrations of PFOS and FOSA in whale at rates observed prior to 2001 and whale meat consumption maintained at 1993 levels (Scenario 1, in orange). Scenario 2 (in green) shows modeled serum concentrations if whale meat consumption had not declined. Filled circles and errorbars indicate modeled means and 95 percent confidence intervals of the $\log_{10}$-normal distribution. Lines and ribbons connect data points from the same cohort. Panel (b) shows the distribution of modeled serum concentrations under scenario 1 against observed distribution of PFOS serum concentrations in children age 5 in 2012. Vertical lines indicate the No Adverse Effect Concentration recommended by EFSA's CONTAM Panel (17.5 ng mL^{-1}),[56] and the Benchmark Dose Level associated with a 10% reduction in antibody response (2.6 ng mL^{-1}).[81]

Figure 3.4: (continued)

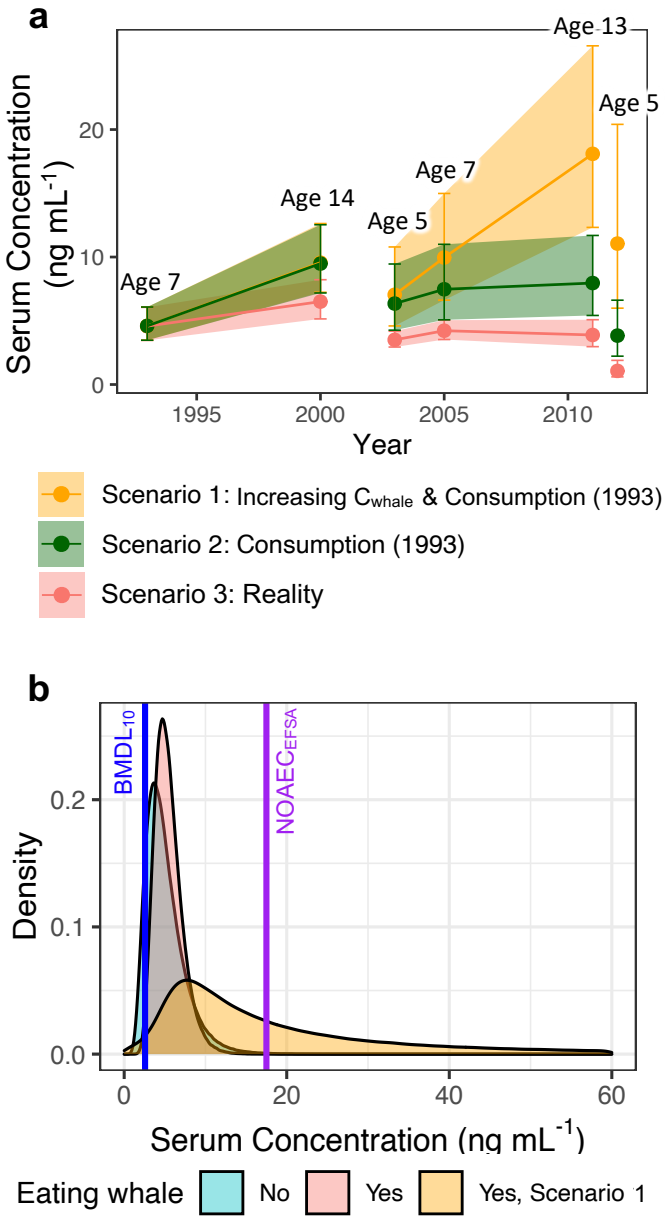

3.3.4 Discussion

We demonstrate in this case study that environmental transport modeling and human exposure modeling are necessary to interpret biomonitoring trends of PFOS. This is especially important for contaminants that are primarily distributed with ocean circulation and whose concentration in the environment does not follow declining trends observed in environmental releases.
FOSA seawater concentrations have declined following the phase out around 2003, but declines in seawater concentrations of PFOS in the North East Atlantic are not yet apparent. Dietary intake dominates uptake of PFOS and its precursor FOSA in pilot whales in the North East Atlantic. While the concentration of FOSA in whale muscle declined by 80%, PFOS concentrations remain stable, following concentration trends in seawater. FOSA continues to contribute 61% to $\sum(PFOS, FOSA)$ concentrations in whale muscle. Fish studies commonly indicate that terminal perfluoroalkyl acids (PFAA) remain the primary PFAS exposure of concern in fish, due in part to substantial precursor biotransformation inferred from low precursor-to-PFAA ratios in fish compared to invertebrates.[74,72,126,174] However, food web studies typically occur in coastal regions, and rarely include higher trophic level invertebrates (i.e. squid) or cetaceans. Our modeling results demonstrate that variability in bioaccumulation and precursor biotransformation rates in some marine organisms can cause PFAS precursors to remain a dominant dietary exposure source for PFOS in humans.

It is possible that atmospheric transport and degradation of precursor substances is responsible for a substantial part of temporal and spatial variation in PFOS concentration trends in biota.[141] Atmospheric modeling studies transport of perfluoralkanecarboxylic acid precursors suggests that atmospheric fate and oxidation yields are variable,[191] but similar studies of perfluoralkanesulfonic acid precursors are warranted to determine their contribution to PFOS in remote environments. Additional characterization of between- and within-species variability in precursor biotransfor-

mation rates will enable broader application of this modeling approach in the absence of robust monitoring data.

Decreases in PFOS exposure since 2003 can be primarily attributed to reduced exposure from sources other than whale meat. As a result of declining direct exposures, the contribution of whale meat to total PFOS burden in whale consuming children has increased. We anticipate slower decreases in PFOS levels in human serum in the future as concentrations in pilot whales and other marine food items respond more slowly to regulation than levels in consumer products. This is especially true as further decreases in whale consumption are unlikely given the cultural value of this wild food for the Faroese population.[60,161] This case study identifies four major areas of uncertainty in assessing effectiveness assessments of international regulations of PFAS that need to be considered to improve regulatory impact evaluations:

1. Timescales and spatial variability of global distribution pathways, including those of precursors
2. Ecosystem structure and inter-species metabolic differences
3. Variability and temporal changes in human (consumption) behavior
4. Intra-human variability in contaminant burden related to age rather than exposure

We show that initial declines of PFOS in human cohort studies have overestimated the pace at which exposure to PFOS and its precursor will decrease in response to regulation. Regulation has been very effective at avoiding further concentration increases of PFOS and its precursors in the environment, avoiding 6 ng mL^{-1} serum concentration in children age 5 that consume whale meat. The significance of this finding extends to other dietary exposure sources[74] and underscores the importance of persistence and resulting environmental accumulation as a major cause of concern.[39]

A

Chapter 1

Table A.1: Air-sea exchange parameterization.

Variable (Units)	Description	Equation	Reference
F (mol m^{-2} sec^{-1})	flux of gas across the air-sea interface	$F = K_w(C_a/K_H - C_w)$	Liss & Slater (1974)
C_a (mol m^{-3})	Air concentration	GEOS-Chem atmospheric simulation	Friedman & Selin (2016)
C_w (mol m^{-3})	Water concentration	MITgcm ocean simulation	This work
K_H	dimensionless gas-over-liquid Henry's law constant	$K_H = C_a/C_w$	–
–	Temperature dependence of K_H	$K_H = K_{H0} \cdot exp(-\Delta H/R \cdot (\frac{1}{T} - \frac{1}{T_0}))$	Johnson (2010)
T_0 (Kelvin)	Standard temperature	25 °C = 298.15 K	–
T (Kelvin)	Temperature of seawater	MITgcm ocean simulation	This work
K_{H0}	Dimensionless gas-over-liquid Henry's law constant at standard temperature and pressure (1 atm)	See Table A.3	–
ΔH (J mol^{-1})	Enthalpy of solution	See Table A.3	–
R (J K^{-1} mol^{-1})	Universal gas constant	8.314	–
K_w (m sec^{-1})	Total water-side transfer velocity	$K_w = (1 - f_{ice}) \cdot [1/k_w + 1/(k_a K_H)]^{-1}$	Johnson (2010)
k_a (m sec^{-1})	Single-phase air-side transfer velocity	$k_a = 1 \cdot 10^{-3} + \frac{u_*}{13.3{S_{c,a}}^{0.5} + C_D^{-0.5} - 5 + \frac{ln(S_{c,a})}{2K}}$	Duce et al. (1991)
k_w (cm h^{-1})	Single-phase waterside transfer velocity	$k_w = (0.222{u_{10}}^2 + 0.333u_{10}) \cdot (S_{c,w}/S_{c,CO_2})^{-0.5}$	Nightingale et al. (2000))
f_{ice} (0 to 1)	Grid box sea ice fraction	MITgcm ocean simulation	This work
S_{c,CO_2}	Schmidt number of CO_2 at 20 °C in freshwater	600	Johnson (2010)
$S_{c,w}$	Schmidt number for the PCB of interest	$S_{c,w} = \mu_w/D_w = \eta_w/(\rho_w D_w)$	Johnson (2010)
μ_w	Kinematic viscosity of water	–	–
D_w (in cm^2 sec^{-1})	Diffusivity of the gas-phase PCB in water	$D_w = \frac{7.4 \cdot 10^{-8} T \sqrt{\Phi M_s}}{\eta_s {V_b}^{0.6}}$	Wilke & Chang (1955)
η_w (kg m^{-1} s^{-1}))	Dynamic viscosity of water	$\eta_w = \frac{t+246}{0.05594t^2 + 5.2842t + 137.37} \cdot 1 \cdot 10^{-3}$	Liss & Slater (1974)
ρ_w (kg m^{-3})	Density of sea water	1.03	Johnson (2010)
t (°C)	Seawater temperature	MITgcm ocean simulation	This work
V_b (cm^3 mol^{-1})	Liquid molar volume	See Table A.3	–

Table A.5 Continued

Variable (Units)	Description	Equation	Reference
η_s (kg m^{-1} s^{-1})	Dynamic viscosity of seawater at 15°C	1.219	ITTC (2006)
M_s	Relative molecular mass of the solvent	18.01 for water	Wilke & Chang (1955)
Φ	Association factor of the solvent	2.6 for water	Wilke & Chang (1955)
u_* (m s^{-1})	Description of ustar	$u_* = u_{10}\sqrt{6.1 \cdot 10^{-4} + u_{10} 6.3 \cdot 10^{-5}}$	Duce et al. (1991)
u_{10} (m s^{-1})	10-meter wind speed	Provided by ERA Re-analysis data	–
C_D	Drag coefficient	$C_D = 6.1 \cdot 10^{-3} + 6.3 \cdot 10^{-5} u_{10}$	Smith (1980)
κ	von Karman constant	0.4	Johnson (2010)
$S_{c,a}$	Schmidt number in air	$Sc, a = \mu_a / D_a = \eta_a / (\rho_a D_a)$	Johnson (2010)
μ_a	Kinematic viscosity of air	–	–
D_a	Diffusion coefficient in air	$D_a = 0.001 T^{1.75} \frac{M_r^{0.5}}{P[V_a^{1/3} + V_b^{1/3}]^2}$	Fuller et al. (1966)
η_a (kg m^{-3})	Dynamic viscosity of air	$\eta_a = S_{V0} + S_{V1} t + S_{V2} t + S_{V3} t^3 + S_{V4} t^4$	Tsilingiris (2008)
ρ_a (kg m^{-3})	Density of air	$\rho_a = S_{D0} + S_{D1} t + S_{D2} t^2 + S_{D3} t^3$	Tsilingiris (2008)
S_V and S_D	Constants	–	Tsilingiris (2008)
P(atm)	Atmospheric pressure	1	–
V_a (cm3 mol^{-1})	Molar volume of air	20.1	Tucker & Nelken (1990)
M_r	Relative molecular mass of air	$M_r = (M_a + M_b)/(M_a M_b)$	Johnson (2010)
M_a (g mol^{-1})	Molar mass of air	28.97	–
M_b (g mol^{-1})	PCB molar mass	See Table A.3	–

Table A.3: Physicochemical properties of PCBs.

	CB-28	CB-101	CB-153	CB-180	Reference
molar mass, M_b (g mol^{-1})	257.54	326.43	360.88	395.32	Li et al. (2003)
molar volume, V_b (cm^3 mol^{-1})	169.14	193.62	205.86	218.1	Schwarzenbach et al. (2003)
log K_{OW} (unitless)	5.92	6.76	7.31	7.66	Schenker et al. (2005)
log K_H (unitless)	-1.93	-2.08	-2.13	-2.51	Schenker et al. (2005)
log K_{OC} *(unitless)	6.99	7.79	8.32	8.65	Schenker et al. (2005), Sobek et al. (2004)
enthalpy of air-water exchange, $\Delta H(kJmol^{-1})$	51.8	65.2	68.2	69	Schenker et al. (2005)
Degradation half-life, $t_{1/2}$ (hours)	5 500	31 000	55 000	55 000	Wania & Daly (2002)

*Calculated using the relationship from Sobek et al. (2004) as follows:
$logK_{OC} = (0.880.07)logK_{OW} + (0.900.47)$.

Table A.4: Modeled and measured dissolved seawater concentrations.

	Surface ocean (<10 m)		
Ocean Basin	**Observed median/ percentiles (pg/L)**		**Modeled median/ percentiles (pg/L)**
CB-28			
Arctic Ocean	0.18 (0.03. 0.57)	(n=41)	0.29 (0.16, 0.54)
North Atlantic	0.42 (0.13, 2.40)	(n=8)	0.09 (0.02, 0.18)
South Atlantic	0.19 (0.06, 1.00)	(n=13)	<0.01
Eq. and S. Pacific	0.76 (0.33, 2.45)	(n=16)	<0.01
Southern Ocean	0.045 (0.024, 0.158)	(n=17)	0.003 (0.001, 0.009)
Global Mean	**0.23 (0.03-2.21)**		**0.09 (<0.41)**
CB-101			
Arctic Ocean	0.040 (0.018, 1.458)	(n=38)	0.038 (0.022, 0.076)
North Atlantic	0.42 (0.05, 0.60)	(n=15)	0.02 (0.01, 0.03)
South Atlantic	0.32 (0.05, 1.54)	(n=50)	<0.01
Eq. and S. Pacific	1.5 (0.3, 6.4)	(n=10)	<0.1
Southern Ocean	0.38 (0.10, 0.91)	(n=19)	<0.01
Global Mean	**0.30 (0.03, 1.78)**		**0.01 (<0.06)**
CB-153			
Arctic Ocean	0.039 (0.005, 1.419)	(n=18)	0.142 (0.097, 0.352)
North Atlantic	0.054 (0.021, 0.143)	(n=4)	0.104 (0.071, 0.111)
South Atlantic	0.045 (0.009, 3.470)	(n=7)	0.002 (<0.033)
Southern Ocean	0.068 (0.035, 0.347)	(n=19)	0.001 (<0.004)
Global Mean	**0.082 (0.010, 1.766)**		**0.122 (<0.427)**
CB-180			
Arctic Ocean	0.020 (0.004, 0.192)	(n=16)	0.008 (0.006, 0.024)
North Atlantic	0.063	(n=1)	0.01
South Atlantic	0.032 (0.028, 0.320)	(n=4)	0.001 (<0.003)
Southern Ocean	0.012 (0.002, 0.117)	(n=18)	<0.001
Global Mean	**0.053 (0.004, 0.603)**		**0.008 (<0.041)**

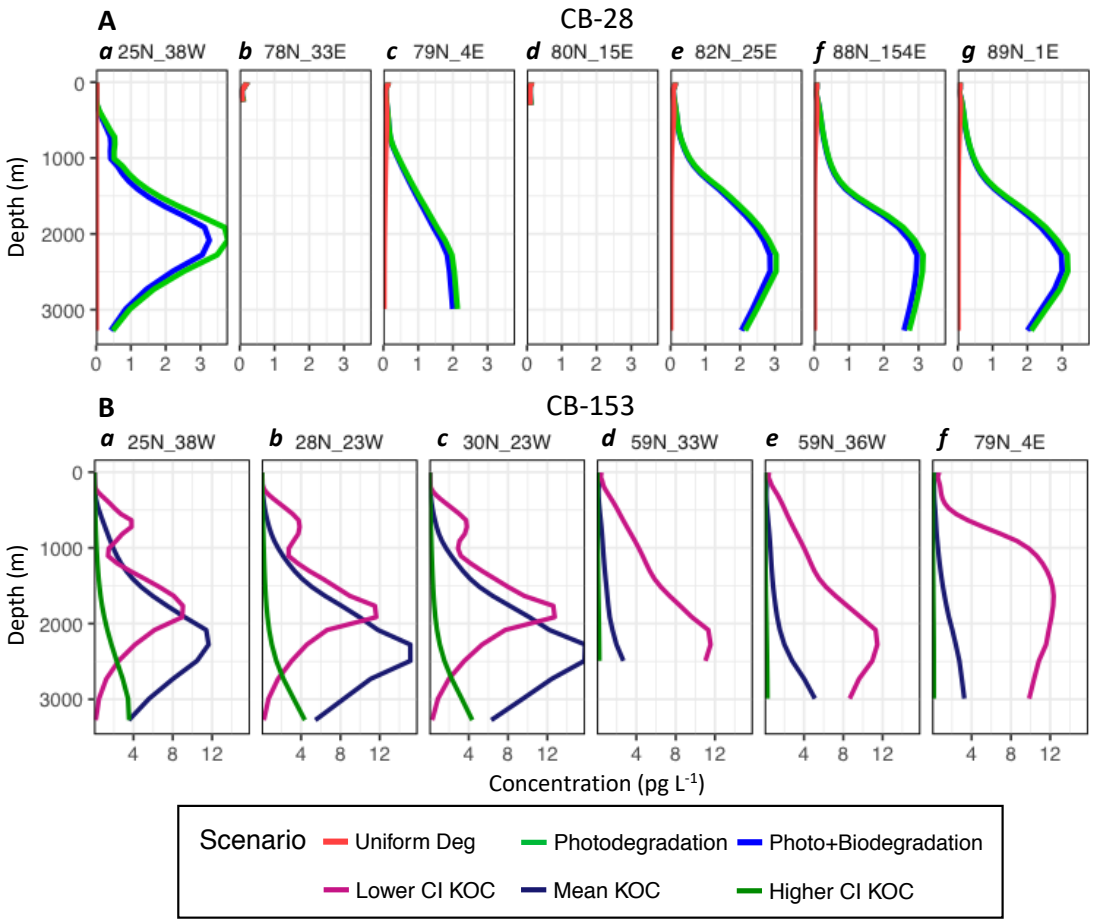

Figure A.1: Modeled vertical profiles from five sensitivity simulations. Panel A shows vertical profiles of CB-28 with uniform degradation (orange), photolytic degradation (green) and combined photolytic and biotic degradation (blue). Panel B shows vertical profiles of CB-153 using logK_{OC} of 5.82 (pink), 7.64 (dark blue) and 8.32 (dark-green).

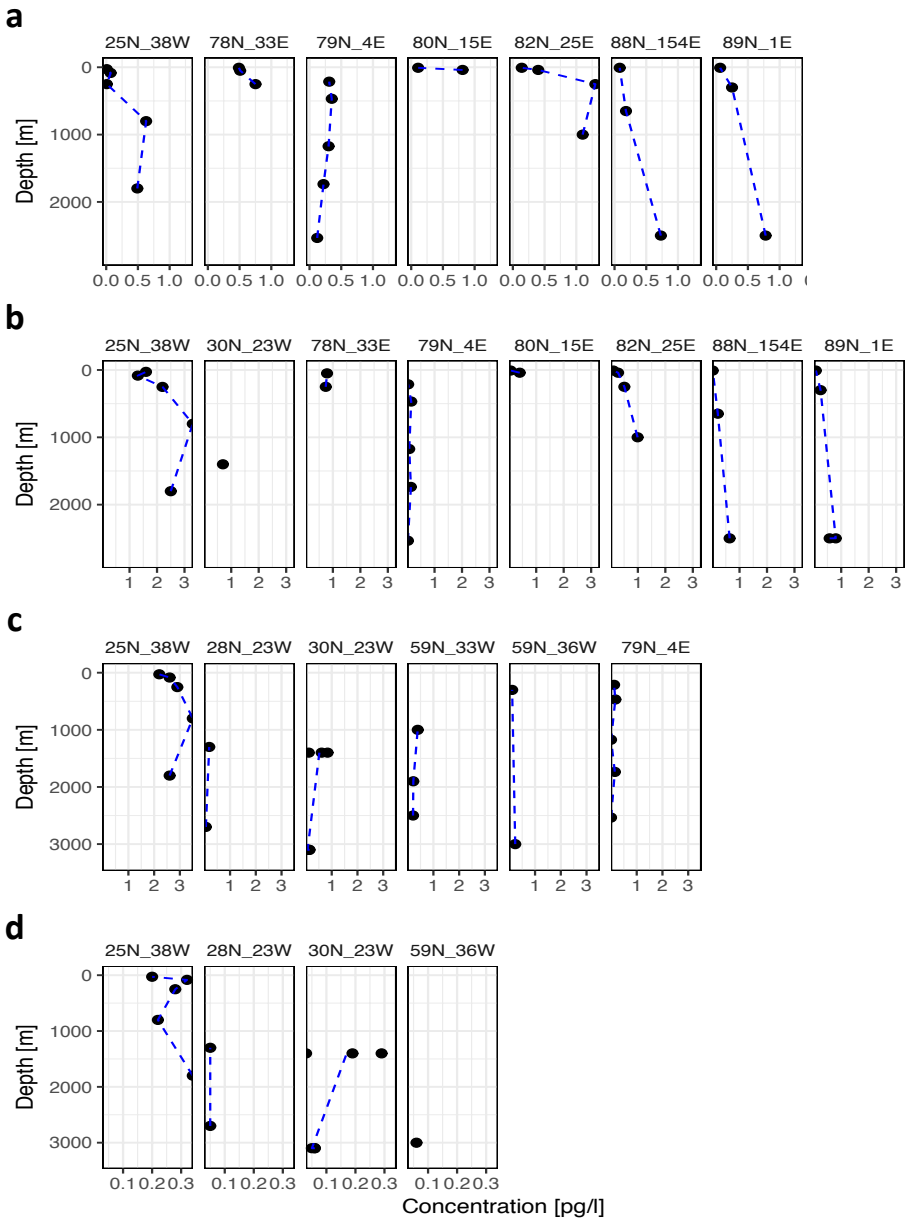

Figure A.2: Measured PCB depth profiles of a) CB-28, b) CB-101, c) CB-153 and d) CB-180. Profiles are from the Tropical Atlantic,[18,187] the North Atlantic[18] and the Arctic Ocean.[86,187] Concentrations at depth exceed the surface concentrations wherever surface concentrations exist and peak between 40 and 2500 m. Reported maximum concentrations are 1.30 pg CB-28 L^{-1}, 3.3 pg CB-101 L^{-1}, 3.5 pg CB-153 L^{-1} and 0.34 pg CB-180 L^{-1}.

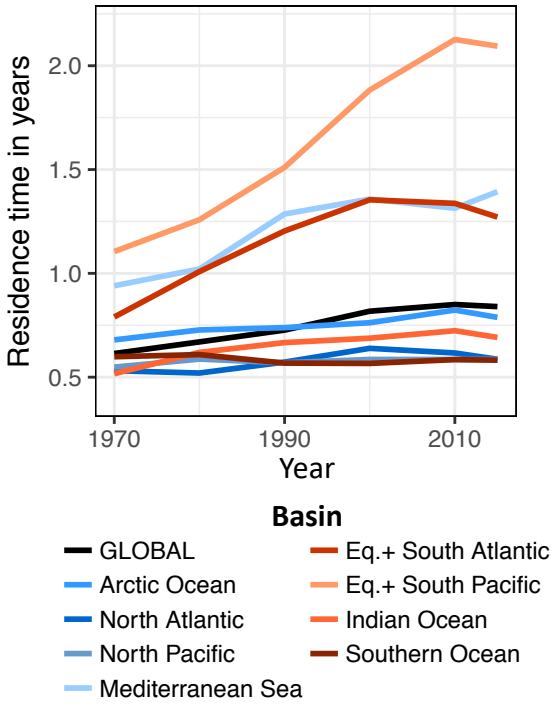

Figure A.3: Changes in PCB residence times in the upper 1000 m between 1970-2015.

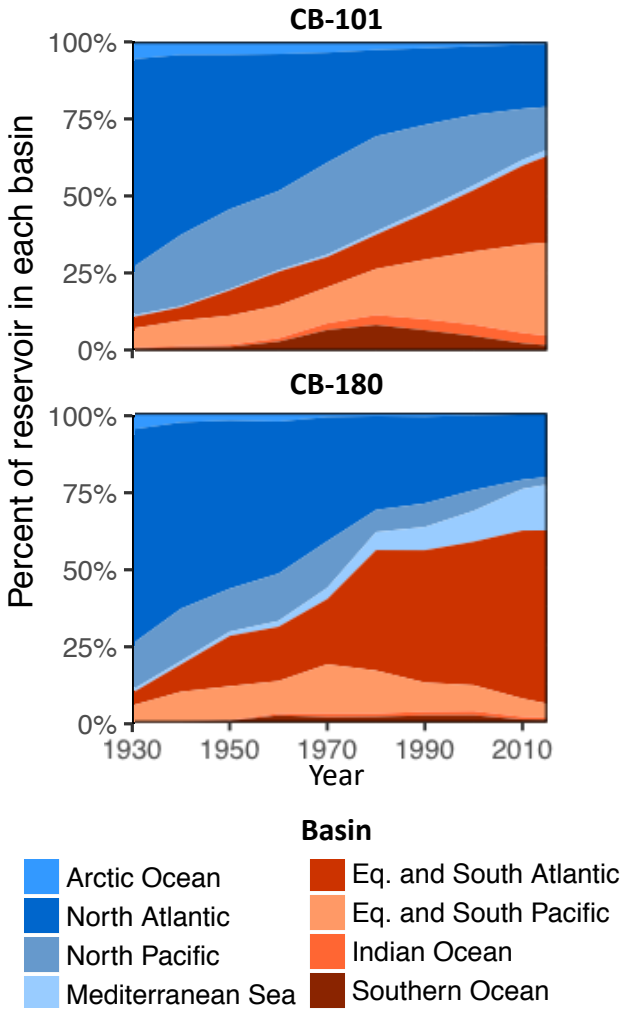

Figure A.4: Changes in CB-101 and CB-180 mass distribution between 1930-2015. Northern Hemisphere basins are shades of blue and Southern Hemisphere basins are shades of red/orange.

Table A.5: Modeled best estimate for 2015 PCB reservoir (kg) and mass flows (kg yr^{-1}) in the upper ocean (top 1000 m) using high K_{OC} and a combination of photolytic and biotic degradation.

	CB-28	CB-101	CB-153	CB-180
Arctic Ocean				
Reservoir	**1 089**	**99**	**1 047**	**98**
Atm. deposition	752	129	1 935	193
Upward/downward	103/-85	5/-4	18/-16	1/-1
vert. transport				
Hor. Transportb	-45	-2	-3	0
Particle sinking	-174	-43	-622	-64
Burial	-151	-51	-944	-96
Degradation	-82	-1	-4	0
Evasion	-369	-31	-163	-8
North Atlantic				
Reservoir	**2 905**	**404**	**3 467**	**339**
Atm. deposition	2 356	418	5 658	623
Upward/downward	192/-227	20/-22	106/-142	9/-13
vert. transport				
Hor. transport	-1 108	-275	-933	-106
Particle sinking	-525	-220	-3 593	-419
Burial	-225	-78	-1 395	-163
Evasion	-907	-113	-645	-40
North Pacific				
Reservoir	**1 644**	**272**	**2 161**	**181**
Atm. deposition	1 846	424	4 520	409
Upward/downward	29/-31	3/-3	13/-20	1/-2
vert. transport				
Hor. transport	-10	-1	-1	0
Particle sinking	-690	-286	-3 439	-318
Burial	-156	-49	-714	-67
Degradation	-492	-23	-39	-2
Evasion	-607	-75	-236	-10
Mediterranean Sea				
Reservoir	**363**	**244**	**1 257**	**117**
Atm. deposition	309	66	688	87
Upward/downward	14/-14	23/-21	76/-71	4/-4
vert. transport				
Hor. transport	0	-1	-17	-3
Particle sinking	-9	-26	-282	-41
Burial	-10	-14	-232	-34
Degradation	-238	-24	-108	-9
Evasion	-69	-22	-161	-13

Table A.5 Continued

	CB-28	CB-101	CB-153	CB-180
Eq. and South Atlantic				
Reservoir	**1 707**	**329**	**1 540**	**142**
Atm. deposition	438	102	894	98
Upward/downward	41/-56	7/-5	24/-17	2/-2
vert. transport				
Hor. transport	871	171	446	20
Particle sinking	-72	-44	-486	-64
Burial	-10	-7	-94	-11
Degradation	-315	-33	-135	-11
Evasion	-99	-38	-255	-20
Eq. and South Pacific				
Reservoir	**1 357**	**252**	**992**	**73**
Atm. deposition	485	145	983	97
Upward/downward	54/-33	15/-13	30/-24	2/-1
vert. transport				
Hor. transport	25	-2	-5	0
Particle sinking	-144	-77	-782	-85
Burial	-5	-6	-69	-8
Degradation	-355	-39	-87	-5
Evasion	-117	-50	-186	-10
Indian Ocean				
Reservoir	**247**	**75**	**353**	**34**
Atm. deposition	266	77	527	58
Upward/downward	23/-14	4/-2	14/-10	1/-1
vert. transport				
Hor. transport	59	26	135	24
Particle sinking	-39	-42	-373	-45
Burial	-4	-6	-65	-8
Degradation	-183	-16	-45	-3
Evasion	-57	-19	-86	-6
Southern Ocean				
Reservoir	**753**	**119**	**889**	**95**
Atm. deposition	680	177	1 729	197
Upward/downward	265/-188	17/-13	77/-71	7/-7
vert. transport				
Hor. transport	208	85	377	66
Particle sinking	-418	-153	-1 620	-188
Burial	-22	-7	-73	-8
Degradation	-102	-2	-3	0
Evasion	-243	-19	-49	-3

B

Chapter 2

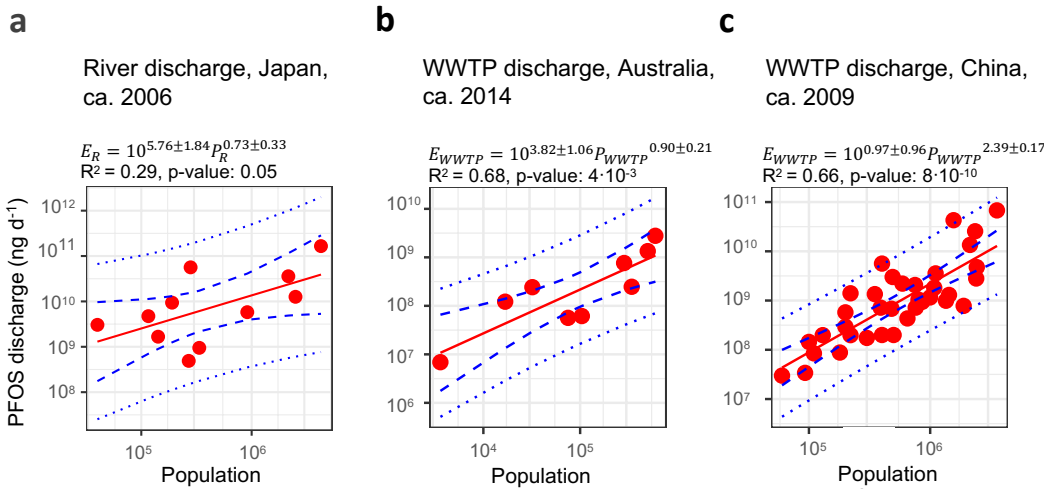

Figure B.1: Regression relationships between a) riverine PFOS discharge and catchment population in Japan and B) WWTP discharge and population served in and c) WWTP discharge and population served in China adapted from Zhang et al. (2017). Solid lines show means, and dashed lines denote 95% confidence intervals around the mean, and outer lines indicate the 95% confidence intervals for predictions.

For Japan (Figure B.1a), measured PFOS concentrations and volumetric river discharges were available for 11 river estuaries sampled in 2005.[143] River basins covered a representative sample of regions and population densities, with basin populations ranging from 40 000-4 250 000 people. The non-linear component of the regression relationship representative of industrial releases was slightly lower than results previously reported for Europe (0.73 vs 1.01), but the per-capita component was much greater for Japan (5.76 and -8.02), where PFOS concentrations in WWTP effluents have been shown to be strongly correlated crotamiton concentrations, a markers of sewage effluents.[143] The regression relationships for PFOS discharges from rivers and population explained less of the variability (R^2=0.29) compared to results previously reported for Europe (R^2=0.68) likely due to the greater number of rivers included in the European study (n=210).[157] We extrapolate power-regression results to other river basins in Japan using catchment population derived from vectorized data from the Geospatial Information Authority of Japan.[75] Resulting log-normally distributed estimates of PFOS discharges to the ocean from Japan, a location of POSF production in the past were $10^{2.23\pm3.70}$ Mg between 1958 and 2015.

For Australia (Figure B.1b), PFOS concentrations from 12 WWTPs were reported by Gallen et al. (2018) for the year 2014 representing each of the eight Australian states. Measured PFOS concentrations ranged from 3-240 ng L^{-1} across WWTPs which served populations between 4000-600000. For six WWTPs where only influent volume was reported we predicted effluent volumes using linear regression (R^2>0.99, p-value<0.01). The regression relationship between PFOS discharge rates and population served by each WWTP explained 68% of the variability in the data. The non-linear component of the power regression relationship associated

with industrial releases was somewhat lower than that previously reported for the United States and Canada (0.90, 1.24 and 1.20), consistent with lower rates of PFAS imports and no primary POSF manufacturing site.[36] The population component (3.82) was higher than that reported for North America (-0.33), where PFOS is still employed in approved uses.[36] In the absence of an existing database of WWTPs in Australia, we compiled an inventory of 113 WWTPs covering 58% of Australia's population from publicly available information contained in government records, provider websites, and news articles. We applied the power-regression relationship to each of the WWTPs and scaled annual discharges for 2014 by changes in global changes in releases to water because no specific emission data for Australia were available.[200] We estimate that Australia, which has never been a producer of POSF and has a small population of 25 million, has discharged $10^{0.42\pm2.22}$ Mg PFOS to the ocean between 1958 and 2015.

For China (Figure B.1c), we applied previously developed regression relationship between PFOS discharges from WWTP and population served for 2009[223] to county-level population data from the national census to extrapolate discharges across the entire Chinese territory[145] Discharges were scaled by emissions to water from Chinese production presented in Wang et al. (2017). Resulting log-normally distributed initial estimates of PFOS discharges to the ocean from China were $10^{1.18\pm1.93}$ Mg (1988-2015), one order of magnitude larger than those from Australia consistent with a much larger population, but lower living standard.

In Brazil, the major sources of PFOS releases is agricultural run-off from direct application to soil of ant baits containing EtFOSA.[130,129,9,223] Prior work showed EtFOSA is a major contributor to PFOS concentrations in surface waters of the South Atlantic.[79,130] In aerobic activated sludge, degradation experiments suggested EtFOSA yields between 4-30% PFOS.[130,138] We thus assume log-distributed uncertainty around a mean conversion rate of 4% with one standard deviation corresponding to 30% for aggregate annual PFOS discharges per catchment area.[116] We initially estimate $10^{1.50\pm0.86}$ Mg of PFOS have been discharged to the ocean from Brazil (1992-2015), comparable to China and reflective of a shorter use period (1992-2015) compared to the historical manufacturing and use regions.

B.0.1 Sample Extraction and Analysis

Seawater samples (n=51) were collected in 1L pre-cleaned (with methanol (MeOH), Milli-Q water and sample water) polypropylene bottles on the 2017 Endeavor and the 2018 Exxpedition cruise. Samples were kept on ice during sample collection and transport and kept frozen at -20°C until extraction and analysis. Prior to extraction, seawater samples were thawed at room temperature, sonicated for 20 seconds and shaken vigorously four times to desorb PFAS from the inner walls of the sample bottle. Samples were weighed, spiked with 40 µL of 0.025 ng μL^{-1} isotopically labeled PFAS internal standard (MPFAC-24ES; Wellington, Guelph, ON, Canada) and equilibrated overnight. Samples were loaded onto preconditioned weak anion exchange SPE cartridges (Water Oasis WAX, 6 mL, 150 mg sorbent) at 1-2 drops per second. The empty sample bottles and cartridges were rinsed with 20 mL Milli-Q water followed by 5 mL of 25 mM ammonium acetate buffer and then centrifuged at 4000 rpm for 3 minutes to remove excess water. The SPE cartridges were eluted with 5 mL of MeOH and 5 mL of 0.1% ammonium hydroxide in MeOH and the extracts were concentrated to 0.5 mL using a ZipVap nitrogen evaporator. Concentrated extracts were diluted 1:1 with Milli-Q water, vortexed, centrifuged and transferred to 1 mL autosampler vials for instrumental analysis.

Analysis. Sample extracts were analyzed for 25 PFAS using an Agilent (Santa Clara, CA) 6460 Triple Quadrupole Liquid Chromatograph Tandem Mass Spectrometer (LC-MS/MS), equipped with an Agilent (Santa Clara, CA) 1290 Infinity Flexible Cube, run in electrospray negative ionization mode following the procedure outlined in Weber et al. (2017). Each 100 µL extract was loaded into an Agilent Zorbax SB-Aq (4.6 × 12.5 mm; 5 µm) online SPE column and eluted with 0.85 mL of 0.1% (v/v) formic acid at a flow rate of 1 mL min^1. Analytes from the SPE column were loaded to an Agilent Poroshell 120 EC-C18 (3.0 × 50 mm; 2.7 µm) reversed-phase HPLC column using ammonium acetate (2 mM) in methanol and water as the mobile phase. A total of 25 PFASs were quantified: perfluorobutanoate (PFBA), perfluoropentanoate (PFPeA), perfluorohexanoate (PFHxA), perfluoroheptanoate (PFHpA), perluorooctanoate (PFOA), perfluorononanoate (PFNA), perfluorodecanoate (PFDA), perfluoroundecanoate (PFUnDA), perfluorododecanoate (PFDoDA), perfluorotridecanoate (PFTriDA), perfluorotetradecanoate (PFTeDA), perfluorobutane sulfonate (PFBS), perfluoropentane sulfonate (PFPeS), perfluorohexane sulfonate (PFHxS), perfluoroheptane sulfonate (PFHpS), perfluorooctane sulfonate (PFOS), perfluorononane sulfonate (PFNS), perfluorodecane sulfonate (PFDS), perfluorooctane sulfonamide (FOSA), 4:2 fluorotelomer sulfonate (4:2 FtS), 6:2 fluorotelomer sulfonate (6:2 FtS), 8:2 fluorotelomer sulfonate (8:2 FtS), N-methyl perfluorooctane sulfonamidoacetic acid (N-MeFOSAA), N-ethyl perfluorooctane sulfonamidoacetic acid (N-EtFOSAA), and dodecafluoro-3H-4,8-dioxanonanoate (NaDONA). The sum of branched and linear PFOS isomers (referred to as PFOS) were quantified together from the Wellington (Guelph, ON, Canada) PFAC-24PAR standard, which includes both branched and linear isomers. Only linear PFHxS isomers were detected and are referred to as PFHxS. Branched isomers of PFOA were included in the quantification with the linear isomer using the calibration standard for the linear isomer.

Quality Assurance/Quality Control. The limit of detection (LOD) and limit of quantification (LOQ) were

defined as the average sample concentration at which the signal-to-noise ratio was 3 and 10, respectively, plus the concentration of any instrumental blank above this value. The method detection limit (MDL) is the LOD corrected for dilution. MDL values for each analyte are reported in Table B.3. Nine field blanks were included in the extraction and analysis (four Endeavor blanks, three field instrument (Niskin) blanks, two Expedition blanks). One Endeavor field blank and one Exxpedition field blank contained PFOS levels above the MDL; the other blanks were below MDL. Samples were corrected for the average of the field blank contamination, where samples below MDL were replaced with $sqrt(2)/2 \cdot MDL$. All instrument blanks run with the analysis were below detection limit for all compounds. Four extraction spikes and three sample spikes (PFAC-24PAR, Wellington, Guelph, ON, Canada) were included with the sample extraction and analysis. Average extraction spike recoveries for PFOS were 100% and 99% for linear and branched isomers, respectively. Average sample matrix spike recoveries for PFOS were 115% and 117% for linear and branched isomers, respectively. The majority of the samples analyzed had concentrations <MDL for most compounds (Table B.3).

Table B.1: Sea spray aerosol (SSA) flux parameterization following Salter et al. (2015).

Variable (unit)	Description	Equation
F_{ent} ($m^3\ m^{-2}$) s^{-1}	Air entrained by wave	$F_{ent} = 2 \times 10^{-8} \times {U_{10}}^{3.74}$
U_{10}	10-m wind speed	MITgcm
A, B, C and D	Polynomial coefficients	See Table B.2
N_{SSA} ($m^{-2}\ s^{-1}$)	Number flux of SSA	$N_{SSA} = F_{ent}(A \times T^3 + B \times T^2 + C \times T + D)$
V (cm^3)	SSA volume	$V = \frac{3}{4}\pi(0.5 \times d \times 1 \times 10^{-4})^3$
$d(\mu m)$	SSA diameter	see Table B.2
ρ_{SSA}	Particle density of SSA	2.16
f_m (dimensionless)	Mass fraction of Na^+ in sea salt	0.31
$C_{Na,SSA}$ ($g\ cm^{-3}$)	Concentration of Na^+ in SSA	$C_{Na,SSA} = f_m \times \rho_{SSA}$
S ($g\ kg^{-1}$)	Salinity of seawater	MITgcm
$C_{Na,w}$ ($g\ cm^{-3}$)	Concentration of Na^+ in seawater	$C_{Na,w} = S \times f_m \times 1 \times 10^{-3}$
$C_{PFOS,w}$ ($g\ cm^{-3}$)	Concentration of PFOS in seawater	this simulation
$C_{PFOS,SSA}$ ($g\ cm^{-3}$)	Concentration of PFOS in SSA	$C_{PFOS,SSA} = EF \times (\frac{C_{PFOS,w}}{C_{Na,w}} \times C_{Na,SSA})$
$C_{PFOS,SSA}$ ($g\ cm^{-3}$)	Concentration of PFOS in SSA	$F_{PFOS,SSA} = (C_{PFOS,SSA} \times N_{SSA} \times V)/M_{PFOS}$
k_{depo} (hr^{-1})	Deposition rate of SSA	$k_{depo} = \frac{1}{-\tau}$
τ (hr)	Residence time against deposition, average for 3 SSA modes	29.6

Table B.2: Parameters used in sea spray aerosol (SSA) parameterization from Johansson et al. (2019).

Variable (unit)	Description	Mode 1	Mode 2	Mode 3
$d(\mu m)$	Model Diameter	0.095	0.6	1.5
EF(dimensionless)	Enrichment factor of PFOS in SSA	62000	62000	55000
A	Polynomial coefficient	5.22×10^5	0	0
B	Polynomial coefficient	3.32×10^7	7.37×10^5	1.42×10^4
C	Polynomial coefficient	6.95×10^8	2.48×10^7	1.47×10^7
D	Polynomial coefficient	1.07×10^10	7.74×10^8	1.71×10^8

B.0.2 Bayesian Inference

We propagate the uncertainty from releases forward and use seawater measurements to constrain regional inputs to the ocean in a Bayesian framework. The conditional probability of PFOS releases from the different sources to the oceans given the available seawater observations can be described as the joint probability of the discharge quantity from each source and observed concentrations given discharges

$$P_{post}(\theta, Y) \propto P(Y|\theta)P_{prior}(\theta)$$

$P_{Prior}(\theta)$ is the $\log_{10}$-normally distributed uncertainty around discharges from WWTPs and rivers as propagated from the regression relationships described above (Figure B.1) and atmospheric inputs. $P(Y|\theta)$ is the likelihood of observed PFOS concentrations in seawater (Y) given a possible combination of releases from different sources. As PFOS is not expected to have an effect on climate and ocean biogeochemistry because of its tracer level concentration, we assume that seawater concentrations (Y) respond linearly to changes in emissions and can be described by

$$Y = M(x, \theta) + \varepsilon$$

Because seawater concentrations vary by orders of magnitude we $\log_{10}$-transform observed and modeled concentration (Y and $M(x, \theta)$) before comparison. Due to the transformation, we were not able to include measurements in locations where the model indicated null concentrations in the comparison (n=38 or 6% of measurements). We consider the random error term ε to follow a Gaussian distribution, that is $\varepsilon = N(0, \sigma^2)$. We consider several error types including observational uncertainty, model parameterization uncertainty, and a residual error, all expressed by their standard deviation (σ).

$$\sigma^2 = \theta_{\varepsilon_1,obs}{\sigma_{obs}}^2 + \theta_{\varepsilon_2,param}{\sigma_{param}}^2 + \theta_{\varepsilon_3,residual}{}^2$$

The observational error σ_{obs} considers how different sampling and analysis methods may affect variability between observations and is assumed to vary by measurement cruise. The uncertainty in the model parameterization σ_{param} considers uncertainty in modeled transport processes dependent on ocean circulation, wind speed, and sea surface temperature and is assumed to vary by ocean basin. The observational error term for each cruise and the model parameterization error for each basin represented by their standard deviation $\theta_{\varepsilon_1,obs}$ and $\theta_{\varepsilon_2,param}$ are inferred in the Bayesian inversion. A residual error term represented by its standard deviation $\theta_{\varepsilon_3,residual}$ is also inferred in the Bayesian inversion.
Using a Metropolis-Hastings implementation of Markov Chain Monte Carlo (MCMC) sampling we can directly sample from the posterior distribution of emissions and calculate the posterior likelihood of statistically plausible emission scenarios from different source regions and deposition of PFOS to the ocean surface. At each sampling iteration a new parameter set $\theta^{(i+1)}$ of emission scaling factors is drawn from a

lognormal distribution with mean θ^i and its probability is compared to the previous set. New proposals are accepted with probability $r = P(\theta^{(i+1)})/P(\theta^i)$ and rejected with probability $(1 - r)$. If the new proposal is rejected, we retain the previous proposal. This procedure is repeated for 10^3 parallel chains with 10^4 iterations. We discard the first 10^5 samples and use the remainder to compute statistics on the posterior distribution of each PFOS source.

Table B.3: Concentrations (pg L^{-1}) of PFAS in seawater samples from 2017 Endeavor and 2018 Exxpedition cruises. QL and QH indicate qualifier flags outside the 30% acceptable range. Values below the method detection limit (MDL) are reported as <MDL value for each compound. Compounds that were blank subtracted (blanks had detectable levels above the MDL) include PFHxA, PFHpA, PFOA, PFNA, PFDA, PFDoA, PFBS, PFHpS, PFOS, 6:2 FtS, 8:2 Fts, FOSA. Samples collected from the ship water intake system are labeled S/U.

		Sampling Location								
ID	Date	Station	Latitude	Longitude	Depth (m)	PFBA	PFPeA	PFHxA	PFHpA	PFOA
1	31/4/2017	1	34 11.82 N	76 24.67 W	1	<786	<86	<46	27	35
2	31/4/2017	1	34 11.82 N	76 24.67 W	23	<786	<86	<46	20	32
3	1/5/2017	2	33 59.40 N	76 06.55 W	5	<322	<69	<109	<109	20
4	1/5/2017	2	33 59.40 N	76 06.55 W	75	<322	<69	<109	<109	<10
5	1/5/2017	2	33 59.40 N	76 06.55 W	405	<322	<69	<109	<109	<10
6	1/5/2017	4	33 06.67 N	76 28.39 W	10	<786	<86	<46	<15	24
7	1/5/2017	4	33 06.67 N	76 28.39 W	100	<786	<86	<46	<15	17
8	1/5/2017	4	33 06.67 N	76 28.39 W	728	<786	<86	<46	<15	10
9	2/5/2017	6	30 12.43 N	76 28.85 W	1	<786	<86	<46	QL	24
10	2/5/2017	6	30 12.43 N	76 28.85 W	3500	<786	<86	<46	<15	<9
11	2/5/2017	6	30 12.43 N	76 28.85 W	3000	<786	<86	<46	<15	<9
12	2/5/2017	6	30 12.43 N	76 28.85 W	2500	<786	<86	<46	<15	<9
13	2/5/2017	6	30 12.43 N	76 28.85 W	2000	<786	<86	<46	<15	<9
14	2/5/2017	6	30 12.43 N	76 28.85 W	1500	<786	<86	<46	<15	<9
15	2/5/2017	6	30 12.43 N	76 28.85 W	880	<786	<86	<46	<15	<9
16	2/5/2017	6	30 12.43 N	76 28.85 W	660	<786	<86	<46	<15	26
17	2/5/2017	6	30 12.43 N	76 28.85 W	500	<786	<86	<46	19	48
18	2/5/2017	6	30 12.43 N	76 28.85 W	300	<786	<86	<46	<15	28
19	2/5/2017	6	30 12.43 N	76 28.85 W	120	<786	<86	<46	22	30
20	2/5/2017	6	30 12.43 N	76 28.85 W	90	<786	<86	<46	19	30
21	2/5/2017	6	30 12.43 N	76 28.85 W	50	<786	<86	<46	22	23
22	2/5/2017	6	30 12.43 N	76 28.85 W	3930	<786	<86	<46	20	<9
23	3/5/2017	8	29 28.73 N	76 36.72 W	10	<786	<86	<46	19	17
24	3/5/2017	8	29 28.73 N	76 36.72 W	120	<786	<86	<46	<15	25
25	3/5/2017	8	29 28.73 N	76 36.72 W	1000	<786	<86	<46	<15	<9
26	3/5/2017	9	28 52.05 N	77 41.17 W	50	<322	<69	<109	<109	<10
27	3/5/2017	9	28 52.05 N	77 41.17 W	150	<322	<69	<109	<109	15
28	3/5/2017	9	28 52.05 N	77 41.17 W	450	<322	<69	<109	<109	17
29	3/5/2017	11	27 35.29 N	79 40.59 W	508	<786	<86	<46	<15	<9
30	3/5/2017	11	27 35.29 N	79 40.59 W	400	<786	<86	<46	<15	18
31	3/5/2017	11	27 35.29 N	79 40.59 W	300	<786	<86	<46	<15	29
32	3/5/2017	11	27 35.29 N	79 40.59 W	200	<786	<86	<46	<15	44
33	3/5/2017	11	27 35.29 N	79 40.59 W	100	<786	91	66	36	71
34	3/5/2017	11	27 35.29 N	79 40.59 W	75	<786	<86	<46	18	20
35	3/5/2017	11	27 35.29 N	79 40.59 W	50	<786	<86	<46	19	21
36	3/5/2017	11	27 35.29 N	79 40.59 W	5	<786	<86	<46	16	19
37	4/5/2017	S/U	27 32.93 N	79 52.12 W	8	<786	<86	<46	26	45
38	30/6/18	1	32 01.12 N	152 32.12W	1	<786	<86	386	202	785
39	1/7/2018	2	33 36.79 N	150 49.69 W	1	<786	<86	<46	30	40
40	2/7/2018	3	35 47.98 N	149 25.50 W	1	<786	<86	<46	28	<9
41	3/7/2018	4	35 09.01 N	148 10.42 W	1	791	<86	262	102	154

Table B.3 Continued

		Sampling Location								
ID	**Date**	**Station**	**Latitude**	**Longitude**	**Depth (m)**	**PFBA**	**PFPeA**	**PFHxA**	**PFHpA**	**PFOA**
42	5/7/2018	5	36 45.93 N	144 22.98 W	1	<786	<86	<46	25	<9
43	6/7/2018	6	38 09.38 N	142 14.32 W	1	<786	<86	<46	QL	<9
44	7/7/2018	7	40 01.91 N	139 48.98 W	1	<786	<86	<46	53	73
45	8/7/2018	8	42 02.31 N	137 39.53W	1	<786	<86	325	162	435
46	9/7/2018	9	43 45.23 N	135 22.20 W	1	<786	<86	<46	113	85
47	10/7/2018	10	45 37.31 N	133 04.74W	1	2556	219	<46	58	63

Table B.3 Continued

		Sampling Location								
ID	Date	Station	Latitude	Longitude	Depth (m)	PFNA	PFDA	PFUA	PFDoA	PFTriA
1	31/4/2017	1	34 11.82 N	76 24.67 W	1	QL	QL	11	21	<43
2	31/4/2017	1	34 11.82 N	76 24.67 W	23	19	<7	<10	<16	<43
3	1/5/2017	2	33 59.40 N	76 06.55 W	5	11	<9	<41	<10	<70
4	1/5/2017	2	33 59.40 N	76 06.55 W	75	QH	<9	<41	<10	<70
5	1/5/2017	2	33 59.40 N	76 06.55 W	405	<8	<9	<41	<10	<70
6	1/5/2017	4	33 06.67 N	76 28.39 W	10	15	<7	<10	<16	<43
7	1/5/2017	4	33 06.67 N	76 28.39 W	100	<10	<7	<10	<16	<43
8	1/5/2017	4	33 06.67 N	76 28.39 W	728	<10	QL	<10	<16	<43
9	2/5/2017	6	30 12.43 N	76 28.85 W	1	12	<7	<10	50	<43
10	2/5/2017	6	30 12.43 N	76 28.85 W	3500	<10	<7	<10	<16	<43
11	2/5/2017	6	30 12.43 N	76 28.85 W	3000	<10	<7	<10	<16	<43
12	2/5/2017	6	30 12.43 N	76 28.85 W	2500	<10	<7	<10	<16	<43
13	2/5/2017	6	30 12.43 N	76 28.85 W	2000	<10	<7	<10	<16	<43
14	2/5/2017	6	30 12.43 N	76 28.85 W	1500	<10	<7	<10	<16	<43
15	2/5/2017	6	30 12.43 N	76 28.85 W	880	<10	<7	<10	<16	<43
16	2/5/2017	6	30 12.43 N	76 28.85 W	660	12	<7	<10	<16	<43
17	2/5/2017	6	30 12.43 N	76 28.85 W	500	21	QL	<10	<16	<43
18	2/5/2017	6	30 12.43 N	76 28.85 W	300	18	<7	<10	<16	<43
19	2/5/2017	6	30 12.43 N	76 28.85 W	120	16	<7	<10	<16	<43
20	2/5/2017	6	30 12.43 N	76 28.85 W	90	15	<7	17	120	<43
21	2/5/2017	6	30 12.43 N	76 28.85 W	50	17	<7	<10	<16	<43
22	2/5/2017	6	30 12.43 N	76 28.85 W	3930	<10	<7	<10	<16	<43
23	3/5/2017	8	29 28.73 N	76 36.72 W	10	<10	<7	<10	<16	<43
24	3/5/2017	8	29 28.73 N	76 36.72 W	120	16	<7	<10	<16	<43
25	3/5/2017	8	29 28.73 N	76 36.72 W	1000	<10	<7	<10	<16	<43
26	3/5/2017	9	28 52.05 N	77 41.17 W	50	QL	<9	<41	<10	<70
27	3/5/2017	9	28 52.05 N	77 41.17 W	150	20	<9	<41	<10	<70
28	3/5/2017	9	28 52.05 N	77 41.17 W	450	14	<9	<41	<10	<70
29	3/5/2017	11	27 35.29 N	79 40.59 W	508	<10	<7	<10	<16	<43
30	3/5/2017	11	27 35.29 N	79 40.59 W	400	<10	<7	<10	<16	<43
31	3/5/2017	11	27 35.29 N	79 40.59 W	300	QH	<7	<10	<16	<43
32	3/5/2017	11	27 35.29 N	79 40.59 W	200	19	<7	<10	<16	<43
33	3/5/2017	11	27 35.29 N	79 40.59 W	100	16	QL	<10	27	<43
34	3/5/2017	11	27 35.29 N	79 40.59 W	75	11	<7	<10	<16	<43
35	3/5/2017	11	27 35.29 N	79 40.59 W	50	QL	QL	13	<16	<43
36	3/5/2017	11	27 35.29 N	79 40.59 W	5	13	QL	<10	<16	<43
37	4/5/2017	S/U	27 32.93 N	79 52.12 W	8	17	<7	<10	<16	<43
38	30/6/18	1	32 01.12 N	152 32.12W	1	208	299	45	53	<43
39	1/7/2018	2	33 36.79 N	150 49.69 W	1	169	10	QH	<16	<43
40	2/7/2018	3	35 47.98 N	149 25.50 W	1	27	<7	<10	<16	<43
41	3/7/2018	4	35 09.01 N	148 10.42 W	1	92	QL	<10	<16	<43
42	5/7/2018	5	36 45.93 N	144 22.98 W	1	18	QL	<10	<16	<43
43	6/7/2018	6	38 09.38 N	142 14.32 W	1	29	QL	<10	<16	<43
44	7/7/2018	7	40 01.91 N	139 48.98 W	1	66	<7	<10	<16	<43
45	8/7/2018	8	42 02.31 N	137 39.53W	1	273	317	95	51	<43
46	9/7/2018	9	43 45.23 N	135 22.20 W	1	147	99	46	29	<43
47	10/7/2018	10	45 37.31 N	133 04.74W	1	72	<7	14	<16	<43

Table B.3 Continued

		Sampling Location								
ID	Date	Station	Latitude	Longitude	Depth (m)	PFTA	PFBS	PFPeS	PFHxS	PFHpS
1	31/4/2017	1	34 11.82 N	76 24.67 W	1	<15	QL	<10	12	<39
2	31/4/2017	1	34 11.82 N	76 24.67 W	23	<15	28	<10	21	<39
3	1/5/2017	2	33 59.40 N	76 06.55 W	5	<35	<64	<2	QH	<20
4	1/5/2017	2	33 59.40 N	76 06.55 W	75	<35	<64	<2	QL	<20
5	1/5/2017	2	33 59.40 N	76 06.55 W	405	<35	<64	<2	QH	<20
6	1/5/2017	4	33 06.67 N	76 28.39 W	10	<15	<17	<10	<8	<39
7	1/5/2017	4	33 06.67 N	76 28.39 W	100	<15	QL	<10	<8	<39
8	1/5/2017	4	33 06.67 N	76 28.39 W	728	<15	<17	<10	<8	<39
9	2/5/2017	6	30 12.43 N	76 28.85 W	1	<15	<17	<10	QH	<39
10	2/5/2017	6	30 12.43 N	76 28.85 W	3500	<15	<17	<10	<8	<39
11	2/5/2017	6	30 12.43 N	76 28.85 W	3000	<15	<17	<10	<8	<39
12	2/5/2017	6	30 12.43 N	76 28.85 W	2500	<15	<17	<10	<8	<39
13	2/5/2017	6	30 12.43 N	76 28.85 W	2000	<15	<17	<10	<8	<39
14	2/5/2017	6	30 12.43 N	76 28.85 W	1500	<15	<17	<10	<8	<39
15	2/5/2017	6	30 12.43 N	76 28.85 W	880	<15	<17	<10	<8	<39
16	2/5/2017	6	30 12.43 N	76 28.85 W	660	<15	<17	<10	<8	<39
17	2/5/2017	6	30 12.43 N	76 28.85 W	500	<15	QL	<10	13	<39
18	2/5/2017	6	30 12.43 N	76 28.85 W	300	<15	<17	<10	<8	<39
19	2/5/2017	6	30 12.43 N	76 28.85 W	120	<15	<17	<10	<8	<39
20	2/5/2017	6	30 12.43 N	76 28.85 W	90	<15	<17	<10	10	<39
21	2/5/2017	6	30 12.43 N	76 28.85 W	50	<15	<17	<10	<8	<39
22	2/5/2017	6	30 12.43 N	76 28.85 W	3930	<15	<17	<10	<8	<39
23	3/5/2017	8	29 28.73 N	76 36.72 W	10	<15	<17	<10	<8	<39
24	3/5/2017	8	29 28.73 N	76 36.72 W	120	<15	<17	<10	<8	<39
25	3/5/2017	8	29 28.73 N	76 36.72 W	1000	<15	<17	<10	<8	<39
26	3/5/2017	9	28 52.05 N	77 41.17 W	50	<35	<64	<2	QH	<20
27	3/5/2017	9	28 52.05 N	77 41.17 W	150	<35	<64	<2	QH	<20
28	3/5/2017	9	28 52.05 N	77 41.17 W	450	<35	<64	QH	QL	<20
29	3/5/2017	11	27 35.29 N	79 40.59 W	508	<15	<17	<10	<8	<39
30	3/5/2017	11	27 35.29 N	79 40.59 W	400	<15	<17	<10	<8	<39
31	3/5/2017	11	27 35.29 N	79 40.59 W	300	<15	<17	<10	11	<39
32	3/5/2017	11	27 35.29 N	79 40.59 W	200	<15	<17	<10	<8	<39
33	3/5/2017	11	27 35.29 N	79 40.59 W	100	<15	64	<10	23	<39
34	3/5/2017	11	27 35.29 N	79 40.59 W	75	<15	<17	<10	<8	<39
35	3/5/2017	11	27 35.29 N	79 40.59 W	50	<15	<17	<10	<8	<39
36	3/5/2017	11	27 35.29 N	79 40.59 W	5	<15	<17	<10	<8	<39
37	4/5/2017	S/U	27 32.93 N	79 52.12 W	8	<15	<17	<10	12	<39
38	30/6/18	1	32 01.12 N	152 32.12W	1	32	<17	15	54	QH
39	1/7/2018	2	33 36.79 N	150 49.69 W	1	<15	<17	<10	QH	QH
40	2/7/2018	3	35 47.98 N	149 25.50 W	1	<15	<17	<10	<8	<39
41	3/7/2018	4	35 09.01 N	148 10.42 W	1	QL	QH	<10	9	<39
42	5/7/2018	5	36 45.93 N	144 22.98 W	1	<15	<17	<10	<8	<39
43	6/7/2018	6	38 09.38 N	142 14.32 W	1	<15	QL	<10	<8	<39
44	7/7/2018	7	40 01.91 N	139 48.98 W	1	<15	<17	<10	<8	QH
45	8/7/2018	8	42 02.31 N	137 39.53W	1	24	QH	119	<8	QH
46	9/7/2018	9	43 45.23 N	135 22.20 W	1	<15	QH	<10	QH	<39
47	10/7/2018	10	45 37.31 N	133 04.74W	1	<15	<17	75	<8	<39

Table B.3 Continued

		Sampling Location									
ID	Date	Station	Latitude	Longitude	Depth (m)	PFOS	PFNS	PFDS	4:2FtS	6:2FtS	8:2FtS
1	31/4/2017	1	34 11.82 N	76 24.67 W	1	137	<6	<6	<6	QL	<5
2	31/4/2017	1	34 11.82 N	76 24.67 W	23	38	<6	<6	<6	36	<5
3	1/5/2017	2	33 59.40 N	76 06.55 W	5	31	<19	<2	QH	QH	<18
4	1/5/2017	2	33 59.40 N	76 06.55 W	75	26	<19	<2	QH	12	<18
5	1/5/2017	2	33 59.40 N	76 06.55 W	405	14	<19	<2	<2	QH	<18
6	1/5/2017	4	33 06.67 N	76 28.39 W	10	15	<6	<6	<6	<5	<5
7	1/5/2017	4	33 06.67 N	76 28.39 W	100	17	<6	<6	<6	22	<5
8	1/5/2017	4	33 06.67 N	76 28.39 W	728	19	<6	<6	<6	116	<5
9	2/5/2017	6	30 12.43 N	76 28.85 W	1	63	<6	<6	<6	32	<5
10	2/5/2017	6	30 12.43 N	76 28.85 W	3500	18	<6	<6	<6	<5	<5
11	2/5/2017	6	30 12.43 N	76 28.85 W	3000	15	<6	<6	<6	<5	<5
12	2/5/2017	6	30 12.43 N	76 28.85 W	2500	16	<6	<6	<6	22	<5
13	2/5/2017	6	30 12.43 N	76 28.85 W	2000	10	<6	<6	<6	22	<5
14	2/5/2017	6	30 12.43 N	76 28.85 W	1500	13	<6	<6	<6	<5	<5
15	2/5/2017	6	30 12.43 N	76 28.85 W	880	21	<6	<6	<6	<5	<5
16	2/5/2017	6	30 12.43 N	76 28.85 W	660	21	<6	<6	<6	QH	<5
17	2/5/2017	6	30 12.43 N	76 28.85 W	500	26	<6	<6	<6	8	<5
18	2/5/2017	6	30 12.43 N	76 28.85 W	300	25	<6	<6	<6	7	<5
19	2/5/2017	6	30 12.43 N	76 28.85 W	120	18	<6	<6	<6	<5	<5
20	2/5/2017	6	30 12.43 N	76 28.85 W	90	19	<6	<6	<6	<5	<5
21	2/5/2017	6	30 12.43 N	76 28.85 W	50	25	<6	<6	<6	<5	<5
22	2/5/2017	6	30 12.43 N	76 28.85 W	3930	11	<6	<6	<6	<5	<5
23	3/5/2017	8	29 28.73 N	76 36.72 W	10	24	<6	<6	<6	189	<5
24	3/5/2017	8	29 28.73 N	76 36.72 W	120	19	<6	<6	<6	36	<5
25	3/5/2017	8	29 28.73 N	76 36.72 W	1000	13	<6	<6	<6	QL	<5
26	3/5/2017	9	28 52.05 N	77 41.17 W	50	38	<19	<2	QH	<3	<18
27	3/5/2017	9	28 52.05 N	77 41.17 W	150	38	<19	<2	QH	QH	<18
28	3/5/2017	9	28 52.05 N	77 41.17 W	450	35	<19	<2	<2	<3	<18
29	3/5/2017	11	27 35.29 N	79 40.59 W	508	13	<6	<6	<6	15	<5
30	3/5/2017	11	27 35.29 N	79 40.59 W	400	26	<6	<6	<6	QH	<5
31	3/5/2017	11	27 35.29 N	79 40.59 W	300	28	<6	<6	<6	<5	<5
32	3/5/2017	11	27 35.29 N	79 40.59 W	200	25	<6	<6	<6	<5	<5
33	3/5/2017	11	27 35.29 N	79 40.59 W	100	64	<6	<6	<6	<5	<5
34	3/5/2017	11	27 35.29 N	79 40.59 W	75	28	<6	<6	<6	12	<5
35	3/5/2017	11	27 35.29 N	79 40.59 W	50	20	<6	<6	<6	28	<5
36	3/5/2017	11	27 35.29 N	79 40.59 W	5	28	<6	<6	<6	<5	<5
37	4/5/2017	S/U	27 32.93 N	79 52.12 W	8	55	<6	<6	<6	14	<5
38	30/6/18	1	32 01.12 N	152 32.12W	1	732	<6	<6	<6	318	98
39	1/7/2018	2	33 36.79 N	150 49.69 W	1	98	<6	<6	<6	QL	<5
40	2/7/2018	3	35 47.98 N	149 25.50 W	1	<1.4	<6	<6	<6	QH	<5
41	3/7/2018	4	35 09.01 N	148 10.42 W	1	42	<6	<6	<6	348	QL
42	5/7/2018	5	36 45.93 N	144 22.98 W	1	3	<6	<6	<6	QH	<5
43	6/7/2018	6	38 09.38 N	142 14.32 W	1	2	<6	<6	<6	<5	<5
44	7/7/2018	7	40 01.91 N	139 48.98 W	1	27	<6	<6	<6	QL	<5
45	8/7/2018	8	42 02.31 N	137 39.53W	1	81	<6	<6	<6	470	<5
46	9/7/2018	9	43 45.23 N	135 22.20 W	1	66	<6	<6	QL	196	<5
47	10/7/2018	10	45 37.31 N	133 04.74W	1	17	<6	<6	<6	42	<5

Table B.3 Continued

		Sampling Location							
ID	Date	Station	Latitude	Longitude	Depth (m)	FOSA	N-MeFOSAA	N-EtFOSAA	NaDONA
1	31/4/2017	1	34 11.82 N	76 24.67 W	1	<4	QH	<5	<2
2	31/4/2017	1	34 11.82 N	76 24.67 W	23	<4	<3	7	<2
3	1/5/2017	2	33 59.40 N	76 06.55 W	5	<2	<41	QL	<2
4	1/5/2017	2	33 59.40 N	76 06.55 W	75	<2	<41	QH	QH
5	1/5/2017	2	33 59.40 N	76 06.55 W	405	<2	<41	QH	<2
6	1/5/2017	4	33 06.67 N	76 28.39 W	10	<4	<3	<5	<2
7	1/5/2017	4	33 06.67 N	76 28.39 W	100	<4	<3	9	<2
8	1/5/2017	4	33 06.67 N	76 28.39 W	728	<4	4	<5	<2
9	2/5/2017	6	30 12.43 N	76 28.85 W	1	<4	<3	<5	<2
10	2/5/2017	6	30 12.43 N	76 28.85 W	3500	<4	<3	<5	<2
11	2/5/2017	6	30 12.43 N	76 28.85 W	3000	<4	<3	<5	<2
12	2/5/2017	6	30 12.43 N	76 28.85 W	2500	<4	<3	<5	<2
13	2/5/2017	6	30 12.43 N	76 28.85 W	2000	<4	<3	<5	<2
14	2/5/2017	6	30 12.43 N	76 28.85 W	1500	<4	<3	<5	<2
15	2/5/2017	6	30 12.43 N	76 28.85 W	880	<4	<3	<5	<2
16	2/5/2017	6	30 12.43 N	76 28.85 W	660	<4	<3	<5	<2
17	2/5/2017	6	30 12.43 N	76 28.85 W	500	<4	<3	<5	<2
18	2/5/2017	6	30 12.43 N	76 28.85 W	300	<4	<3	<5	<2
19	2/5/2017	6	30 12.43 N	76 28.85 W	120	<4	<3	<5	<2
20	2/5/2017	6	30 12.43 N	76 28.85 W	90	<4	<3	<5	<2
21	2/5/2017	6	30 12.43 N	76 28.85 W	50	<4	<3	<5	<2
22	2/5/2017	6	30 12.43 N	76 28.85 W	3930	<4	<3	<5	<2
23	3/5/2017	8	29 28.73 N	76 36.72 W	10	5	<3	<5	<2
24	3/5/2017	8	29 28.73 N	76 36.72 W	120	<4	<3	<5	<2
25	3/5/2017	8	29 28.73 N	76 36.72 W	1000	<4	<3	<5	<2
26	3/5/2017	9	28 52.05 N	77 41.17 W	50	<2	<41	QL	<2
27	3/5/2017	9	28 52.05 N	77 41.17 W	150	<2	<41	QL	<2
28	3/5/2017	9	28 52.05 N	77 41.17 W	450	<2	<41	<2	<2
29	3/5/2017	11	27 35.29 N	79 40.59 W	508	<4	<3	<5	<2
30	3/5/2017	11	27 35.29 N	79 40.59 W	400	<4	<3	<5	<2
31	3/5/2017	11	27 35.29 N	79 40.59 W	300	<4	<3	<5	<2
32	3/5/2017	11	27 35.29 N	79 40.59 W	200	<4	<3	<5	<2
33	3/5/2017	11	27 35.29 N	79 40.59 W	100	<4	<3	<5	<2
34	3/5/2017	11	27 35.29 N	79 40.59 W	75	<4	<3	25	<2
35	3/5/2017	11	27 35.29 N	79 40.59 W	50	<4	<3	<5	<2
36	3/5/2017	11	27 35.29 N	79 40.59 W	5	<4	<3	<5	<2
37	4/5/2017	S/U	27 32.93 N	79 52.12 W	8	<4	<3	<5	<2
38	30/6/18	1	32 01.12 N	152 32.12W	1	<4	QL	QL	<2
39	1/7/2018	2	33 36.79 N	150 49.69 W	1	<4	QH	6	<2
40	2/7/2018	3	35 47.98 N	149 25.50 W	1	<4	QL	<5	<2
41	3/7/2018	4	35 09.01 N	148 10.42 W	1	<4	13	<5	<2
42	5/7/2018	5	36 45.93 N	144 22.98 W	1	<4	4	<5	<2
43	6/7/2018	6	38 09.38 N	142 14.32 W	1	<4	<3	<5	<2
44	7/7/2018	7	40 01.91 N	139 48.98 W	1	<4	<3	QL	<2
45	8/7/2018	8	42 02.31 N	137 39.53W	1	<4	6	10	<2
46	9/7/2018	9	43 45.23 N	135 22.20 W	1	<4	7	<5	<2
47	10/7/2018	10	45 37.31 N	133 04.74W	1	<4	<3	<5	<2

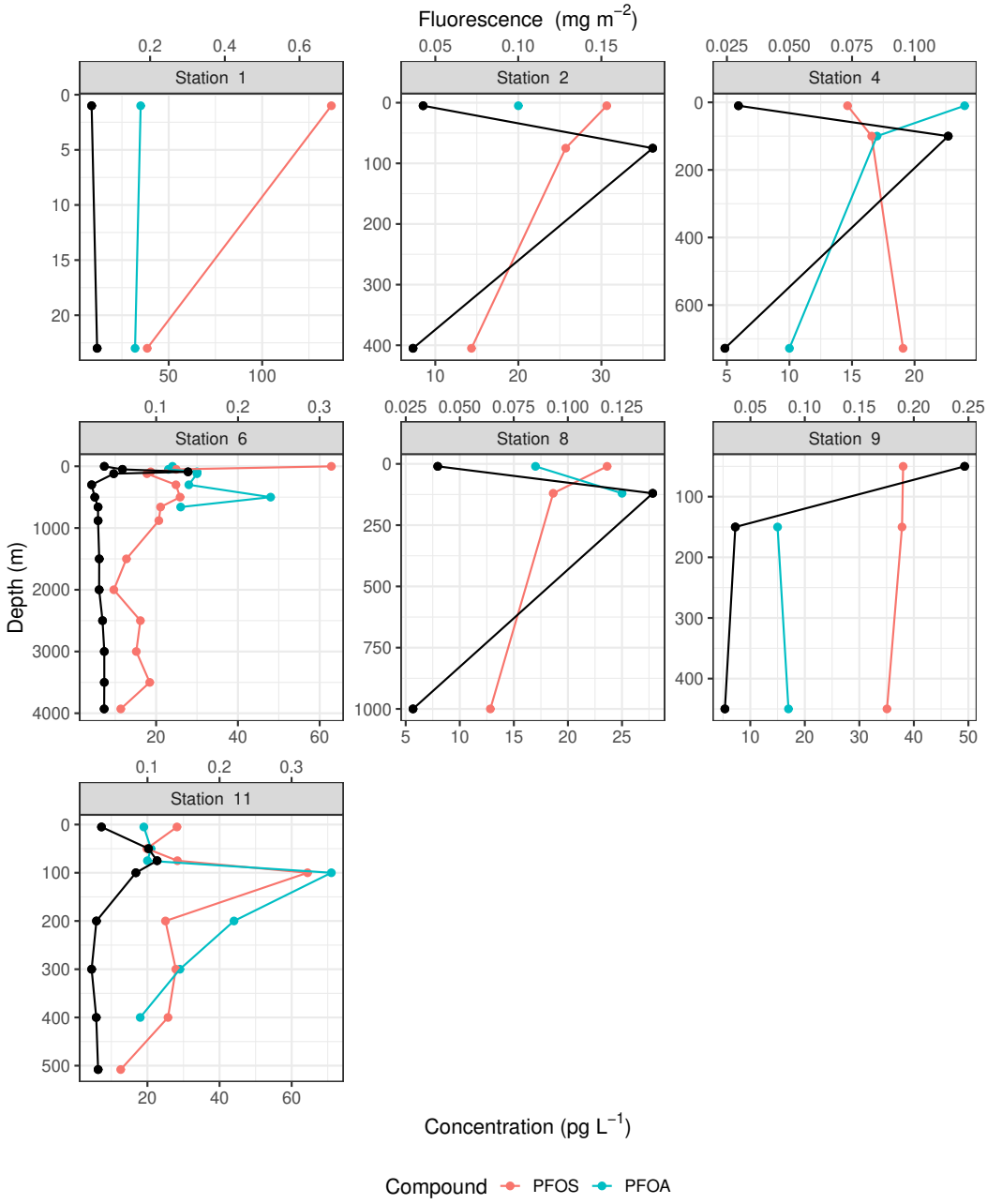

Figure B.2: Vertical profiles of PFOS and PFOA concentration in samples collected on the R/V Endeavor in 2017 and fluorescence (in black) at corresponding depths. Note different scale used for fluorescence. Connecting lines between samples >MDL are for visualization purposes only.

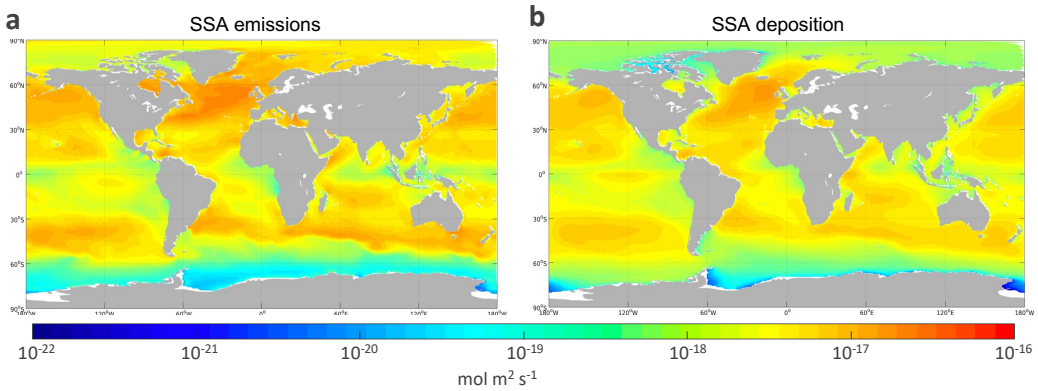

Figure B.3: Modeled (a) emission and (b) deposition flux with SSA (ca. 2015). Fluxes are indicated in $\log_{10}$-scale.

Chapter 3

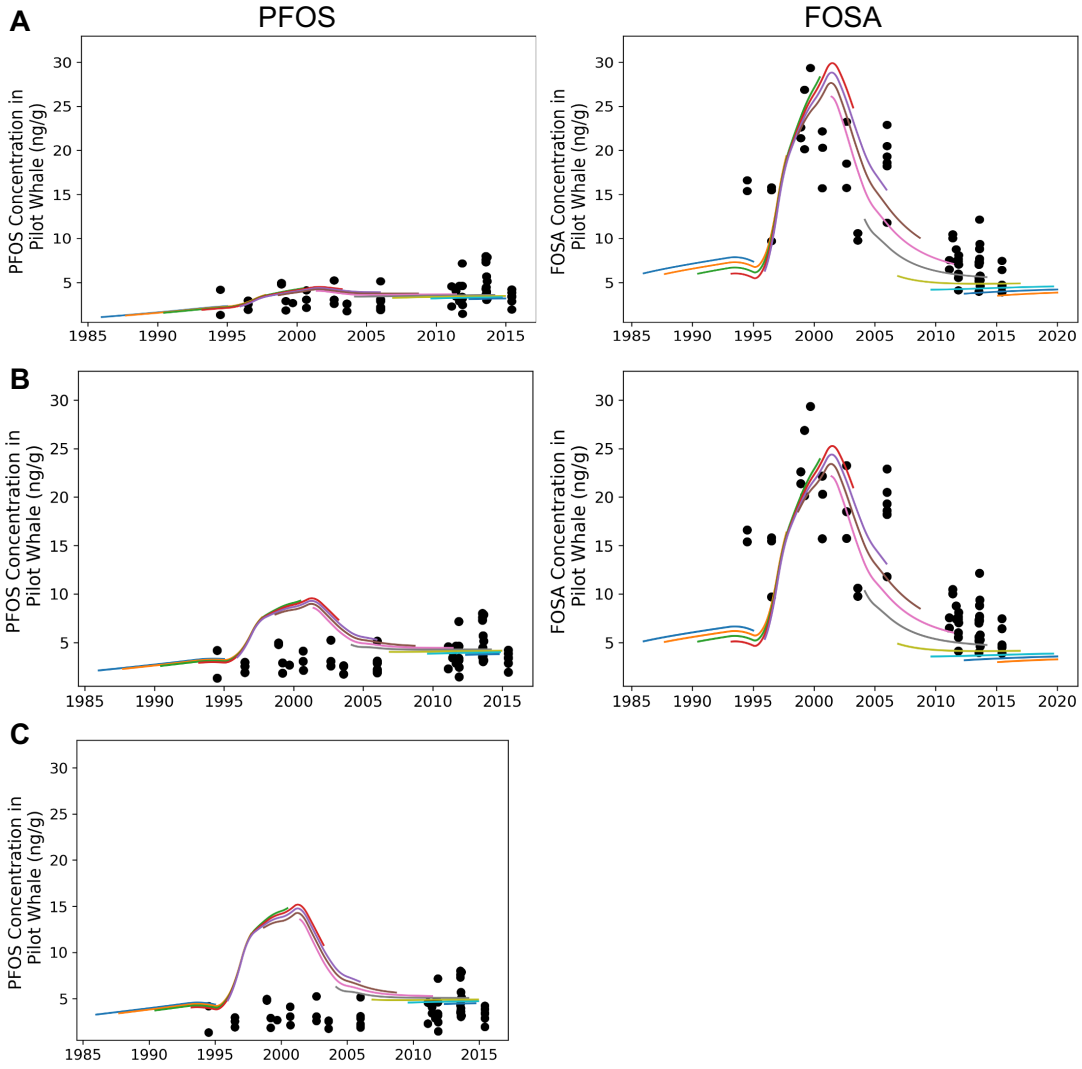

Figure C.1: Modeled concentrations of perfluorooctane sulfonamide (FOSA) and perfluorooctane sulfonate (PFOS) in whales with (a) 5%, (b) 20% and (c) 100% biotransformation in fish. FOSA concentrations in Panel C) are not shown since all FOSA is biotransformed to PFOS in this scenario.

Bibliography

[1] Abramowicz, D. (1990). Aerobic and anaerobic biodegradation of PCBs: A review. *Critical Reviews in Biotechnology*, 10(3), 241–251.

[2] Adams, R. G., Lohmann, R., Fernandez, L. A., & MacFarlane, J. K. (2007). Polyethylene devices: Passive samplers for measuring dissolved hydrophobic organic compounds in aquatic environments. *Environmental Science & Technology*, 41(4), 1317–1323.

[3] Ahrens, L., Barber, J. L., Xie, Z., & Ebinghaus, R. (2009). Longitudinal and latitudinal distribution of perfluoroalkyl compounds in the surface water of the Atlantic Ocean. *Environmental Science & Technology*, 43(9), 3122–3127.

[4] Ahrens, L., Gerwinski, W., Theobald, N., & Ebinghaus, R. (2010a). Sources of polyfluoroalkyl compounds in the North Sea, Baltic Sea and Norwegian Sea: Evidence from their spatial distribution in surface water. *Marine Pollution Bulletin*, 60(2), 255–260.

[5] Ahrens, L., Shoeib, M., Del Vento, S., Codling, G., & Halsall, C. (2011). Polyfluoroalkyl compounds in the Canadian Arctic atmosphere. *Environmental Chemistry*, 8(4), 399–406.

[6] Ahrens, L., Xie, Z., & Ebinghaus, R. (2010b). Distribution of perfluoroalkyl compounds in seawater from Northern Europe, Atlantic Ocean, and Southern Ocean. *Chemosphere*, 78(8), 1011–1016.

[7] AMAP (2016a). AMAP assessment 2015: Temporal trends in persistent organic pollutants in the Arctic. *Arctic Monitoring and Assessment Programme (AMAP)*, (pp. vi+71).

[8] AMAP (2016b). Influence of climate change on transport, levels, and effects of contaminants in northern areas – part 2. By: P. Carlsson, J. H. Christensen, K. Borgå, R. Kallenborn, K. Aspmo Pfaffhuber, J. Ø. Odland, L.-O. Reiersen, and J.F. Pawlak. (pp.52).

[9] Armitage, J. M., Schenker, U., Martin, J., Scheringer, M., Macleod, M., & Cousins, I. T. (2009). Modeling the global fate and transport of perfluorooctane sulfonate (PFOS) and precursor compounds in relation to temporal trends in wildlife exposure. *Environmental Science & Technology*, 43(24), 9274–80.

[10] Armitage, J. M. & Wania, F. (2013). Exploring the potential influence of climate change and particulate organic carbon scenarios on the fate of neutral organic contaminants in the Arctic environment. *Environmental Science: Processes & Impacts*, 15, 2263–2272.

[11] Arnot, J. A. & Gobas, F. A. P. C. (2004). A food web bioaccumulation model for organic chemicals in aquatic ecosystems. *Environmental Toxicology and Chemistry*, 23(10), 2343–2355.

[12] Arrigo, K. R. & van Dijken, G. L. (2011). Secular trends in Arctic ocean net primary production. *Journal of Geophysical Research: Oceans*, 116(C9).

[13] Axelman, J. & Gustafsson, O. (2002). Global sinks of PCBs: A critical assessment of the vapor-phase hydroxy radical sink emphasizing field diagnostics and model assumptions. *Global Biogeochemical Cycles*, 16(4), 58–1–58–13.

[14] Bengtson Nash, S., Rintoul, S. R., Kawaguchi, S., Staniland, I., Hoff, J. v. d., Tierney, M., & Bossi, R. (2010). Perfluorinated compounds in the antarctic region: Ocean circulation provides prolonged protection from distant sources. *Environmental Pollution*, 158(9), 2985–2991.

[15] Benskin, J. P., Muir, D. C. G., Scott, B. F., Spencer, C., De Silva, A. O., Kylin, H., Martin, J. W., Morris, A., Lohmann, R., Tomy, G., Rosenberg, B., Taniyasu, S., & Yamashita, N. (2012). Perfluoroalkyl acids in the Atlantic and Canadian Arctic Oceans. *Environmental Science & Technology*, 46(11), 5815–5823.

[16] Berrojalbiz, N., Dachs, J., Del Vento, S., Ojeda, M. J., Valle, M. C., Castro-Jiménez, J., Mariani, G., Wollgast, J., & Hanke, G. (2011). Persistent organic pollutants in Mediterranean seawater and processes affecting their accumulation in plankton. *Environmental Science & Technology*, 45(10), 4315–4322.

[17] Bjerregaard-Olesen, C., Bach, C. C., Long, M., Ghisari, M., Bossi, R., Bech, B. H., Nohr, E. A., Henriksen, T. B., Olsen, J., & Bonefeld-Jørgensen, E. C. (2016). Time trends of perfluorinated alkyl acids in serum from danish pregnant women 2008–2013. *Environment International*, 91, 14–21.

[18] Booij, K., van Bommel, R., van Aken, H. M., van Haren, H., Brummer, G.-J. A., & Ridderinkhof, H. (2014). Passive sampling of nonpolar contaminants at three deep-ocean sites. *Environmental Pollution*, 195, 101–108.

[19] Boyd, P. W. & Trull, T. W. (2007). Understanding the export of biogenic particles in oceanic waters: Is there consensus? *Progress in Oceanography*, 72(4), 276–312.

[20] Brandsma, S. H., Smithwick, M., Solomon, K., Small, J., de Boer, J., & Muir, D. C. G. (2011). Dietary exposure of rainbow trout to 8:2 and 10:2 fluorotelomer alcohols and perfluorooctanesulfonamide: Uptake, transformation and elimination. *Chemosphere*, 82(2), 253–258.

[21] Breivik, K., Sweetman, A., Pacyna, J. M., & Jones, K. C. (2002). Towards a global historical emission inventory for selected PCB congeners — a mass balance approach: 2. emissions. *Science of the Total Environment*, 290(1–3), 199–224.

[22] Breivik, K., Sweetman, A., Pacyna, J. M., & Jones, K. C. (2007). Towards a global historical emission inventory for selected PCB congeners — a mass balance approach 3. an update. *Science of the Total Environment*, 377(2-3), 296–307.

[23] Brouwer, A., Ahlborg, U. G., Rolaf van Leeuwen, F. X., Mark Feeley, M., G. Ahlborg, U., Beck, H., Brouwer, B., Carlsen, A., Feeley, M., Helge, H., Larsen, J.-J., Larsen, J. C., Larsen, E., Neubert, D., Rolaf van Leeuwen, F. X., & Younes, M. (1998). Report of the who working group on the assessment of health risks for human infants from exposure to PCDDS, PCDFS and PCBs. *Chemosphere*, 37(9), 1627–1643.

[24] Brouwer, A., Longnecker, M. P., Birnbaum, L. S., Cogliano, J., Kostyniak, P., Moore, J., Schantz, S., & Winneke, G. (1999). Characterization of potential endocrine-related health effects at low-dose levels of exposure to PCBs. *Environmental Health Perspectectives*, 107, 639–649.

[25] Brumovský, M., Karásková, P., Borghini, M., & Nizzetto, L. (2016). Per- and polyfluoroalkyl substances in the Western Mediterranean Sea waters. *Chemosphere*, 159, 308–316.

[26] Brusseau, M. L. (2018). Assessing the potential contributions of additional retention processes to PFAS retardation in the subsurface. *Science of The Total Environment*, 613-614, 176–185.

[27] Buck, R. C., Franklin, J., Berger, U., Conder, J. M., Cousins, I. T., de Voogt, P., Jensen, A. A., Kannan, K., Mabury, S. A., & van Leeuwen, S. P. J. (2011). Perfluoroalkyl and polyfluoroalkyl substances in the environment: Terminology, classification, and origins. *Integrated Environmental Assessment and Management*, 7(4), 513–541.

[28] Burkhard, L. P. (2000). Estimating dissolved organic carbon partition coefficients for nonionic organic chemicals. *Environmental Science & Technology*, 34(22), 4663–4668.

[29] Busch, J., Ahrens, L., Xie, Z., Sturm, R., & Ebinghaus, R. (2010). Polyfluoroalkyl compounds in the East Greenland Arctic Ocean. *Journal of Environmental Monitoring*, 12(6), 1242–1246.

[30] Cai, M., Zhao, Z., Yin, Z., Ahrens, L., Huang, P., Cai, M., Yang, H., He, J., Sturm, R., Ebinghaus, R., & Xie, Z. (2012). Occurrence of perfluoroalkyl compounds in surface waters from the North Pacific to the Arctic Ocean. *Environmental Science & Technology*, 46(2), 661–668.

[31] Carr, M.-E., Friedrichs, M. A. M., Schmeltz, M., Noguchi Aita, M., Antoine, D., Arrigo, K. R., Asanuma, I., Aumont, O., Barber, R., Behrenfeld, M., Bidigare, R., Buitenhuis, E. T., Campbell, J., Ciotti, A., Dierssen, H., Dowell, M., Dunne, J., Esaias, W., Gentili, B., Gregg, W., Groom, S., Hoepffner, N., Ishizaka, J., Kameda, T., Le Quéré, C., Lohrenz, S., Marra, J., Mélin, F., Moore, K., Morel, A., Reddy, T. E., Ryan, J., Scardi, M., Smyth, T., Turpie, K., Tilstone, G., Waters, K., & Yamanaka, Y. (2006). A comparison of global estimates of marine primary production from ocean color. *Deep Sea Research Part II: Topical Studies in Oceanography*, 53(5), 741–770.

[32] Casas, G., Martínez-Varela, A., Roscales, J. L., Vila-Costa, M., Dachs, J., & Jiménez, B. (2020). Enrichment of perfluoroalkyl substances in the sea-surface microlayer and sea-spray aerosols in the southern ocean. *Environmental Pollution*, 267, 115512.

[33] Chan, H. M., Fediuk, K., Hamilton, S., Rostas, L., Caughey, A., Kuhnlein, H., Egeland, G., & Loring, E. (2006). Food security in Nunavut, Canada: barriers and recommendations. *International Journal of Circumpolar Health*, 65(5), 416–431.

[34] Chen, M., Qiang, L., Pan, X., Fang, S., Han, Y., & Zhu, L. (2015). In vivo and in vitro isomer-specific biotransformation of perfluorooctane sulfonamide in common carp (*cyprinus carpio*). *Environmental Science & Technology*, 49(23), 13817–13824.

[35] Chiou, C. T. (1985). Partition coefficients of organic compounds in lipid-water systems and correlations with fish bioconcentration factors. *Environmental Science & Technology*, 19(1), 57–62.

[36] Coggan, T. L., Moodie, D., Kolobaric, A., Szabo, D., Shimeta, J., Crosbie, N. D., Lee, E., Fernandes, M., & Clarke, B. O. (2019). An investigation into per- and polyfluoroalkyl substances (PFAS) in nineteen australian wastewater treatment plants (WWTPs). *Heliyon*, 5(8), e02316.

[37] Corsolini, S. & Sarà, G. (2017). The trophic transfer of persistent pollutants (HCB, DDTs, PCBs) within polar marine food webs. *Chemosphere*, 177, 189–199.

[38] Cousins, I. T., Kong, D., & Vestergren, R. (2011). Reconciling measurement and modelling studies of the sources and fate of perfluorinated carboxylates. *Environmental Chemistry*, 8(4), 339–354.

[39] Cousins, I. T., Ng, C. A., Wang, Z., & Scheringer, M. (2019). Why is high persistence alone a major cause of concern? *Environmental Science: Processes & Impacts*, 21(5), 781–792.

[40] Cowan, D. F. (1966). Observations on the pilot whale *globicephala melaena*: Organweight and growth. *The Anatomical Record*, 155(4), 623–628.

[41] Dachs, J., Lohmann, R., Ockenden, W. A., Méjanelle, L., Eisenreich, S. J., & Jones, K. C. (2002). Oceanic biogeochemical controls on global dynamics of persistent organic pollutants. *Environmental Science & Technology*, 36(20), 4229–4237.

[42] Dam, M. & Bloch, D. (2000). Screening of mercury and persistent organochlorine pollutants in long-finned pilot whale (*globicephala melas*) in the Faroe Islands. *Marine Pollution Bulletin*, 40(12), 1090–1099.

[43] Dassuncao, C., Hu, X. C., Nielsen, F., Weihe, P., Grandjean, P., & Sunderland, E. M. (2018). Shifting global exposures to poly- and perfluoroalkyl substances (PFASs) evident in longitudinal birth cohorts from a seafood-consuming population. *Environmental Science & Technology*, 52(6), 3738–3747.

[44] Dassuncao, C., Pickard, H., Pfohl, M., Tokranov, A. K., Li, M., Mikkelsen, B., Slitt, A., & Sunderland, E. M. (2019). Phospholipid levels predict the tissue distribution of poly- and perfluoroalkyl substances in a marine mammal. *Environmental Science & technology letters*, 6(3), 119–125.

[45] Dassuncao, D., Hu, X. C., Zhang, X., Bossi, R., Mikkelsen, B., & Sunderland, E. M. (2017). Rapidly changing poly- and perfluoroalkyl substances in North Atlantic pilot whales indicate dominant contribution of atmospheric precursors to past exposures. *Environmental Science & Technology*.

[46] De Silva, A. O., Armitage, J. M., Bruton, T. A., Dassuncao, C., Heiger-Bernays, W., Hu, X. C., Kärrman, A., Kelly, B., Ng, C., Robuck, A., Sun, M., Webster, T. F., & Sunderland, E. M. (2021). PFAS exposure pathways for humans and wildlife: A synthesis of current knowledge and key gaps in understanding. *Environmental Toxicology and Chemistry*, 40(3), 631–657.

[47] Delworth, T. L., Zeng, F., Vecchi, G. A., Yang, X., Zhang, L., & Zhang, R. (2016). The North Atlantic oscillation as a driver of rapid climate change in the Northern Hemisphere. *Nature Geoscience*, 9, 509.

[48] Ding, Q., Schweiger, A., L'Heureux, M., Battisti, D. S., Po-Chedley, S., Johnson, N. C., Blanchard-Wrigglesworth, E., Harnos, K., Zhang, Q., Eastman, R., & Steig, E. J. (2017). Influence of high-latitude atmospheric circulation changes on summertime Arctic sea ice. *Nature Climate Change*, 7, 289.

[49] Dreyer, A., Weinberg, I., Temme, C., & Ebinghaus, R. (2009). Polyfluorinated compounds in the atmosphere of the Atlantic and Southern Oceans: Evidence for a global distribution. *Environmental Science & Technology*, 43(17), 6507–6514.

[50] Duce, R. A., Liss, P. S., Merrill, J. T., Atlas, E. L., Buat-Menard, P., Hicks, B. B., Miller, J. M., Prospero, J. M., Arimoto, R., Church, T. M., Ellis, W., Galloway, J. N., Hansen, L., Jickells,

T. D., Knap, A. H., Reinhardt, K. H., Schneider, B., Soudine, A., Tokos, J. J., Tsunogai, S., Wollast, R., & Zhou, M. (1991). The atmospheric input of trace species to the world ocean. *Global Biogeochemical Cycles*, 5(3), 193–259.

[51] Duinker, J. C., Schultz, D. E., & Petrick, G. (1988). Selection of chlorinated biphenyl congeners for analysis in environmental samples. *Marine Pollution Bulletin,*, 19(1), 19–25.

[52] Dutkiewicz, S., Follows, M. J., & Bragg, J. G. (2009). Modeling the coupling of ocean ecology and biogeochemistry. *Global Biogeochemical Cycles*, 23(4), GB4017.

[53] Dutkiewicz, S., Ward, B. A., Monteiro, F., & Follows, M. J. (2012). Interconnection of nitrogen fixers and iron in the Pacific Ocean: Theory and numerical simulations. *Global Biogeochemical Cycles*, 26(1), GB1012.

[54] Eakins, B. & Sharman, G. (2010). Volumes of the world's oceans from etopo1.

[55] Eckley, N. (2001). Traveling toxices — the science, policy, an management of persistent organic pollutants. *Environment: Science and Policy for Sustainable Development*, 43(7), 24–36.

[56] EFSA Panel on Contaminants in the Food Chain, Schrenk, D., B. M., Bodin, L., Chipman, J. K., del Mazo, J., Grasl-Kraupp, B., Hogstrand, C., Hoogenboom, L. R., Leblanc, J.-C., Nebbia, C., Nielsen, E., Ntzani, E., Petersen, A., Sand, S., Vleminckx, C., H, W., L, B., Ceccatelli, S., Cravedi, J. P., Halldorsson, T. I., Haug, L. S., Johansson, N., Knutsen, H., Rose, M., Roudot, A.-C., VanLoveren, H., Vollmer, G., Mackay, K., Riolo, F., & Schwerdtle, T. (2020). Scientific opinion on the risk to human health related to the presence of perfluoroalkyl substances in food. *EFSA Journal*, 18(6223).

[57] Ellis, D. A., Martin, J. W., Mabury, S. A., Hurley, M. D., Sulbaek Andersen, M. P., & Wallington, T. J. (2003). Atmospheric lifetime of fluorotelomer alcohols. *Environmental Science & Technology*, 37(17), 3816–3820.

[58] European Space Agency (2010). GlobCover 2009.

[59] Feigin, V. L., Vos, T., Nichols, E., Owolabi, M. O., Carroll, W. M., Dichgans, M., Deuschl, G., Parmar, P., Brainin, M., & Murray, C. (2020). The global burden of neurological disorders: translating evidence into policy. *Lancet Neurology*, 19(3), 255–265.

[60] Fielding, R. (2010). Environmental change as a threat to the pilot whale hunt in the Faroe Islands. *Polar Research*, 29(3), 430–438.

[61] Food & Agriculture Organisation of the United Nations, F. (2020). *State of the World Fisheries and Aquaculture Statistics*. Report.

[62] Forget, G., Campin, J. M., Heimbach, P., Hill, C. N., Ponte, R. M., & Wunsch, C. (2015a). ECCO version 4: An integrated framework for non-linear inverse modeling and global ocean state estimation. *Geoscientific Model Development*, 8(10), 3071–3104.

[63] Forget, G., Ferreira, D., & Liang, X. (2015b). On the observability of turbulent transport rates by ARGO: Supporting evidence from an inversion experiment. *Ocean Science*, 11(5), 839–853.

[64] Forget, G. & Ponte, R. M. (2015). The partition of regional sea level variability. *Progress in Oceanography,*, 137, 173–195.

[65] Friedman, C. L. & Selin, N. E. (2016). PCBs in the Arctic atmosphere: Determining important driving forces using a global atmospheric transport model. *Atmospheric Chemistry and Physics*, 16(5), 3433–3448.

[66] Friesen, K. J., Muir, D. C. G., & Webster, G. R. B. (1990). Evidence of sensitized photolysis of polychlorinated dibenzo-p-dioxins in natural waters under sunlight conditions. *Environmental Science & Technology*, 24(11), 1739–1744.

[67] Fuller, E. N., Schettler, P. D., & Giddings, J. C. (1966). New method for prediction of binary gas-phase diffusion coefficients. *Industrial & Engineering Chemistry*, 58(5), 18–27.

[68] Galatius, A., Bossi, R., Sonne, C., Rigét, F. F., Kinze, C. C., Lockyer, C., Teilmann, J., & Dietz, R. (2013). PFAS profiles in three north sea top predators: metabolic differences among species? *Environmental Science and Pollution Research*, 20(11), 8013–8020.

[69] Galbán-Malagón, C., Berrojalbiz, N., Ojeda, M.-J., & Dachs, J. (2012). The oceanic biological pump modulates the atmospheric transport of persistent organic pollutants to the Arctic. *Nature Communications*, 3, 862.

[70] Galbán-Malagón, C. J., Del Vento, S., Berrojalbiz, N., Ojeda, M.-J., & Dachs, J. (2013). Polychlorinated biphenyls, hexachlorocyclohexanes and hexachlorobenzene in seawater and phytoplankton from the southern ocean (weddell, south scotia, and bellingshausen seas). *Environmental Science & Technology*, 47(11), 5578–5587.

[71] Gallen, C., Eaglesham, G., Drage, D., Nguyen, T. H., & Mueller, J. F. (2018). A mass estimate of perfluoroalkyl substance (PFAS) release from australian wastewater treatment plants. *Chemosphere*, 208, 975–983.

[72] Gebbink, W. A., Bignert, A., & Berger, U. (2016). Perfluoroalkyl acids (PFAAs) and selected precursors in the Baltic Sea environment: Do precursors play a role in food web accumulation of PFAAs? *Environmental Science & Technology*, 50(12), 6354–6362.

[73] Gebbink, W. A., Glynn, A., & Berger, U. (2015a). Temporal changes (1997–2012) of perfluoroalkyl acids and selected precursors (including isomers) in swedish human serum. *Environmental Pollution*, 199, 166–173.

[74] Gebbink, W. A., Glynn, A., Darnerud, P. O., & Berger, U. (2015b). Perfluoroalkyl acids and their precursors in swedish food: The relative importance of direct and indirect dietary exposure. *Environmental Pollution*, 198, 108–115.

[75] Geospatial Information Authority of Japan (2011). Global map Japan version 2 vector data.

[76] Giesy, J. P. & Kannan, K. (2001). Global distribution of perfluorooctane sulfonate in wildlife. *Environmental Science & Technology*, 35(7), 1339–1342.

[77] Gioia, R., Lohmann, R., Dachs, J., Temme, C., Lakaschus, S., Schulz-Bull, D., Hand, I., & Jones, K. C. (2008a). Polychlorinated biphenyls in air and water of the North Atlantic and Arctic Ocean. *Journal of Geophysical Research: Atmospheres*, 113(D19), n/a–n/a.

[78] Gioia, R., Nizzetto, L., Lohmann, R., Dachs, J., Temme, C., & Jones, K. C. (2008b). Polychlorinated biphenyls (PCBs) in air and seawater of the Atlantic Ocean: Sources, trends and processes. *Environmental Science & Technology*, 42(5), 1416–1422.

[79] González-Gaya, B., Dachs, J., Roscales, J. L., Caballero, G., & Jiménez, B. (2014). Perfluoroalkylated substances in the global tropical and subtropical surface oceans. *Environmental Science & Technology*, 48(22), 13076–13084.

[80] Grandjean, P., Andersen, E. W., Budtz-Jørgensen, E., Nielsen, F., Mølbak, K., Weihe, P., & Heilmann, C. (2012). Serum vaccine antibody concentrations in children exposed to perfluorinated compounds. *JAMA*, 307(4), 391–397.

[81] Grandjean, P. & Budtz-Jørgensen, E. (2013). Immunotoxicity of perfluorinated alkylates: calculation of benchmark doses based on serum concentrations in children. *Environmental Health*, 12(1), 35.

[82] Grandjean, P., Heilmann, C., Weihe, P., Nielsen, F., Mogensen, U., Timmermann, C. A. G., & Budtz-Jørgensen, E. (2017a). *Estimated exposures to perfluorinated compounds in infancy predict attenuated vaccine antibody concentrations at age 5-years*, volume 14.

[83] Grandjean, P., Heilmann, C., Weihe, P., Nielsen, F., Mogensen, U. B., & Budtz-Jørgensen, E. (2017b). Serum vaccine antibody concentrations in adolescents exposed to perfluorinated compounds. *Environmental Health Perspectives*, 125(7).

[84] Grandjean, P., Heilmann, C., Weihe, P., Nielsen, F., Mogensen, U. B., Timmermann, A., & Budtz-Jørgensen, E. (2017c). Estimated exposures to perfluorinated compounds in infancy predict attenuated vaccine antibody concentrations at age 5-years. *Journal of Immunotoxicology*, 14(1), 188–195.

[85] Grandjean, P. & Landrigan, P. J. (2014). Neurobehavioural effects of developmental toxicity. *Lancet Neurology*, 13(3), 330–338.

[86] Gustafsson, O., Andersson, P., Axelman, J., Bucheli, T. D., Kömp, P., McLachlan, M. S., Sobek, A., & Thörngren, J. O. (2005). Observations of the PCB distribution within and in-between ice, snow, ice-rafted debris, ice-interstitial water, and seawater in the Barents Sea marginal ice zone and the North Pole area. *Environmental Science & Technology*, 342(1–3), 261–279.

[87] Gustafsson, O., Axelman, J., Broman, D., Eriksson, M., & Dahlgaard, H. (2001). Process-diagnostic patterns of chlorobiphenyl congeners in two radiochronologically characterized sediment cores from the northern Baffin Bay. *Chemosphere*, 45(6), 759–766.

[88] Gustafsson, O., Gschwend, P. M., & Buesseler, K. O. (1997). Settling removal rates of PCBs into the Northwestern Atlantic derived from ^{238}U–^{234}Th disequilibria. *Environmental Science & Technology*, 31(12), 3544–3550.

[89] Hansell, D. A., Carlson, C. A., Repeta, D. J., & Schlitzer, R. (2009). Dissolved organic matter in the ocean - a controversy stimulates new insights. *Oceanography*, 22(4), 202–211.

[90] Hansen, B., Østerhus, S., Turrell, W. R., Jónsson, S., Valdimarsson, H., Hátún, H., & Olsen, S. M. (2008). *The Inflow of Atlantic Water, Heat, and Salt to the Nordic Seas Across the Greenland–Scotland Ridge*, (pp. 15–43). Springer Netherlands: Dordrecht.

[91] Haukås, M., Berger, U., Hop, H., Gulliksen, B., & Gabrielsen, G. W. (2007). Bioaccumulation of per- and polyfluorinated alkyl substances (PFAS) in selected species from the barents sea food web. *Environmental Pollution*, 148(1), 360–371.

[92] Hawker, D. W. & Connell, D. W. (1988). Octanol-water partition coefficients of polychlorinated biphenyl congeners. *Environmental Science & Technology*, 22(4), 382–387.

[93] Helsel, D. R. (2011). *Computing Summary Statistics and Totals*, (pp. 62–98).

[94] Henson, S. A., Sanders, R., Madsen, E., Morris, P. J., Le Moigne, F., & Quartly, G. D. (2011). A reduced estimate of the strength of the ocean's biological carbon pump. *Geophysical Research Letters*, 38(4).

[95] Houde, M., Bujas, T. A. D., Small, J., Wells, R. S., Fair, P. A., Bossart, G. D., Solomon, K. R., & Muir, D. C. G. (2006). Biomagnification of perfluoroalkyl compounds in the bottlenose dolphin (*Tursiops truncatus*) food web. *Environmental Science & Technology*, 40(13), 4138–4144.

[96] Hung, H., Katsoyiannis, A. A., Brorström-Lundén, E., Olafsdottir, K., Aas, W., Breivik, K., Bohlin-Nizzetto, P., Sigurdsson, A., Hakola, H., Bossi, R., Skov, H., Sverko, E., Barresi, E., Fellin, P., & Wilson, S. (2016). Temporal trends of persistent organic pollutants (POPs) in Arctic air: 20 years of monitoring under the Arctic Monitoring and Assessment Programme (AMAP). *Environmental Pollution*, 217, 52–61.

[97] International Panel on Climate Change (IPCC) (2014). *Climate Change 2014: Synthesis Report. Contribution of Working Groups I, II and III to the Fifth Assessment Report of the Intergovernmental Panel on Climate Change [Core Writing Team: Pachauri, P. K. and Meyer, L. A. (eds.)]*. Geneva, Switzerland: IPCC, 151 pp.

[98] International Whaling Commission, I. (1993). *Biology of Northern Hemisphere Pilot Whales*. Report.

[99] ITTC (2006). *Recommended Procedures and Guidelines, Testing and Extrapolation Methods*. Report.

[100] Iudicone, D., Speich, S., Madec, G., & Blanke, B. (2008). The global conveyor belt from a southern ocean perspective. *Journal of Physical Oceanography*, 38(7), 1401–1425.

[101] Jamieson, A. J., Malkocs, T., Piertney, S. B., Fujii, T., & Zhang, Z. (2017). Bioaccumulation of persistent organic pollutants in the deepest ocean fauna. *Nature Ecology & Evolution*, 1, 0051.

[102] Joerss, H., Xie, Z., Wagner, C. C., von Appen, W.-J., Sunderland, E. M., & Ebinghaus, R. (2020). Transport of legacy perfluoroalkyl substances and the replacement compound HFPO-DA through the Atlantic gateway to the Arctic Ocean — Is the Arctic a sink or a source? *Environmental Science & Technology*, 54(16), 9958–9967.

[103] Johansson, J. H., Salter, M. E., Acosta Navarro, J. C., Leck, C., Nilsson, E. D., & Cousins, I. T. (2019). Global transport of perfluoroalkyl acids via sea spray aerosol. *Environmental Science: Processes & Impacts*, 21(4), 635–649.

[104] Johnson, M. T. (2010). A numerical scheme to calculate temperature and salinity dependent air-water transfer velocities for any gas. *Ocean Science*, 6(4), 913–932.

[105] Ju, X., Jin, Y., Sasaki, K., & Saito, N. (2008). Perfluorinated surfactants in surface, subsurface water and microlayer from Dalian coastal waters in China. *Environmental Science & Technology*, 42(10), 3538–3542.

[106] Jurado, E., Jaward, F. M., Lohmann, R., Jones, K. C., Simó, R., & Dachs, J. (2004). Atmospheric dry deposition of persistent organic pollutants to the Atlantic and inferences for the global oceans. *Environmental Science & Technology*, 38(21), 5505–5513.

[107] Jönsson, A., Gustafsson, O., Axelman, J., & Sundberg, H. (2003). Global accounting of PCBs in the continental shelf sediments. *Environmental Science & Technology*, 37(2), 245–255.

[108] Kannan, K., Corsolini, S., Falandysz, J., Fillmann, G., Kumar, K. S., Loganathan, B. G., Mohd, M. A., Olivero, J., Wouwe, N. V., Yang, J. H., & Aldous, K. M. (2004). Perfluorooctanesulfonate and related fluorochemicals in human blood from several countries. *Environmental Science & Technology*, 38(17), 4489–4495.

[109] Kelly, B. C., Ikonomou, M. G., Blair, J. D., Morin, A. E., & Gobas, F. A. P. C. (2007). Food web-specific biomagnification of persistent organic pollutants. *Science*, 317(5835), 236.

[110] Kwok, R., Cunningham, G. F., Wensnahan, M., Rigor, I., Zwally, H. J., & Yi, D. (2009). Thinning and volume loss of the arctic ocean sea ice cover: 2003–2008. *Journal of Geophysical Research: Oceans*, 114(C7), n/a–n/a.

[111] Laliberté, M. (2007). Model for calculating the viscosity of aqueous solutions. *Journal of Chemical & Engineering Data*, 52(2), 321–335.

[112] Lammel, G., Meixner, F. X., Vrana, B., Efstathiou, C. I., Kohoutek, J., Kukučka, P., Mulder, M. D., Přibylová, P., Prokeš, R., Rusina, T. P., Song, G. Z., & Tsapakis, M. (2016). Bidirectional air–sea exchange and accumulation of POPs (PAHs, PCBs, OCPs and PBDEs) in the nocturnal marine boundary layer. *Atmospheric chemistry and Physics*, 16(10), 6381–6393.

[113] Lammel, G. & Stemmler, I. (2012). Fractionation and current time trends of PCB congeners: evolvement of distributions 1950-2010 studied using a global atmosphere-ocean general circulation model. *Atmospheric Chemistry and Physics*, 12(15), 7199.

[114] Land, M., de Wit, C. A., Bignert, A., Cousins, I. T., Herzke, D., Johansson, J. H., & Martin, J. W. (2018). What is the effect of phasing out long-chain per- and polyfluoroalkyl substances on the concentrations of perfluoroalkyl acids and their precursors in the environment? A systematic review. *Environmental Evidence*, 7(1), 4.

[115] Landrigan, P. J., Fuller, R., Acosta, N. J. R., Adeyi, O., Arnold, R., Basu, N., Baldé, A. B., Bertollini, R., Bose-O'Reilly, S., Boufford, J. I., Breysse, P. N., Chiles, T., Mahidol, C., Coll-Seck, A. M., Cropper, M. L., Fobil, J., Fuster, V., Greenstone, M., Haines, A., Hanrahan, D., Hunter, D., Khare, M., Krupnick, A., Lanphear, B., Lohani, B., Martin, K., Mathiasen, K. V., McTeer, M. A., Murray, C. J. L., Ndahimananjara, J. D., Perera, F., Potočnik, J., Preker, A. S., Ramesh, J., Rockström, J., Salinas, C., Samson, L. D., Sandilya, K., Sly, P. D., Smith, K. R., Steiner, A., Stewart, R. B., Suk, W. A., van Schayck, O. C. P., Yadama, G. N., Yumkella, K., & Zhong, M. (2018). The lancet commission on pollution and health. *The Lancet*, 391(10119), 462–512.

[116] Lehner, B. & Grill, G. (2013). Global river hydrography and network routing: baseline data and new approaches to study the world's large river systems. *Hydrological Processes*, 27(15), 2171–2186.

[117] Letcher, R. J., Chu, S., McKinney, M. A., Tomy, G. T., Sonne, C., & Dietz, R. (2014). Comparative hepatic in vitro depletion and metabolite formation of major perfluorooctane sulfonate precursors in arctic polar bear, beluga whale, and ringed seal. *Chemosphere*, 112, 225–231.

[118] Li, J., Xie, Z., Mi, W., Lai, S., Tian, C., Emeis, K.-C., & Ebinghaus, R. (2017). Organophosphate esters in air, snow, and seawater in the North Atlantic and the Arctic. *Environmental Science & Technology*, 51(12), 6887–6896.

[119] Li, N., Wania, F., Lei, Y. D., & Daly, G. L. (2003). A comprehensive and critical compilation, evaluation, and selection of physical–chemical property data for selected polychlorinated biphenyls. *J. Phys. Chem. Ref. Data*, 32(4), 1545–1590.

[120] Lim, T. C., Wang, B., Huang, J., Deng, S., & Yu, G. (2011). Emission inventory for PFOS in China: review of past methodologies and suggestions. *TheScientificWorldJournal*, 11, 1963–1980.

[121] Liss, P. S. & Slater, P. G. (1974). Flux of gases across the air-sea interface. *Nature*, 247(5438), 181–184.

[122] Lohmann, R. & Belkin, I. M. (2014). Organic pollutants and ocean fronts across the Atlantic Ocean: A review. *Progress in Oceanography*, 128, 172–184.

[123] Lohmann, R., Breivik, K., Dachs, J., & Muir, D. (2007). Global fate of POPs: Current and future research directions. *Environmental Pollution*, 150(1), 150–165.

[124] Lohmann, R., Jaward, F. M., Durham, L., Barber, J. L., Ockenden, W., Jones, K. C., Bruhn, R., Lakaschus, S., Dachs, J., & Booij, K. (2004). Potential contamination of shipboard air samples by diffusive emissions of PCBs and other organic pollutants: Implications and solutions. *Environmental Science & Technology*, 38(14), 3965–3970.

[125] Lohmann, R., Klanova, J., Kukucka, P., Yonis, S., & Bollinger, K. (2012). PCBs and OCPs on a east-to-west transect: The importance of major currents and net volatilization for PCBs in the Atlantic Ocean. *Environmental Science & Technology*, 46(19), 10471–10479.

[126] Loi, E. I. H., Yeung, L. W. Y., Taniyasu, S., Lam, P. K. S., Kannan, K., & Yamashita, N. (2011). Trophic magnification of poly- and perfluorinated compounds in a subtropical food web. *Environmental Science & Technology*, 45(13), 5506–5513.

[127] Loose, B., McGillis, W. R., Perovich, D., Zappa, C. J., & Schlosser, P. (2014). A parameter model of gas exchange for the seasonal sea ice zone. *Ocean Science*, 10(1), 17–28.

[128] Lordan, C., Collins, M. A., Key, L. N., & Browne, E. D. (2001). The biology of the ommastrephid squid, *todarodes sagittatus*, in the North-East Atlantic. *Journal of the Marine Biological Association of the United Kingdom*, 81(2), 299–306.

[129] Löfstedt Gilljam, J., Leonel, J., Cousins, I. T., & Benskin, J. P. (2016a). Additions and correction to is ongoing sulfluramid use in South America a significant source of perfluorooctanesulfonate (PFOS)? production inventories, environmental fate, and local occurrence. *Environmental Science & Technology*, 50(14), 7930–7933.

[130] Löfstedt Gilljam, J., Leonel, J., Cousins, I. T., & Benskin, J. P. (2016b). Is ongoing sulfluramid use in South America a significant source of perfluorooctanesulfonate (PFOS)? production inventories, environmental fate, and local occurrence. *Environmental Science & Technology*, 50(2), 653–659.

[131] Macdonald, R. W., Harner, T., & Fyfe, J. (2005). Recent climate change in the arctic and its impact on contaminant pathways and interpretation of temporal trend data. *Science of The Total Environment*, 342(1–3), 5–86.

[132] MacInnis, J. J., French, K., Muir, D. C. G., Spencer, C., Criscitiello, A., De Silva, A. O., & Young, C. J. (2017). Emerging investigator series: a 14-year depositional ice record of perfluoroalkyl substances in the High Arctic. *Environmental Science: Processes & Impacts*, 19(1), 22–30.

[133] Mackay, D. & Paterson, S. (1991). Evaluating the multimedia fate of organic chemicals: a level iii fugacity model. *Environmental Science & Technology*, 25(3), 427–436.

[134] Mackay, D. & Wania, F. (1995). Transport of contaminants to the Arctic: partitioning, processes and models. *Science of the Total Environment*, 160, 25–38.

[135] Martin, J. W., Asher, B. J., Beesoon, S., Benskin, J. P., & Ross, M. S. (2010). PFOS or PreFOS? are perfluorooctane sulfonate precursors (prefos) important determinants of human and environmental perfluorooctane sulfonate (PFOS) exposure? *Journal of Environmental Monitoring*, 12(11), 1979–2004.

[136] Martin, J. W., Ellis, D. A., Mabury, S. A., Hurley, M. D., & Wallington, T. J. (2006). Atmospheric chemistry of perfluoroalkanesulfonamides: Kinetic and product studies of the oh radical and cl atom initiated oxidation of n-ethyl perfluorobutanesulfonamide. *Environmental Science & Technology*, 40(3), 864–872.

[137] McLachlan, M. S., Zou, H., & Gouin, T. (2017). Using benchmarking to strengthen the assessment of persistence. *Environmental Science & Technology*, 51(1), 4–11.

[138] Mejia Avendaño, S. & Liu, J. (2015). Production of pfos from aerobic soil biotransformation of two perfluoroalkyl sulfonamide derivatives. *Chemosphere*, 119, 1084–1090.

[139] Miaz, L. T., Plassmann, M. M., Gyllenhammar, I., Bignert, A., Sandblom, O., Lignell, S., Glynn, A., & Benskin, J. P. (2020). Temporal trends of suspect- and target-per/polyfluoroalkyl substances (PFAS), extractable organic fluorine (EOF) and total fluorine (TF) in pooled serum from first-time mothers in Uppsala, Sweden, 1996–2017. *Environmental Science: Processes & Impacts*, 22(4), 1071–1083.

[140] Mortensen, H. S., Pakkenberg, B., Dam, M., Dietz, R., Sonne, C., Mikkelsen, B., & Eriksen, N. (2014). Quantitative relationships in *delphinid neocortex*. *Frontiers in neuroanatomy*, 8, 132–132.

[141] Muir, D., Bossi, R., Carlsson, P., Evans, M., De Silva, A., Halsall, C., Rauert, C., Herzke, D., Hung, H., Letcher, R., Rigét, F., & Roos, A. (2019). Levels and trends of poly- and perfluoroalkyl substances in the arctic environment – an update. *Emerging Contaminants*, 5, 240–271.

[142] Muir, D. & Miaz, L. T. (2021). Spatial and temporal trends of perfluoroalkyl substances in global ocean and coastal waters. *Environmental Science & Technology*.

[143] Murakami, M., Imamura, E., Shinohara, H., Kiri, K., Muramatsu, Y., Harada, A., & Takada, H. (2008). Occurrence and sources of perfluorinated surfactants in rivers in Japan. *Environmental Science & Technology*, 42(17), 6566–6572.

[144] Nascimento, R. A., Nunoo, D. B. O., Bizkarguenaga, E., Schultes, L., Zabaleta, I., Benskin, J. P., Spanó, S., & Leonel, J. (2018). Sulfluramid use in Brazilian agriculture: A source of per- and polyfluoroalkyl substances (PFASs) to the environment. *Environmental Pollution*, 242, 1436–1443.

[145] National Bureau of Statistics of China (2013). 2010 Population Census.

[146] Nielsen, S. T., Mortensen, R., Katrin Hoydal, K., Erenbjerg, S., & Dam, M. (2012). *AMAP Faroe Islands Heavy Metals and POPs Core Programme 2009-2012*. Report, Environment Agency.

[147] Nightingale, P. D., Malin, G., Law, C. S., Watson, A. J., Liss, P. S., Liddicoat, M. I., Boutin, J., & Upstill-Goddard, R. C. (2000). In situ evaluation of air-sea gas exchange parameterizations using novel conservative and volatile tracers. *Global Biogeochemical Cycles*, 14(1), 373–387.

[148] Nizzetto, L., Lohmann, R., Gioia, R., Dachs, J., & Jones, K. C. (2010). Atlantic ocean surface waters buffer declining atmospheric concentrations of persistent organic pollutants. *Environmental Science & Technology*, 44(18), 6978–6984.

[149] Olsen, G. W., Burris, J. M., Ehresman, D. J., Froehlich, J. W., Seacat, A. M., Butenhoff, J. L., & Zobel, L. R. (2007a). Half-life of serum elimination of perfluorooctanesulfonate,perfluorohexanesulfonate, and perfluorooctanoate in retired fluorochemical production workers. *Environmental health perspectives*, 115(9), 1298–1305.

[150] Olsen, G. W., Mair, D. C., Reagen, W. K., Ellefson, M. E., Ehresman, D. J., Butenhoff, J. L., & Zobel, L. R. (2007b). Preliminary evidence of a decline in perfluorooctanesulfonate (PFOS) and perfluorooctanoate (PFOA) concentrations in american red cross blood donors. *Chemosphere*, 68(1), 105–111.

[151] Pan, C.-G., Ying, G.-G., Liu, Y.-S., Zhang, Q.-Q., Chen, Z.-F., Peng, F.-J., & Huang, G.-Y. (2014). Contamination profiles of perfluoroalkyl substances in five typical rivers of the Pearl River Delta region, South China. *Chemosphere*, 114, 16–25.

[152] Panagopoulos, D., Kierkegaard, A., Jahnke, A., & MacLeod, M. (2016). Evaluating the salting-out effect on the organic carbon/water partition ratios (KOC and KDOC) of linear and cyclic volatile methylsiloxanes: Measurements and polyparameter linear free energy relationships. *Journal of Chemical & Engineering Data*, 61(9), 3098–3108.

[153] Panneer Selvam, B., Lapierre, J.-F., Guillemette, F., Voigt, C., Lamprecht, R. E., Biasi, C., Christensen, T. R., Martikainen, P. J., & Berggren, M. (2017). Degradation potentials of dissolved organic carbon (DOC) from thawed permafrost peat. *Scientific Reports*, 7, 45811.

[154] Paul, A. G., Jones, K. C., & Sweetman, A. J. (2009). A first global production, emission, and environmental inventory for perfluorooctane sulfonate. *Environmental Science & Technology*, 43(2), 386–392.

[155] Persky, V., Turyk, M., Anderson, H. A., Hanrahan, L. P., Falk, C., Steenport, D. N., Chatterton, R., Freels, S., & Great Lakes Consortium (2001). The effects of PCB exposure and fish consumption on endogenous hormones. *Environmental Health Perspectives*, 109(12), 1275–1283.

[156] Pickard, H. M., Criscitiello, A. S., Spencer, C., Sharp, M. J., Muir, D. C. G., De Silva, A. O., & Young, C. J. (2018). Continuous non-marine inputs of per- and polyfluoroalkyl substances to the High Arctic: A multi-decadal temporal record. *Atmospheric Chemistry & Physics*, 18(7), 5045–5058.

[157] Pistocchi, A. & Loos, R. (2009). A map of european emissions and concentrations of PFOS and PFOA. *Environmental Science & Technology*, 43(24), 9237–9244.

[158] Polyakov, I. V., Alekseev, G. V., Bekryaev, R. V., Bhatt, U., Colony, R. L., Johnson, M. A., Karklin, V. P., Makshtas, A. P., Walsh, D., & Yulin, A. V. (2002). Observationally based assessment of polar amplification of global warming. *Geophysical Research Letters*, 29(18), 25–1–25–4.

[159] Polyakov, I. V., Walsh, J. E., & Kwok, R. (2012). Recent changes of arctic multiyear sea ice coverage and the likely causes. *Bulletin of the American Meteorological Society*, 93(2), 145–151.

[160] Powley, C. R., George, S. W., Russell, M. H., Hoke, R. A., & Buck, R. C. (2008). Polyfluorinated chemicals in a spatially and temporally integrated food web in the western Arctic. *Chemosphere*, 70(4), 664–672.

[161] Pufall, E. L., Jones, A. Q., McEwen, S. A., Lyall, C., Peregrine, A. S., & Edge, V. L. (2011). Perception of the importance of traditional country foods to the physical, mental, and spiritual health of labrador inuit. *Arctic*, 64(2), 242–250.

[162] Rahmstorf, S., Box, J. E., Feulner, G., Mann, M. E., Robinson, A., Rutherford, S., & Schaffernicht, E. J. (2015). Exceptional twentieth-century slowdown in Atlantic Ocean overturning circulation. *Nature Climate Change*, 5, 475.

[163] Richter-Menge, J., Overland, J. E., Mathis, J., & Osborne, E. (2017). *Arctic Report Card 2017*. Report.

[164] Rodrigo, A. P. & Costa, P. M. (2017). The role of the cephalopod digestive gland in the storage and detoxification of marine pollutants. *Frontiers in Physiology*, 8, 232.

[165] Salter, M. E., Zieger, P., Acosta Navarro, J. C., Grythe, H., Kirkevåg, A., Rosati, B., Riipinen, I., & Nilsson, E. D. (2015). An empirically derived inorganic sea spray source function incorporating sea surface temperature. *Atmospheric Chemistry & Physics*, 15(19), 11047–11066.

[166] Sander, R. (1999). Modeling atmospheric chemistry: Interactions between gas-phase species and liquid cloud/aerosol particles. *Surveys in Geophysics*, 20(1), 1–31.

[167] Schenker, U., MacLeod, M., Scheringer, M., & Hungerbühler, K. (2005). Improving data quality for environmental fate models: A least-squares adjustment procedure for harmonizing physicochemical properties of organic compounds. *Environmental Science & Technology*, 39(21), 8434–8441.

[168] Scheringer, M., Strempel, S., Hukari, S., Ng, C. A., Blepp, M., & Hungerbuhler, K. (2012). How many persistent organic pollutants should we expect? *Atmospheric Pollution Research*, 3(4), 383–391.

[169] Scheringer, M., Wegmann, F., Fenner, K., & Hungerbühler, K. (2000). Investigation of the cold condensation of persistent organic pollutants with a global multimedia fate model. *Environmental Science & Technology*, 34(9), 1842–1850.

[170] Schwarzenbach, R. P., Gschwend, P. M., & Imboden, D. M. (2003). *Environmental Organic Chemistry*. New York: John Wiley & Sons, 2nd edition.

[171] Sha, B., Johansson, J. H., Benskin, J. P., Cousins, I. T., & Salter, M. E. (2020). Influence of water concentrations of perfluoroalkyl acids (PFAAs) on their size-resolved enrichment in nascent sea spray aerosols. *Environmental Science & Technology*.

[172] Simcik, M. F. & Dorweiler, K. J. (2005). Ratio of perfluorochemical concentrations as a tracer of atmospheric deposition to surface waters. *Environmental Science & Technology*, 39(22), 8678–8683.

[173] Simonich, S. L. & Hites, R. A. (1995). Global distribution of persistent organochlorine compounds. *Science*, 269(5232), 1851.

[174] Simonnet-Laprade, C., Budzinski, H., Maciejewski, K., Le Menach, K., Santos, R., Alliot, F., Goutte, A., & Labadie, P. (2019). Biomagnification of perfluoroalkyl acids (PFAAs) in the food web of an urban river: Assessment of the trophic transfer of targeted and unknown precursors and implications. *Environmental Science: Processes & Impacts*, 21(11), 1864–1874.

[175] Sinkkonen, S. & Paasivirta, J. (2000). Degradation half-life times of PCDDs, PCDFs and PCBs for environmental fate modeling. *Chemosphere*, 40(9–11), 943–949.

[176] Smart, B. E. (2001). Fluorine substituent effects (on bioactivity). *Journal of Fluorine Chemistry*, 109(1), 3–11.

[177] Smith, S. D. (1980). Wind stress and heat flux over the ocean in gale force winds. *Journal of Physical Oceanography*, 10(5), 709–726.

[178] Sobek, A. & Gustafsson, O. (2004). Latitudinal fractionation of polychlorinated biphenyls in surface seawater along a 62° N–89° N transect from the Southern Norwegian Sea to the North Pole Area. *Environmental Science & Technology*, 38(10), 2746–2751.

[179] Sobek, A. & Gustafsson, O. (2014). Deep water masses and sediments are main compartments for polychlorinated biphenyls in the Arctic Ocean. *Environmental Science & Technology*, 48(12), 6719–6725.

[180] Sobek, A., Gustafsson, O., Hajdu, S., & Larsson, U. (2004). Particle–water partitioning of PCBs in the photic zone: A 25-month study in the open Baltic Sea. *Environmental Science & Technology*, 38(5), 1375–1382.

[181] Speich, S., Blanke, B., & Cai, W. (2007). Atlantic meridional overturning circulation and the Southern Hemisphere supergyre. *Geophysical Research Letters*, 34(23).

[182] Stemmler, I. & Lammel, G. (2013). Evidence of the return of past pollution in the ocean: A model study. *Geophys. Res. Lett.*, 40(7), 1373–1378.

[183] Stenzel, A., Goss, K.-U., & Endo, S. (2013). Experimental determination of polyparameter linear free energy relationship (pp-lfer) substance descriptors for pesticides and other contaminants: New measurements and recommendations. *Environmental Science & Technology*, 47(24), 14204–14214.

[184] Stock, N. L., Furdui, V. I., Muir, D. C. G., & Mabury, S. A. (2007). Perfluoroalkyl contaminants in the Canadian Arctic: Evidence of atmospheric transport and local contamination. *Environmental Science & Technology*, 41(10), 3529–3536.

[185] Stramska, M. & Stramski, D. (2005). Variability of particulate organic carbon concentration in the north polar Atlantic based on ocean color observations with sea-viewing wide field-of-view sensor (SeaWiFS). *Journal of Geophysical Research: Oceans*, 110(C10).

[186] Stroeve, J., Holland Marika, M., Meier, W., Scambos, T., & Serreze, M. (2007). Arctic sea ice decline: Faster than forecast. *Geophysical Research Letters*, 34(9).

[187] Sun, C., Soltwedel, T., Bauerfeind, E., Adelman, D. A., & Lohmann, R. (2016). Depth profiles of persistent organic pollutants in the North and Tropical Atlantic Ocean. *Environmental Science & Technology*, 50(12), 6172–6179.

[188] Sunderland, E. M. (2007). Mercury exposure from domestic and imported estuarine and marine fish in the U.S. seafood market. *Environmental health perspectives*, 115(2), 235–242.

[189] Sunderland, E. M., Hu, X. C., Dassuncao, C., Tokranov, A. K., Wagner, C. C., & Allen, J. G. (2018). A review of the pathways of human exposure to poly- and perfluoroalkyl substances (PFASs) and present understanding of health effects. *Journal of Exposure Science & Environmental Epidemiology*.

[190] Sühring, R., Diamond, M. L., Scheringer, M., Wong, F., Pućko, M., Stern, G., Burt, A., Hung, H., Fellin, P., Li, H., & Jantunen, L. M. (2016). Organophosphate esters in Canadian Arctic air: Occurrence, levels and trends. *Environmental Science & Technology*, 50(14), 7409–7415.

[191] Thackray, C. P., Selin, N. E., & Young, C. J. (2020). A global atmospheric chemistry model for the fate and transport of PFCAs and their precursors. *Environmental Science: Processes & Impacts*, 22(2), 285–293.

[192] Theobald, N., Caliebe, C., Gerwinski, W., Hühnerfuss, H., & Lepom, P. (2011). Occurrence of perfluorinated organic acids in the North and Baltic Seas. part 1: distribution in sea water. *Environmental Science and Pollution Research*, 18(7), 1057–1069.

[193] Thompson, J., Roach, A., Eaglesham, G., Bartkow, M. E., Edge, K., & Mueller, J. F. (2011). Perfluorinated alkyl acids in water, sediment and wildlife from sydney harbour and surroundings. *Marine Pollution Bulletin*, 62(12), 2869–2875.

[194] Tsilingiris, P. T. (2008). Thermophysical and transport properties of humid air at temperature range between 0 and 100°c. *Energy Conversion and Management*, 49(5), 1098–1110.

[195] Tucker, W. A. & Nelken, L. H. (1990). *Diffusion coefficients in air and water*, (pp. 17. 1–17. 25). Washington, DC. USA.

[196] UNEP (2001). Stockholm Convention on Persistent Organic Pollutants, opened for signature May 23, 2001, UN Doc. UNEP/POPS/CONF/4, App. II (2001). *Available online at the United Nations Environment Programme's (UNEP's) POPs Web site, <http://irptc.unep.ch/pops/>.*

[197] United Nations Environment Program (2009). Sc-4/17: Listing of perfluorooctane sulfonic acid, its salts and perfluorooctane sulfonyl fluoride.

[198] Van Oostdam, J., Donaldson, S. G., Feeley, M., Arnold, D., Ayotte, P., Bondy, G., Chan, L., Dewaily, E., Furgal, C. M., Kuhnlein, H., Loring, E., Muckle, G., Myles, E., Receveur, O., Tracy, B., Gill, U., & Kalhok, S. (2005). Human health implications of environmental contaminants in arctic canada: A review. *Science of The Total Environment*, 351-352, 165–246.

[199] Vento, S. D., Halsall, C., Gioia, R., Jones, K., & Dachs, J. (2012). Volatile per- and polyfluoroalkyl compounds in the remote atmosphere of the western Antarctic peninsula: an indirect source of perfluoroalkyl acids to Antarctic waters? *Atmospheric Pollution Research*, 3(4), 450–455.

[200] Wang, Z., Boucher, J. M., Scheringer, M., Cousins, I. T., & Hungerbühler, K. (2017). Toward a comprehensive global emission inventory of c4–c10 perfluoroalkanesulfonic acids (PFSAs) and related precursors: Focus on the life cycle of c8-based products and ongoing industrial transition. *Environmental Science & Technology*, 51(8), 4482–4493.

[201] Wang, Z., Cousins, I. T., Scheringer, M., Buck, R. C., & Hungerbühler, K. (2014a). Global emission inventories for c4–c14 perfluoroalkyl carboxylic acid (PFCA) homologues from 1951 to 2030, part i: production and emissions from quantifiable sources. *Environment International*, 70, 62–75.

[202] Wang, Z., Cousins, I. T., Scheringer, M., Buck, R. C., & Hungerbühler, K. (2014b). Global emission inventories for c4–c14 perfluoroalkyl carboxylic acid (PFCA) homologues from 1951 to 2030, part ii: The remaining pieces of the puzzle. *Environment International*, 69, 166–176.

[203] Wang, Z., Walker, G. W., Muir, D. C. G., & Nagatani-Yoshida, K. (2020). Toward a global understanding of chemical pollution: A first comprehensive analysis of national and regional chemical inventories. *Environmental Science & Technology*, 54(5), 2575–2584.

[204] Wania, F. & Daly, G. L. (2002). Estimating the contribution of degradation in air and deposition to the deep sea to the global loss of PCBs. *Atmospheric Environment*, 36(36–37), 5581–5593.

[205] Wania, F. & Mackay, D. (1993). Global fractionation and cold condensation of low volatility organochlorine compounds in polar regions. *Ambio*, 22(1), 10–18.

[206] Weber, A. K., Barber, L. B., LeBlanc, D. R., Sunderland, E. M., & Vecitis, C. D. (2017). Geochemical and hydrologic factors controlling subsurface transport of poly- and perfluoroalkyl substances, Cape Cod, Massachusetts. *Environmental Science & Technology*, 51(8), 4269–4279.

[207] Wei, S., Chen, L. Q., Taniyasu, S., So, M. K., Murphy, M. B., Yamashita, N., Yeung, L. W. Y., & Lam, P. K. S. (2007). Distribution of perfluorinated compounds in surface seawaters between Asia and Antarctica. *Marine Pollution Bulletin*, 54(11), 1813–1818.

[208] Weihe, P., Debes, F., Halling, J., Petersen, M. S., Muckle, G., Odland, J. O., Dudarev, A., Ayotte, P., Dewailly, E., Grandjean, P., & Bonefeld-Jørgensen, E. (2016). Health effects associated with measured levels of contaminants in the Arctic. *International Journal of Circumpolar Health*, 75, 33805–33805.

[209] Weihe, P. & Joensen, H. D. (2012). Dietary recommendations regarding pilot whale meat and blubber in the Faroe Islands. *International Journal of Circumpolar Health*, 71, 18594–18594.

[210] Weihe, P., Kato, K., Calafat, A. M., Nielsen, F., Wanigatunga, A. A., Needham, L. L., & Grandjean, P. (2008). Serum concentrations of polyfluoroalkyl compounds in faroese whale meat consumers. *Environmental Science & Technology*, 42(16), 6291–6295.

[211] Wilke, C. R. & Chang, P. (1955). Correlation of diffusion coefficients in dilute solutions. *American Institute of Chemical Engineers Journals*, 1(2), 264–270.

[212] Wong, F., Shoeib, M., Katsoyiannis, A., Eckhardt, S., Stohl, A., Bohlin-Nizzetto, P., Li, H., Fellin, P., Su, Y., & Hung, H. (2018). Assessing temporal trends and source regions of per- and polyfluoroalkyl substances (PFASs) in air under the Arctic Monitoring and Assessment Programme (AMAP). *Atmospheric Environment*, 172, 65–73.

[213] Xie, Z., Wang, Z., Mi, W., Möller, A., Wolschke, H., & Ebinghaus, R. (2015). Neutral poly-/perfluoroalkyl substances in air and snow from the Arctic. *Scientific Reports*, 5(1), 8912.

[214] Yamashita, N., Kannan, K., Taniyasu, S., Horii, Y., Okazawa, T., Petrick, G., & Gamo, T. (2004). Analysis of perfluorinated acids at parts-per-quadrillion levels in seawater using liquid chromatography-tandem mass spectrometry. *Environmental Science & Technology*, 38(21), 5522–5528.

[215] Yamashita, N., Kannan, K., Taniyasu, S., Horii, Y., Petrick, G., & Gamo, T. (2005). A global survey of perfluorinated acids in oceans. *Marine Pollution Bulletin*, 51(8), 658–668.

[216] Yamashita, N., Taniyasu, S., Petrick, G., Wei, S., Gamo, T., Lam, P. K. S., & Kannan, K. (2008). Perfluorinated acids as novel chemical tracers of global circulation of ocean waters. *Chemosphere*, 70(7), 1247–1255.

[217] Yamazaki, E., Taniyasu, S., Ruan, Y., Wang, Q., Petrick, G., Tanhua, T., Gamo, T., Wang, X., Lam, P. K. S., & Yamashita, N. (2019). Vertical distribution of perfluoroalkyl substances in water columns around the Japan Sea and the Mediterranean Sea. *Chemosphere*, 231, 487–494.

[218] Yeung, L. W. Y., Dassuncao, C., Mabury, S., Sunderland, E. M., Zhang, X., & Lohmann, R. (2017). Vertical profiles, sources, and transport of PFASs in the arctic ocean. *Environmental Science & Technology*, 51(12), 6735–6744.

[219] Young, C. J. & Marbury, S. A. (2010). *Atmospheric Perfluorinated Acid Precursors: Chemistry, Occurrence, and Impacts*. New York, New York, NY: Springer.

[220] Zhang, L. & Lohmann, R. (2010a). Cycling of PCBs and HCB in the surface ocean-lower atmosphere of the open Pacific. *Environmental Science & Technology*, 44(10), 3832–3838.

[221] Zhang, L. & Lohmann, R. (2010b). Cycling of PCBs and HCB in the surface ocean-lower atmosphere of the open Pacific. *Environmental Science & Technology*, 44(10), 3832–3838.

[222] Zhang, X., Lohmann, R., & Sunderland, E. M. (2019). Poly- and perfluoroalkyl substances in seawater and plankton from the northwestern Atlantic margin. *Environmental Science & Technology*, 53(21), 12348–12356.

[223] Zhang, X., Zhang, Y., Dassuncao, C., Lohmann, R., & Sunderland, E. M. (2017). North Atlantic Deep Water formation inhibits high Arctic contamination by continental perfluorooctane sulfonate discharges. *Global Biogeochemical Cycles*, 31(8), 1332–1343.

[224] Zhang, Y., Jacob, D. J., Dutkiewicz, S., Amos, H. M., Long, M. S., & Sunderland, E. M. (2015). Biogeochemical drivers of the fate of riverine mercury discharged to the global and Arctic ceans. *Global Biogeochemical Cycles*, 29(6), 854–864.

[225] Zhao, Z., Tang, J., Mi, L., Tian, C., Zhong, G., Zhang, G., Wang, S., Li, Q., Ebinghaus, R., Xie, Z., & Sun, H. (2017). Perfluoroalkyl and polyfluoroalkyl substances in the lower atmosphere and surface waters of the Chinese Bohai Sea, Yellow Sea, and Yangtze river estuary. *Science of The Total Environment*, 599-600, 114–123.

[226] Zhao, Z., Xie, Z., Möller, A., Sturm, R., Tang, J., Zhang, G., & Ebinghaus, R. (2012). Distribution and long-range transport of polyfluoroalkyl substances in the Arctic, Atlantic Ocean and Antarctic coast. *Environmental Pollution*, 170, 71–77.

[227] Zhou, Y., Wang, T., Li, Q., Wang, P., Li, L., Chen, S., Zhang, Y., Khan, K., & Meng, J. (2018). Spatial and vertical variations of perfluoroalkyl acids (PFAAs) in the Bohai and Yellow Seas: Bridging the gap between riverine sources and marine sinks. *Environmental Pollution*, 238, 111–120.

This thesis was typeset using LaTeX, originally developed by Leslie Lamport and based on Donald Knuth's TeX. The body text is set in 11 point Egenolff-Berner Garamond, a revival of Claude Garamont's humanist typeface. The above illustration, "Science Experiment 02", was created by Ben Schlitter and released under CC BY-NC-ND 3.0. A template that can be used to format a PhD thesis with this look and feel has been released under the permissive MIT (X11) license, and can be found online at github.com/suchow/Dissertate or from its author, Jordan Suchow, at suchow@post.harvard.edu.